Quantitative Insight into Two Complex Physical Systems: Desoxyribonucleic Acid and Solid Electrolytes

Dissertation
zur Erlangung der naturwissenschaftlichen Doktorwürde (Dr. sc. nat.)
vorgelegt der
Mathematisch-naturwissenschaftlichen Fakultät der Universität Zürich

Conrad Escher
von Zürich

Promotionskomitee

Prof. Dr. Hans-Werner Fink
Prof. Dr. Thomas Greber

Zürich 2007

Gutachter:

Prof. Dr. Dieter Pohl

Prof. Dr. Christian Schönenberger

Zusammenfassung

Die vorliegende Arbeit ist in zwei Teilen abgefasst. Der Erste, *On the Energetics of Individual DNA Molecules in the Liquid Phase*, beschäftigt sich mit dem Studium langer, fadenförmiger DNS-Moleküle betreffend Fragen aus dem Bereich der Polymerphysik. Im zweiten Teil, *On the Dynamics of the Conduction Mechanism and Field Ion Emission from a Solid Electrolyte*, wird die Erfindung einer neuartigen Ionenquelle vorgestellt und deren Verwendung zur Untersuchung des Leitungsmechanismus in Festkörperelektrolyten diskutiert.

Die Experimente mit einzelnen DNS-Molekülen werden unter dem (optischen) Fluoreszenz-Mikroskop durchgeführt. Dies ermöglicht Untersuchungen an den Molekülen in wässriger Lösung; unter natürlichen Bedingungen also. Das Hauptmerkmal des experimentellen Aufbaus ist die Möglichkeit temperaturabhängige Messungen ausführen zu können und stellt eine notwendige Voraussetzung dar, um Fragen zur Energetik thermisch aktivierter Prozesse angehen zu können.
In einem ersten Experiment wird der Diffusionskoeffizient des Massenmittelpunktes eines einzelnen DNS-Moleküls, der ein Mass für die Mobilität des Moleküls darstellt, bei verschiedenen Temperaturen bestimmt. Die Ergebnisse werden verglichen mit den entsprechenden Diffusionsdaten einer Styrol-Kugel, die einen Durchmesser von *100nm* und somit ca. die achtfache Masse des DNS-Moleküls aufweist. Es stellt sich heraus, dass, trotz seiner kleineren Masse, das Fadenmolekül deutlich langsamer diffundiert als die starre Kugel. Ein Vergleich der Diffusionsdaten verschiedener Temperaturen erlaubt es darüber hinaus, auf die Aktivierungsenergie des Diffusionsprozesses zu schliessen. Letztere ist die bestimmende Grösse hinsichtlich der Dynamik thermisch aktivierter Prozesse.
In einem zweiten Experiment wird der Übergang zwischen der vollständig gestreckten und der zufällig verknäuelten Konfiguration eines einzelnen DNS-Moleküls in Lösung beobachtet. Bezüglich der Entropie zeichnen sich die genannten Konfigurationen dadurch aus, dass erstere den Zustand niedrigster Entropie, letztere den Zustand grösster Entropie darstellt. Die Übergangszeiten zwischen den beiden Konfigurationen werden bei verschiedenen Temperaturen zwischen *-5°C* und *50°C* ermittelt und daraus eine Aktivierungsbarriere abgeleitet, die für besagten Übergang relevant ist.
Die Untersuchungen betreffend den Leitungsmechanismus in Festkörper-Elektrolyten werden mit Hilfe des Feldemissions-Mikroskops durchgeführt. Dazu wird *(AgI)(AgPO$_3$)*, einer der besten Ag^+ Ionenleiter unter den Festkörper-Elektrolyten, zu einer scharfen Spitze geformt. Wie sich herausstellt, lassen sich aus einer solchen Spitze bereits Ag^+ Ionen emittieren, wenn sie auf ein Potential von der Grössenordnung *10kV* gelegt wird.
In einem ersten Teil wird das Verhalten dieser neuartigen Ionenquelle studiert. Insbesondere werden *I/V*-Charakteristika aufgenommen und die Langzeit-Stabilität des Emissionsstromes geprüft. Dabei zeigt sich, dass die Quelle durchaus Potential für technologische Anwendungen im Zusammenhang mit fokussierten Ionenstrahlen aufweist.
In einem zweiten Teil werden die Feldemissionsmuster analysiert. Auf der Elektrolyt-Spitze können ausgeprägte Emissionszentren ausgemacht werden. Diese lassen sich interpretieren als die Ausgänge von Leitungs-Kanälen, die sich im Festkörper-Elektrolyten ausgebildet haben. Auto- und Cross-Korrelationsmessungen führen auf charakteristische Zeiten und Distanzen betreffend die Dynamik des Ionen-Leitungsmechanismus in *(AgI)(AgPO$_3$)*.

Abstract

The work presented here is divided into two sections. The first section *On the Energetics of Individual DNA Molecules in the Liquid Phase* examines long, filiform DNA molecules and addresses questions concerning polymer physics. In the second section *On the Dynamics of the Conduction Mechanism and Field Ion Emission from a Solid Electrolyte* the invention of a novel ion emission source is introduced and its application to investigate the conduction mechanism of solid electrolytes is discussed.

The experiments with individual DNA molecules are carried out under the (optical) fluorescence microscope. This method allows investigation in aqueous solution, i.e. under natural environmental conditions for the DNA molecule. The key feature of the experimental set up is the possibility to accomplish temperature dependent measurements and represents an essential prerequisite to approach questions concerning the energetics of thermally activated processes.

In a first experiment the diffusion coefficient of the centre of mass of a single DNA molecule – a quantity describing the overall mobility of the molecule – is determined at different temperatures. The results are compared with corresponding diffusion data of a *100nm* diameter styrene bead eight times heavier than the DNA molecule. Despite its smaller mass, the chain-like DNA is found to clearly slower diffuse than the rigid bead.

In a second experiment the transition between the straight and the random coil configuration of individual DNA molecules under thermo dynamical equilibrium conditions is studied. In terms of entropy these two configurations are prominent: The latter represents an entropic maximum, whereas the former represents minimal entropy. Transition times between these two configurations are acquired at various temperatures ranging from -5°C to 50°C to derive an overall activation barrier relevant for the transition under study.

The studies on the conduction mechanism of solid electrolytes are accomplished in the field emission microscope. Therefore *(AgI)(AgPO$_3$)* - known to be one of the best Ag^+ conductors among solid electrolytes - is shaped into a sharp tip. As it turns out, Ag^+ ions can readily be field emitted from the tip when put on high potential of the order of *10kV*.

In the first part the performance of this novel ion source is characterized. In particular *I/V*-characteristics are recorded and long-term stability of the emission current is verified revealing potential for focussed ion beam applications.

In the second part field ion emission patterns are analysed. Distinct emission sites on the tip apex are identified and interpreted as departure gates of the conduction pathways formed inside the solid electrolyte. Auto- and cross-correlation measurements reveal characteristic times and distances involved in the ion conduction dynamics of *(AgI)(AgPO$_3$)*.

Contents:

Section II

Section I

On the Energetics of Individual DNA Molecules in the Liquid Phase

I.0. Introduction to Section I

This introduction is meant to provide a compendium of the field of research from which the presented manuscripts accrue. A modest theoretical background presents the basic models and quantities related to polymer physics of individual molecules in dilute solution. Thereafter the most important previous experimental findings and methods are discussed briefly to expound the experimental precincts.

I.1. Description of a Polymer Chain in Dilute Solution

A polymer is a large molecule made up of many rather simple chemical units (monomers), joined together by chemical reaction. For example there are the hydrocarbon or hydrosilicon chains (plastic, rubber etc.) made up of typically $10^2 - 10^4$ monomers or there is the DNA biopolymer composed of up to 10^8 units.

Probably the first products that nowadays are assigned to polymer chemistry have been used by the North American Indians. They made rubber balls, bottles, shoe soles and so forth from caoutchouc[1]. Unfortunately this natural rubber disintegrates fairly rapid in air as the polymers are cut in smaller pieces and cross links are cracked by oxygen. In 1839 Charles Goodyear found a method, the so-called vulcanising, to prevent the caoutchouc from disintegration. By now a considerable variety of natural as well as synthetic polymers of high durability is known. Several great scientists (e.g. P. Debye, W. Kuhn, P. Flory, P.G. de Gennes) have been and are involved to gain insight into the fascinating discipline of polymer physics.

Materials composed of these very long molecules display properties that are completely different from materials composed of small molecules or atoms. Classifications like *gas*, *liquid* and *crystalline phase* are no more appropriate. Polymers are rather classified as *semi-crystalline*, *visco-elastic* (e.g. polymer melt), *highly elastic* (e.g. rubber) and *vitreous* (e.g. acrylic glass).

Furthermore, polymers are very often in solution such as liquid crystals or resists and the polymer concentration becomes a crucial parameter for the physics of such a system. In a very dilute solution the individual polymer essentially only interacts with the surrounding solvent molecules whereas in a concentrated solution the interaction between entangled polymers is dominant. In the following we shall focus on an isolated single polymer chain in solution and describe it by means of statistical mechanics.

[1] The word “caoutchouc” comes from cahuchu (= crying tree; *hevea brasiliensis*). By cutting the bark of this plant a milky looking jus (latex) can be collected and processed into rubber.

I.1.1. The Random Chain

A first approach to describe the equilibrium configuration of an individual long polymer chain in solution is to regard the molecule as a random chain [I.1], also referred to as freely jointed chain (FJC) [I.2]. The random chain denotes a chain that is thought to be made up of a string of *N* rigid chain links of equal length *l* that are freely rotatable with respect to each other. Following the molecule from one end to the other is equivalent to a random walk with unit step size l. Hence, the chain is characterised by a Gaussian end-to-end distribution $P(\vec{r}_{ee},N)$:

$$P(\vec{r}_{ee},N)=\left(\frac{3}{2\pi N\cdot l^2}\right)^{3/2}\exp\left(-\frac{3\vec{r}_{ee}^{\,2}}{2N\cdot l^2}\right)$$

eqn.I.1

Here $\vec{r}_{ee}$ is the end-to-end vector. From the end-to-end distribution important physical quantities can be derived. In particular for the mean square end-to-end distance results:

$$\left\langle \vec{r}_{ee}^{\,2}\right\rangle = N\cdot l^2$$

eqn.I.2

In other words: $\left\langle \vec{r}_{ee}^{\,2}\right\rangle$ scales with *N* (to the power of 1), i.e. with the degree of polymerisation or the length of the polymer.

The random walk model assumes the orientation of each link is random and completely independent of the orientation of the previous link. This allows the polymer to fold back onto itself, which is physically impossible, as two different links of the molecule cannot occupy the same region in space. To adjust the model to these short-range interactions[2] let *z* be the total number of possible directions in the coordinate system. This leaves *(z-1)* possible directions to each chain link, if folding back on the previous link is excluded. This modification will certainly influence the mean square end-to-end distance. For the model including short-range interactions and very large *N* one finds:

$$\left\langle \vec{r}_{ee}^{\,2}\right\rangle = N\cdot l^2\left(\frac{z}{z-2}\right)$$

eqn.I.3

Note that with a large number *z* of possible directions eqn.I.3 and eqn.I.2 do not differ much. But in particular the following proportionality holds also for the modified model:

$$\left\langle \vec{r}_{ee}^{\,2}\right\rangle \propto N$$

eqn.I.4

In general is true: As long as the interaction between the links of a very long chain extends only up to a finite distance along the polymer it behaves like an ideal chain, independent of the microscopic structure. And one can write:

[2] „Short-range" refers to distances along the chain and not to distances in space.

$$\left\langle \vec{r}_{ee}^{\,2} \right\rangle = \overline{N} \cdot l_{eff}^2$$

eqn.I.5

Here l_{eff} is a characteristic effective length of a chain segment after which the direction of the molecule is random again and often referred to as Kuhn length; see fig.I.1. $\overline{N}$ is the number of segments of Kuhn length l_{eff} in the polymer chain. In particular for the so-called freely rotating chain (FRC) - an important model for several polymers - above description is valid. The FRC-model assumes that the bond angles are fixed but are free to rotate, giving rise to a uniform distribution of dihedral angles [I.1].

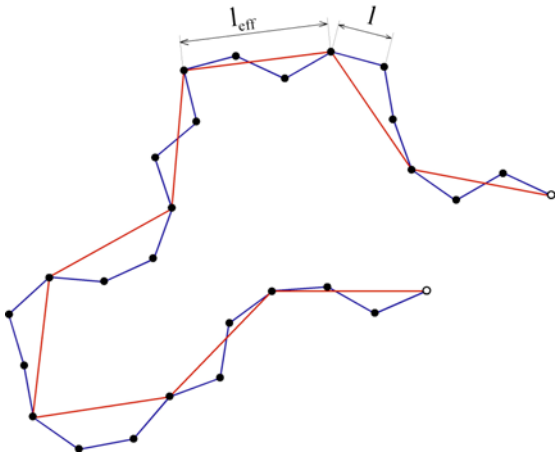

fig.I.1

I.1.2. The Worm Like Chain

To describe somewhat stiffer (semi-flexible) polymers the worm like chain model (WLC-model) [I.2], also referred to as the Kratky-Porod model, is often used. The WLC-model is an important model for many systems. It was developed out of the FRC-model but introduces the notion of continuously curved chain morphology. The model envisions an isotropic rod that is continuously flexible and thus is particularly suited for describing stiffer polymers. At room temperature, the polymer adopts a conformational ensemble that is smoothly curved; at *0K*, the polymer adopts a rigid rod conformation. For its description a unit tangent vector $\vec{t}(s)$ to the polymer chain is defined:

$$\vec{t}(s) = \frac{\partial \vec{r}(s)}{\partial s}$$

eqn.I.6

Here $\vec{r}(s)$, with s $\in$ [*0*,*L*], is the position vector along the chain of contour length *L*.

Then the end-to-end vector is given by:

$$\vec{r}_{ee} = \int_0^L \vec{t}(s)ds$$

eqn.I.7

To measure the stiffness of the polymer chain the orientation correlation function is introduced and it can be shown that correlation decays exponentially:

$$\left\langle \vec{t}(s) \cdot \vec{t}(0) \right\rangle = \exp(-s/p)$$

eqn.I.8

Here p is by definition the polymers characteristic persistence length. Similar to the Kuhn-length the persistence length is a measure to describe how far the polymer extends in a given direction before becoming random.
For the mean square end-to-end distance one finds:

$$\left\langle \vec{r}_{ee}^{\,2} \right\rangle = 2pL\left\{1 - p/L\left[1 - \exp(-L/p)\right]\right\}$$

eqn.I.9

And for very long chains, i.e. $L >> p$:

$$\left\langle \vec{r}_{ee}^{\,2} \right\rangle = 2pL$$

eqn.I.10

Note that the comparison of eqn.I.10 with eqn.I.5 shows: For a semi-flexible molecule the "random chain-approximation" leads to a "characteristic stiffness" (=Kuhn-length) that is twice the persistence length.
Moreover, it has been shown [I.3] that for a worm like chain the force to extend the chain within the entropic elasticity regime is approximately given by [3]:

$$F(x) = \frac{k_B T}{p}\left[\frac{x}{L} + \frac{1}{4(1 - x/L)^2} - \frac{1}{4}\right]$$

eqn.I.11

While the first, linear term in eqn.I.11 dominates in the $x << L$ regime, i.e. for small extensions, the second term describes a sharp increase in the force when the extension x approaches contour length L.

[3] The force to extend a FJC diverges less strongly as $x \to L$: $F(x) \propto (1 - x/L)^{-1}$

I.1.3. The Radius of Gyration

Since the average of the square end-to-end distance is not easy to measure experimentally other quantities need to be introduced to express the dimension of a polymer chain in solution. A measure for the spatial distribution of the segments of the chain is the radius of gyration. It is defined as:

$$\vec{r}_{gyr}^{\,2} = \frac{1}{2N^2}\sum_{n=1}^{N}\sum_{m=1}^{N}\left\langle(\vec{r}_n - \vec{r}_m)^2\right\rangle$$

eqn.I.12

Here $\vec{r}_n$ ($n \in \{1,2,\ldots,N\}$) denotes the position vector of the nth segment. The radius of gyration can be directly measured in experiments and can also be defined for polymers with branched structure not only for linear polymer chains. The position of the centre of mass of the chain is given by:

$$\vec{r}_{CM} = \frac{1}{N}\sum_{n=1}^{N}\vec{r}_n$$

eqn.I.13

Using this the radius of gyration can be expressed as

$$\vec{r}_{gyr}^{\,2} = \frac{1}{N}\sum_{n=1}^{N}\left\langle\left(\vec{r}_n - \vec{r}_{CM}\right)^2\right\rangle$$

eqn.I.14

$\vec{r}_{gyr}^{\,2}$ equals thus the square of the average distance between the segments and the centre of mass of the polymer. Moreover, it can be shown that for an ideal chain the following relation between the radius of gyration and the end-to-end distance holds

$$\vec{r}_{gyr}^{\,2} = \frac{1}{6}N\cdot l^2 = \frac{1}{6}\left\langle\vec{r}_{ee}^{\,2}\right\rangle$$

eqn.I.15

In other words: The size of an ideal chain (i.e. a random chain, that ignores long-range interaction[4]) scales with $N^{1/2}$.

I.1.4. The Non-Ideal Chain

Starting from the simplest random chain the polymer models have been modified to exclude that two adjacent segments occupy the same site (FRC and WLC). Therefore short-range interactions between segments that are close to each other along the chain have been taken into account. Still these models permit a chain to loop back so that segments that are far apart along the chain will occupy the same region in space (long-range interaction), which of course is unphysical. The condition that accounts for this difficulty is called the excluded volume

[4] „Long-range" refers to distances along the chain and not to distances in space; see paragraph I.1.4.

effect. If a polymer chain is again envisioned as the trace of a walk, the excluded volume effect corresponds to the condition that the path cannot pass trough any sites that have been traversed previously (self avoiding walk). This condition becomes very important when evolution of configurations is discussed. Ignoring the excluded volume effect one part of a chain crossing **over** another part could unhamperedly transect and be crossing **under** the latter just an instant later. Again, this is unphysical. The ideal chain corresponds to a random chain that ignores the (long-range) excluded volume effect and thus is often referred to as phantom chain; see fig.I.2.

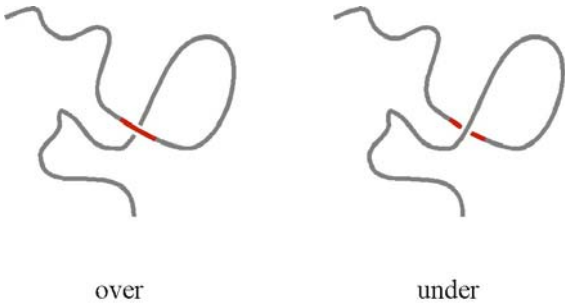

fig.I.2

The inclusion of long-range interaction of course causes a deviation in the statistical quantities from the ideal chain. In particular one expects the average size of a non-ideal chain to be larger. Since the same site can no more be shared by multiple segments, very dense configurations are excluded. The statistical properties of excluded volume chains have been extensively investigated in numerical simulations. For large N the following formula has been found:

$$r_{gyr} \cong N^{0.588} \cdot l$$

eqn.I.16

I.1.5. The Influence of the Solvent

Finally, discussing the size of an individual polymer in solution one needs to be aware that the size of the polymer will greatly depend on the liquid by which it is surrounded. If there is a high affinity between the solvent molecules and the segments of the chain, the polymer is easily dissolved and the solvent is called “good” solvent. On the other hand, in a solvent that does not well dissolve the polymer (poor solvent), the chain will remain more compact. Thus, to explain the dependence of the polymer size on the type of solvent the interactions between the polymer and the solvent must be considered. The interaction energies between adjacent polymer segments (E_{PP}) as well as interaction energies between polymer segments and solvent molecules (E_{PS}) and the ones between neighbouring solvent molecules (E_{SS}) come into play. Mostly these energies originate from van der Waals attraction but also from Coulomb interaction. In a more detailed derivation it can be shown [I.4] that the influence of the solvent on the size of a polymer essentially is characterized by the interaction term:

$$\Delta E = \frac{E_{PP} - E_{SS}}{2} - E_{PS}$$

eqn.I.17

In a good solvent there is a pronounced attractive interaction between the solvent and the polymer segments, whereas in a poor solvent the attractive interaction between solvent molecules on the one side and the attractive interaction between adjacent polymer segments on the other side are dominant. Hence, small or negative values for ΔE are characteristic for a good solvent, whereas high values for ΔE characterise a poor solvent. Note that in a poor solvent the effect of the solvent counteracts the excluded volume effect. The former tends to reduce the size of the molecule while the latter favours an enlarged polymer size. By increasing the temperature of the solution the interaction between the polymer chain and the solvent is enhanced. There is a critical temperature (defined as θ-temperature) when the repulsive excluded volume effect balances the attractive forces between the segments. At this temperature the polymer behaves as an ideal chain.

I.1.6. The Random Coil

Above discussion on the random configuration of polymer chains in solution (in addition maybe with the introduction of the radius of gyration) might have suggested the perception, that the most probable configuration (random coil) of a long polymer has an overall spherical shape. But it has been shown [I.1] that this is not the case. It turns out that the random coil is more likely to have an ellipsoidal (bean like) shape with a typical ratio of the axes of *6:2.3:1*. Only a few years ago these predictions of the aspherical random coil conformation have been verified for the first time experimentally. Therefore individual, long DNA molecules were observed at equilibrium by means of fluorescence microscopy and an average aspect ratio of *4.1:2.3:1* was determined [I.5].

I.1.7. Dynamical Models

Above discussion was focussing on the basic conformational aspects of a long polymer chain in dilute solution. Such a molecule has an extremely large number of freedoms. Thus, its shape is incessantly changing and the associated random motions are very complex. On the one side the motion of an individual segment is influenced by the net momentum transfer of the solvent (Brownian motion) but on the other side there are the intra molecular forces of the adjacent segments. Moreover the motion of an individual segment is influenced by hydrodynamic perturbance caused by the motion of the other segments.

I.1.7.1. The Rouse Model

One relatively simple model to describe the dynamical aspects of an individual polymer chain in dilute solution is the so-called Rouse model [I.6, I.7]. The polymer is envisioned as an ideal chain divided in segments sufficiently large to display rubber like elasticity. The polymer is then treated like a chain of beads connected with Hookean springs (spring-bead model; Gaussian chain). Assuming the beads experience a drag force proportional to their velocity as they are moved through the solvent, the following (Langevin-) equation for the position $\vec{r}_n(t)$ of the beads holds:

$$\frac{d\vec{r}_n}{dt} = -\frac{1}{\zeta}\frac{\partial U}{\partial \vec{r}_n} + \vec{g}_n \qquad \text{with: } \zeta = 6\pi\eta a$$

eqn.I.18

Here ζ is the friction coefficient of a bead, *a* denotes the (Stokes-) radius of the bead and η the viscosity of the solvent. $U(\vec{r})$ is a potential that varies with position. According to the first term on the right side in eqn.I.18 the particle is pulled in the direction of decreasing potential. As there is also an influence on the velocity of the bead due to Brownian motion the velocity fluctuates around an average value. The second summand on the right in eqn.I.18 accounts for these fluctuations; $\vec{g}_n(t)$ is a probability function that varies randomly with time. Letting *k* be the spring constant eqn.I.18 can be rewritten:

$$\frac{d\vec{r}_n}{dt} = \frac{k}{\zeta}(\vec{r}_{n+1} + \vec{r}_{n-1} - 2\vec{r}_n) + \vec{g}_n$$

eqn.I.19

It is convenient to assume that the beads are continuously distributed along the chain, i.e. *n* becomes a continuous variable. Writing $\vec{r}(n,t)$ instead of $\vec{r}_n(t)$, eqn.I.19 takes the form:

$$\frac{\partial \vec{r}(n,t)}{\partial t} = \frac{k}{\zeta}\frac{\partial^2 \vec{r}(n,t)}{\partial n^2} + \vec{g}(n,t)$$

eqn.I.20

This represents a linear harmonic oscillator. Hence, introducing normalized coordinates the motion of the chain can be decomposed into independent modes (Rouse modes). Each of these modes has its characteristic relaxation time (Rouse time) given by:

$$\tau_p = \frac{1}{p^2}\frac{\zeta N^2 b^2}{3\pi^2 k_B T} \qquad p = 1,2,3,...$$

eqn.I.21

The slowest relaxation time ($p = 1$) is often referred to as the *fundamental relaxation time* τ_R.

From the solution of eqn.I.20 the motion of the polymer ranging from rearrangements of single segments to the diffusion of the whole molecule can be described. In fact, one of the most important dynamical quantities is the diffusion coefficient. Einstein's relation eqn.I.22 says: The diffusion coefficient (a physical quantity describing thermal fluctuations) can be calculated from the viscosity coefficient (a quantity describing the response of the system under an external force)[5].

$$D = \frac{k_B T}{\zeta}$$

eqn.I.22

Introducing this to the Rouse model one finally finds a diffusion coefficient for the centre of mass of the spring-bead chain:

[5] See also fluctuation-dissipation theorem.

$$D_{CM} = \frac{k_B T}{N\zeta}$$

eqn.I.23

Note that D_{CM} scales with N^{-1}. It turns out that the Rouse model is a reasonable description for a relatively short chain. However, it fails for longer chains. In fact, the following dependencies have been measured experimentally, using dynamic light scattering methods [I.8, I.9]:

$$D_{CM} \propto N^{-\nu}$$

eqn.I.24

With $\nu = 1/2$ in the θ-state and $\nu = 3/5$ for a good solvent.[6]

I.1.7.2. The Zimm Model

The Rouse model assumes the average velocity of a particular bead is determined only by the external force acting on it, but is independent of the motion of the other beads. A more accurate model must take into account the fact that if one bead moves, the surrounding solvent will also move and as a consequence other beads are dragged along. This type of interaction transmitted by the motion of the solvent is called "hydrodynamic interaction", also referred to as "backflow effects".

An advancement of the Rouse model that accounts for these effects is the Zimm model [I.10]. As the hydrodynamic interactions do not influence the (spring-) potential $U(\vec{r})$ in eqn.I.18 but they alter the mobility of the segments, the mobility tensor H_{nm} is introduced. Consequently eqn.I.19 takes the following form:

$$\frac{d\vec{r}_n}{dt} = k\sum_m H_{nm} \cdot (\vec{r}_{m+1} + \vec{r}_{m-1} - 2\vec{r}_m) + \vec{g}_n$$

eqn.I.25

Unfortunately H_{nm} depends on $\vec{r}_n$. Thus, eqn.I.25 is non-linear in $\vec{r}_n(t)$ and almost impossible to solve. Therefore Zimm replaces H_{nm} with its equilibrium average value $\langle H_{nm} \rangle_{eq}$.[7] Due to the long-range nature of the hydrodynamic interactions this approximation is appropriate. Passing over to the continuous model with this modification eqn.I.25 finally can be written:

$$\frac{\partial \vec{r}(n,t)}{\partial t} = k\int_0^N h(n-m)\frac{\partial^2 \vec{r}(m,t)}{\partial m^2}dm + \vec{g}(n,t)$$

$$\text{here:} \qquad h(n-m) = \frac{1}{(6\pi^3|n-m|)^{1/2}\eta \cdot l}$$

eqn.I.26

Rewriting this with normalized coordinates again allows for deriving the diffusion coefficient of the centre of mass of the polymer:

[6] ν is often called the *Flory-parameter*.

[7] This approximation is called *pre-averaging approximation*.

$$D_{CM} = \frac{8k_BT}{3(6\pi^3)^{1/2}\eta N^{1/2}l} = 0.196\frac{k_BT}{\eta N^{1/2}l}$$

eqn.I.27

Note that with the Zimm model D_{CM} scales with N^{ν}, where $\nu = 1/2$. This agrees well with experiments carried out in solutions in the θ-state.

In terms of the exponent ν scaling concepts have been formulated [I.11] proposing that the dynamical properties of a polymer will scale similarly to its static properties (depending on the solvent quality). For example if the number of segments in a chain is changed from N to N/λ (where λ is a constant) then the physical properties can be held constant by simply changing the segment length from l to $l\lambda^{\nu}$ since these properties do not depend on the local structure of the chain. By this transformation any invariant dynamical or static property A should change from A to $A\lambda^{x}$ where x depends on ν.

Sophisticated concepts and formalisms are developed (e.g. in the framework of path integrals [I.12]) to calculate the scaling exponents.

I.2. Desoxyribonucleic Acid

Desoxyribonucleic acid (DNA) is the carrier of the genetic information of all life form and thus often referred to as “the molecule of life”. It is a 2*nm* thin filiform biopolymer made up of two complementary strands of desoxyribonucleotides wound around each other; see fig.I.3a.[8] A single nucleotide is chemically composed of a sugar ring connecting a phosphate group and a base. While the sugar-phosphate groups assume responsibility for the structural purposes and form the so-called backbones of the strands, the bases (or rather their sequence) harbour the genetic code. There are only 4 different bases involved, namely Adenin (**A**), Cytosin (**C**), Guanin (**G**) and Thymin (**T**). The two strands of nucleotides are held together via hydrogen bonds between opposed bases, thereby **A** only ever pairs with **T** and **G** only with **C**; see fig.I.3b. In this sense the two strands are complementary to each other permitting efficient replication. In addition, the DNA molecule is negatively charged all along the backbones (poly ion).

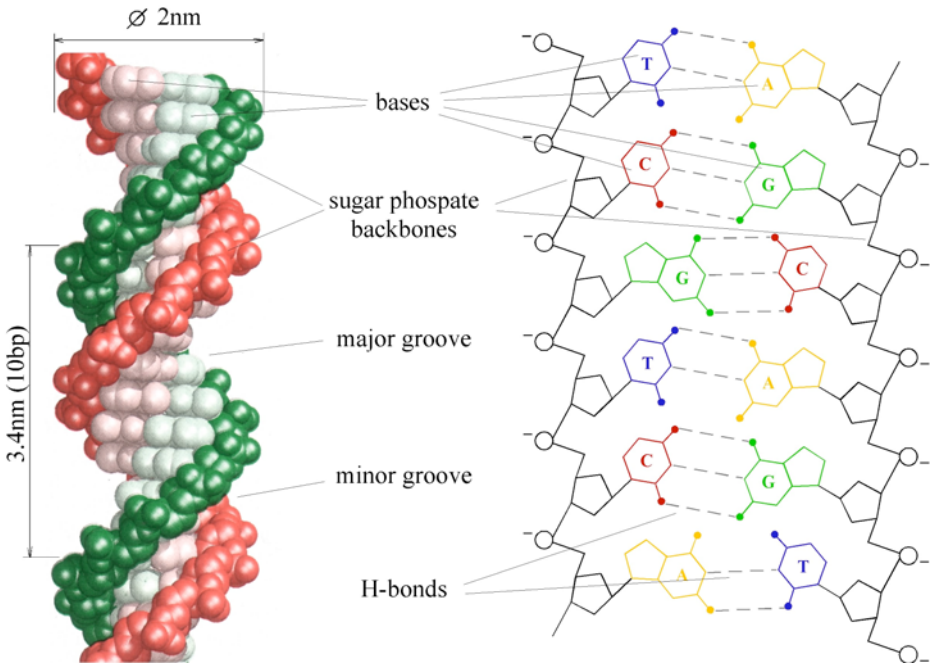

a) b)

fig.I.3

Ever since the discovery of its famous double helical structure and associated therewith the interpretation of the effectiveness of its exact replication in 1953 [I.13, I.14] the DNA molecule is occupying the central position in molecular biology. Over the last decades several powerful biological tools such as PCR, sequencing, labelling, etc. have been developed and allow reliably copying, designing and modifying DNA molecules in great quantities. Nowadays DNA can be combined with basically any chemical side group. For example it can be attached to electrically active molecular elements, such as metal clusters or fullerenes. Of particular importance with regard to the experiments presented here is the ability to strongly bind individual DNA molecules to surfaces. The most common way is certainly to make use of the non-covalent bond between biotin (vitamin H) and streptavidin (protein). On the one hand there are nucleotide-biotin complexes available that can easily be

[8] DNA always refers to the so-called double stranded B-form DNA in this text. It is believed to be the most common DNA structure in natural environment but there are other DNA helices known, namely the A-DNA-helix and the Z-DNA-helix.

attached to the ends of DNA molecules by enzymatic reaction. On the other hand surfaces, such as glass and styrene can reliably be coated with streptavidin. Thus, streptavidin-coated objects provide an efficient anchor for biotinylated DNA molecules.

I.2.1. The Physical Properties of DNA

Beyond their importance in molecular biology these tools have opened up possibilities to manipulate individual DNA molecules and to start exploring their physical properties.

There have been dedicated experiments on the elasticity of single DNA molecules [I.15-I.19]. In these experiments individual DNA molecules have been attached to micro beads and thus could be held at both ends with either glass pipettes, laser tweezers, AFM cantilevers etc. Then the molecules were stretched and the force-extension respond was measured. DNA was found to be an extensible molecule. A force of *2* to *3pN* is able to stretch DNA in aqueous solution to 90% of its contour length at room temperature. Approaching contour length the force rises sharply up to *~65pN* where the molecule undergoes a rapid (reversible) transition into a stable form of about *1.7* times its contour length. With further extension the force rises sharply again. Comparing the extension force data beyond the contour length with theory (eqn.I.11) revealed DNA to be described by a worm like chain rather than a freely joint chain [I.3, I.20].

But also the electrical conductance of DNA has been investigated. Here the findings are most controversial. First direct electrical transport measurements were carried out on freestanding *600nm* long ropes of a few DNA molecules. Under visual control with the Low Energy Electron Point Source (LEEPS) microscope single ropes could be contacted with a tungsten tip and linear *I/V*-characteristics were recorded. Resistivity values derived from these measurements indicate that DNA (under vacuum conditions) is a good semiconductor [I.21].
Another experiment was done using *10.4nm* short DNA molecules of known sequence (i.e. 30 base pairs long poly**G**-poly**C** DNA). Single DNA molecules in aqueous environment were positioned between two electrodes using a field trapping technique. The sample was then dried in a nitrogen flow. It was found that the DNA oligomer does not conduct charge for biases below *1V* at room temperature. This non linear *I/V*-characteristics signify that poly**G**-poly**C** DNA behaves like a semiconductor with a large bandgap [I.22].
More measurements on the resistivity of DNA were performed using scanning-probe techniques. DNA molecules were deposited on a mica surface and Au-contacts were shadow-evaporated onto the molecules at one end. The visual control was accomplished with the scanning force microscope (SFM). In order to carry out the conductivity experiments, a metallised SFM cantilever was finally brought to mechanical contact with the molecule. With a lower resistivity limit of $10^6 \Omega cm$ DNA was found to be an insulator [I.23].
But also proximity-induced superconductivity of DNA was found! DNA molecules were combed across submicron wide slits between rhenium/carbon metallic contacts. From room temperature down to *1K* ohmic conduction was measured. The resistance of a single molecule was determined to be less than $100k\Omega$ and only weakly depending on temperature. Below *1K*, i.e. at the superconducting transition temperature of the contacts, proximity-induced superconductivity was observed [I.24].

The reasons for the discrepancies are still under debate and it is not yet clear whether these opposing results reflect the large set of parameters involved (e.g. the influence of different ambient surroundings or molecule-electrode interface) or if they are due to possible artefacts in some experiments.

I.2.2. Experimental Polymer Physics

But also for polymer physics DNA has become of great importance. The convenient fact that DNA molecules of various precise lengths can be obtained, in particular the fabrication of concatamers[9] of many tens of micrometers in length excels DNA as an outstanding candidate to study the dynamics of single filiform molecules and accordant scaling laws. And thanks to the achievements in fluorescence microscopy accompanying the development of a variety of fluorochromes[10] it has become possible to study individual DNA molecules in the liquid phase [I.25].

For example single fluorescently labelled DNA molecules of various length have been attached to micro spheres to be held by means of optical tweezers. That way the labelled molecules could be trailed through an entangled solution of DNA and simultaneously be monitored by the fluorescence microscope [I.26]. Tube-like motion was observed in agreement with theoretical predictions [I.27, I.28]. Moreover, fluorescently labelled DNA molecules were attached to magnetic beads and pulled by a calibrated magnetic force through the solution of unlabelled DNA. From the force-velocity diagram the friction coefficient ζ of a single DNA molecule was directly measured [I.29]. ζ was found to be highly velocity dependent due to sharp conformational transitions for increasing velocities.

Similarly prepared DNA molecules were held in dilute solution with optical tweezers at one end and stretched to full extension in the solvent flow. Their relaxation was observed after the flow stopped. Characteristic relaxation times (Rouse times) were determined and their scaling with the length of the molecule was analysed [I.30]. Based on this, theoretical calculations and computer simulations showed that the Rouse times decrease as a function of extension of the polymer and split in longitudinal and transverse relaxation times [I.31]. Models to describe the transitions between the random coil configuration and the fully extended configuration based either on the freely joint chain model [I.32, I.33] or the worm like chain model [I.34, I.35] have been developed.

Self-diffusion of single DNA molecules has also been studied. Fluorescently labelled DNA fragments of different lengths in good solvent conditions revealed "Zimm"-like scaling behaviour ($\nu = 0.61 \approx 3/5$) [I.36]; see eqn.I.24. In another experiment DNA fragments were strongly adsorbed to a fluid lipid membrane without inhibiting the lateral DNA mobility in two dimensions. The diffusion constant was obtained from the centre-of-mass time correlation function of single molecules and was found to behave "Rouse"-like, i.e. D_{CM} scaled with $\nu = 1$ (eqn.I.23) [I.37]. (Similar experiments carried out with polyethylene glycol instead of DNA revealed a

[9] Concatamers denote reiterative strings of one unit-DNA. Hence, their length is an exact multiple of the length of the unit-DNA.

[10] Fluorochromes (fluorescence molecules) are composed of an associative group and a fluorophore group. The latter is responsible for the ability to fluoresce, whereas the former allows binding to a specific site. To suppress background signal the fluorochrome ideally only fluoresces when specifically bound; see also chapter I.3.

diffusion coefficient D_{CM} that scales with $N^{-3/2}$ [I.38].) Very recently diffusion of DNA of different size and conformation (linear and circular)[11] has been studied both, in water as well as in mucus. For linear DNA molecules no deceleration of the diffusion was observed, whereas the diffusion of circular DNA conformation was reduced significantly in mucus compared to diffusion in water. Scaling exponents were determined and for the linear DNA chains "Zimm"-like behaviour was found ($\nu = -0.63$) [I.39].
Furthermore the dynamics of single DNA molecules were studied in planar extensional flows. Different conformational shapes of the polymer were observed revealing different dynamic behaviour in the flow [I.40]. It could be shown that the conformation of the molecule in the flow may depend on the deformation history [I.41].

There have also been studies of the dynamics of tethered DNA molecules in shear flow. Surprisingly, conformations of polymers perpendicular to the shear flow direction have been observed. Such conformations are not considered in classical models [I.42]. Moreover, the temporal fluctuations in the chain extension were observed and it was found that below a critical shear rate the rate of these fluctuations decreased with increasing shear rate! These anomalous dynamics could be explained as cyclic dynamics of the polymer chain arising from the coupling of the chain velocity in the flow direction to thermally driven fluctuations in the shear gradient direction [I.43]. Again in shear flow DNA molecules of different lengths were slowly stretched to full extension. Scaling laws were derived and compared to simulations. The deformation dynamics were shown to be dependent on both the nonlinear force-extension relation and fluctuations of the chain transverse to the flow direction [I.44].

In rather recent ambitious experiments fluorescently labelled DNA molecules of different contour lengths were electrophoretically stretched, i.e. in an electric field and the dynamics such as relaxation times were studied at semi-dilute concentrations [I.45, I.46]. From the analysis of the data the scaling exponents ν for the slowest relaxation times τ_R were derived. Moreover, the data provided a first quantitative test for the latest theory about hydrodynamic and electrorphoretic stretch of tethered DNA [I.47]. Experiment and theory were found to be in good agreement.

But also the effect of confinement on the dynamics of polymers was studied by observing the transient extension and relaxation of single fluorescently labelled DNA molecules as they interacted with obstacles. The experiments were done in electrophoretic flows and the observations lead to the perception that an electric field, i.e. an electrophoretic force, acts on the anchored molecule equivalently to a hydrodynamic flow [I.48].

[11] Many native DNA molecules are in a circular conformation (closed chain). By enzymatic reaction the chain can be cut at one precise site and thus transfers to the linear conformation (opened chain).

I.3. Fluorescence Microscopy

Above described experiments as well as the experiments on the energetics of single DNA molecules in aqueous solution that are subject of this thesis have all been carried out under the fluorescence microscope. Therefore, it appears reasonable to explain this useful technique in some more detail:

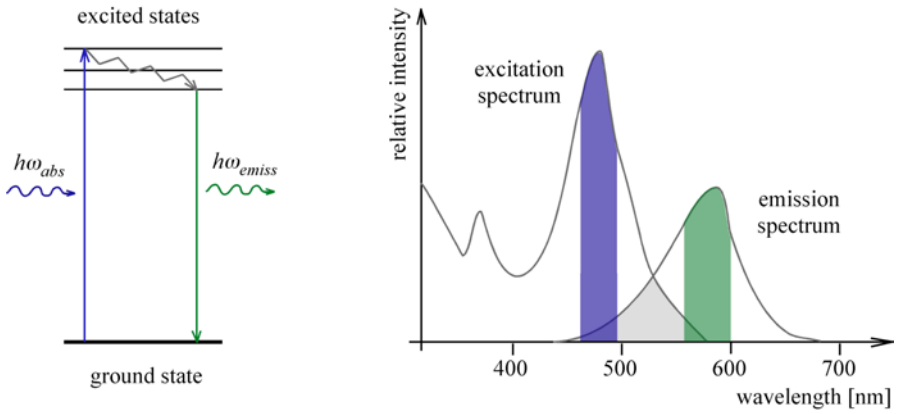

a) b)

fig.I.4

Excitation of molecules by light is not always an elastic process like Rayleigh scattering. There are molecules that decay from the excited state into the ground state via an intermediate state; see fig.I.4a. Thereby some of the energy of the absorbed photon is consumed by internal conversion (e.g. vibrational relaxation) so that the reemitted photon carries less energy. Due to this energy difference excitation and emission signal can be distinguished as long as the overlap of the total excitation and emission spectra is small enough; see fig.I.4b. The characteristic decay times are relatively short, i.e. of the order of $10^{-7}sec$, since fluorescence includes transitions between states of equal spin only. By contrast phosphorescence involves spin forbidden transitions leading to decay times of seconds up to hours.

Fluorescence microscopy is characterized on the one side by a specific optical microscope equipped with a powerful light source (e.g. a mercury lamp) and a restrictive filter system to create monochromatic excitation light and to separately detect the fluorescence signal. On the other side there is the sample preparation, crucial to achieve a fluorescence signal with satisfactory signal/noise- ratio and contrast at a given excitation wavelength.

I.3.1. The Fluorescence Microscope

The essential parts of a fluorescence microscope are shown in fig.I.5. To adjust an appropriate intensity[12] the light of the source of the microscope first passes a neutral density filter system. The next (band-) filter block allows only light of a certain wavelength to continue its path onto the dichroic mirror from where it is deflected into the objective and finally focussed onto the sample. Provided some parts of the sample fluoresce, emission light of lower energy is created there. Consequently - following the reverse optical path - there is incidence of

[12] The loss of signal due to bleaching of the sample is often a severe problem in fluorescence microscopy. Therefore the intensity is kept as low as possible.

light of two different wavelengths through the objective. At the dichroic plate the excitation light is separated from the fluorescence light as the former is still deflected whereas for the latter the plate is transparent. Hence, only the fluorescence signal is lead to the detector but not the dominant excitation signal.

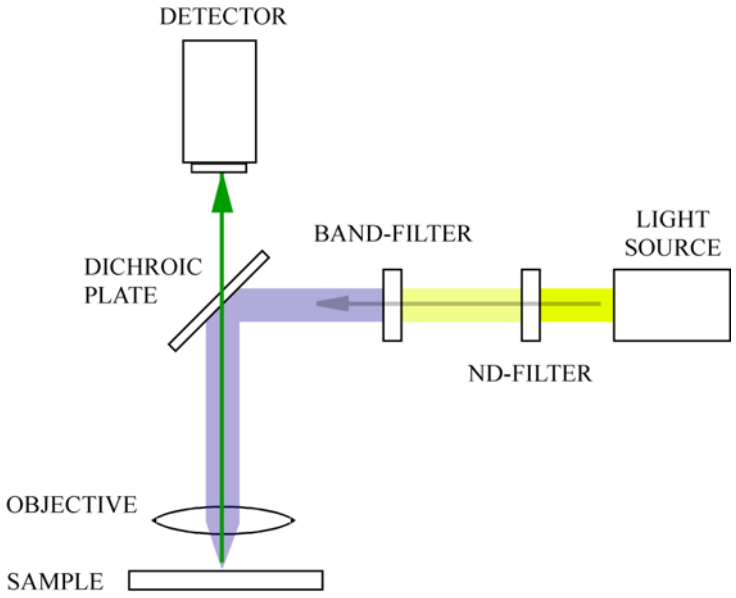

fig.I.5

I.3.2. Staining of DNA

Only a few molecules naturally fluoresce (e.g. green fluorescent protein (GFP)). Therefore most samples need to be stained with synthesized fluorescent dyes (so-called markers, labels etc.) prior to the investigation under the fluorescence microscope. There is a tremendous amount of different dyes for various purposes[13]. However, for all the experiments described here the nucleic acid stains from the so-called *TOTO*-family (cyanine dimers; *Molecular Probes*) has been used; see fig.I.6a. These cyanine dimers consist of a spacer of a certain length connecting two monomers that can act as fluorophores. The monomers (benzazolium/quinolinium ring system) are designed in such a way, that they fit nicely between the base pairs of the DNA molecule while the spacer comes to lay in the minor groove of the DNA double helix [I.49]; see fig.I.6b.

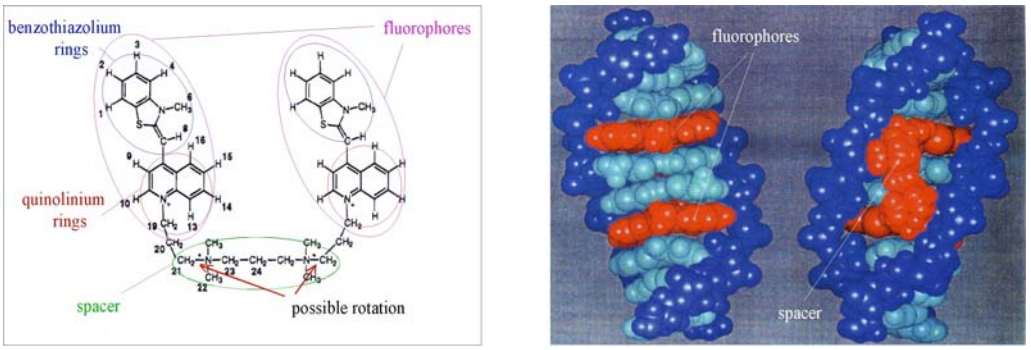

a) b)

fig.I.6

[13] See: *Handbook of Fluorescent Probes and Research Products, Molecular Probes.*

Hereby the DNA molecule gets slightly longer and the helix somewhat unwound. Intercalated like this the benzazolium/quinolinium ring system becomes fluorescent under excitation. Whereas when the fluorochrome is not attached to any DNA molecule the two monomers start rotating around the linker under excitation but do not fluoresce. Therefore the free intercalators in solution do not contribute to any disturbing fluorescence background signal. Adding intercalators to the DNA solution in appropriate concentration cyanine dimers may intercalate between base pairs all along the DNA molecule. After approximately one hour of incubation the fluorescence signal is strong enough to observe individual DNA molecules under the fluorescence microscope. Note that with a thickness of only 2*nm* DNA is a hundred times too thin to be optically resolved. Thus, fluorescent DNA appears much thicker than it actually is. But for polymers of several micrometers in length the method still allows to study their overall kinetics.

I.4. Introduction of the Presented Experiments with Individual DNA Molecules

The experiments presented here are carried out with individual λ-DNA molecules (*Fermentas*), i.e. DNA molecules of the λ-phage[14]. The molecules are stained with the nucleic acid stain *YOYO-1* (*Molecular Probes*) and observed in the liquid phase[15] under the epi-fluorescence microscope (*Nikon; Eclipse E600-FN*) with an *100x* oil-immersion objective (numerical aperture:*1.4*). Unstained λ-DNA molecules are *16*μ*m* long. Staining with a ratio intercalator to base pairs of *1*:*10* leads to an approximate length of *18*μ*m*, as each intercalation extends the molecule about *0,4nm* [I.50]. The persistence length of DNA has been found to be of the order of *50nm* [I.51], a value that is somewhat uncertain but generally accepted.

Both, the diffusion experiments as well as the straight to random coil transition experiments are carried out in a thin aqueous film of an approximate depth of *8*μ*m* and *10*μ*m* respectively. To study the transition between the straight and the random coil configuration the DNA is anchored at one end and electrophoretically straightened similarly to the experiments mentioned above.

The absorption and emission maxima of *YOYO-1* are at wavelengths of *491nm* and *509nm* respectively. (The band pass filters and the dichroic mirror are set accordingly.) The data are acquired with a low light camera (*Proxitronic; Proxicam HL4S*) and a *DVCAM*-video recorder (*Sony; DSR-45P*) with a temporal resolution of *25Hz*.

The novel aspect of the experiments presented here is the temperature dependence of the measurements required to gain insight into the energetics of the studied processes.

[14] λ-phage denotes a bacterio-phage whose host is the bacterium Escherichia Coli.
[15] Water is a good solvent for the poly ionic DNA molecule.

I.5. Reference List I

[I.1] W. Kuhn, Kolloid-Z. **68** (1), 2(1934).

[I.2] P.J. Flory, *Statistical Mechanics of Chain Molecules*, Interscience Publishers, New York (1969).

[I.3] C. Bustamante, J.F. Marko, E.D. Siggia, S. Smith, Science **265**, 1599 (1994).

[I.4] M. Doi, *Introduction to Polymer Physics*, Oxford Science Publications (1996).

[I.5] C. Haber, S.A. Ruiz, D. Wirtz, PNAS **97** (20), 10792 (2000).

[I.6] P.E. Rouse, J. Chem. Phys. **21** (7), 1272 (1953).

[I.7] F. Bueche, J. Chem. Phys. **22** (4), 603 (1954).

[I.8] C.C. Han, A. Z. Akcasu, Macromolecules **14**, 1080 (1981).

[I.9] Y. Tsunashima, M. Hirata, N. Nemoto, M. Kurata, Macromolecules **20**, 1992 (1987).

[I.10] B.H. Zimm, J. Chem. Phys. **24** (2), 269 (1956).

[I.11] P.G. de Gennes, *Scaling Concepts in Polymer Physics*, Cornell University Press, Ithaca, NY (1979).

[I.12] S. Stepanow, J. Phys. A: Math. Gen. **17**, 3041 (1984).

[I.13] R. Franklin, R.G. Gosling, Nature **171,** 740 (1953).

[I.14] J.D. Watson, F.H.C Crick, Nature **171**, 737 (1953).

[I.15] S.B. Smith, L. Finzi, C. Bustamante, Science **258,** 1122 (1992).

[I.16] P. Cluzel, A. Lebrun, Ch. Heller, R. Lavery, J.-L. Voivy, D. Chatenay, F. Caron, Science **271,** 792 (1996).

[I.17] S.B. Smith, Y. Cui, C. Bustamante, Science **271,** 795 (1996).

[I.18] T.R. Strick, J.-F. Allemand, D. Bensimon, A. Bensimon, V. Croquette, Science **271,** 1835 (1996).

[I.19] G.V. Shivasshankar, A. Libchaber, Appl. Phys. Lett. **71** (25), 3727 (1997).

[I.20] J.F. Marko, E.D. Siggia, Macromolecules **28**, 8759 (1995).

[I.21] H-W. Fink, Ch. Schönenberger, Nature **398**, 407 (1999).

[I.22] D. Porath, A. Bezryadin, S. deVries, C. Dekker, Nature **403**, 635 (2000).

[I.23] P.J. de Pablo, F. Moreno-Herrero, J. Colchero, J. Gomez Herrero, P. Herrero, A.M. Baro, P. Ordejon, J.M. Soler, E. Artacho, Phys. Rev. Lett. **85** (23), 4992 (2000).

[I.24] A.Y. Kasumov, M. Kociak, S. Guéron, B. Reulet, V.T. Volkov, D.V. Klinov, H. Bouchiat, Science **291,** 280 (2001).

[I.25] R.H. Austin, J.P. Brody, E.D. Cox, T. Duke, W. Volkmuth, Physics Today, 32, (Feb. 1997).

[I.26] T.T. Perkins, D.E. Smith, S. Chu, Science **264**, 819 (1994).

[I.27] P.G. de Gennes, Macromolecules **9**, 587 (1976).

[I.28] M. Doi, S.F. Edwards, J. Chem. Soc. Faraday Trans. **74** (2), 1789 (1978).

[I.29] D. Wirtz, Phys. Rev. Lett. 75 (12), 2436 (1995).

[I.30] T.T. Perkins, S.R. Quake, D.E. Smith, S. Chu, Science **264**, 822 (1994).

[I.31] J.W. Hatfield, S.R. Quake, Phys. Rev. Lett. **82** (17), 3548 (1999).

[I.32] F. Brochard-Wyart, H. Hervet, P. Pincus, Europhys. Lett. **26** (7), 511 (1994).

[I.33] F. Brochard-Wyart, Europhys. Lett. **30** (7), 387 (1995).

[I.34] Y. Bohbot-Raviv, W.Z. Zhao, M. Feingold, C.H. Wiggins, R. Granek, Phys. Rev. Lett. **92** (9), 098101 (2004).

[I.35] B.H. Zimm, Macromolecules **31**, 6089 (1998).

[I.36] D.E. Smith, T.T. Perkins, S. Chu, Macromolecules **29**, 1372 (1996).

[I.37] B. Maier, J.O. Rädler, Phys. Rev. Lett. **82** (9), 1911 (1999).

[I.38] S.A. Sukhishvili, Y. Chen, J.D. Müller, E. Gratton, K.S. Schweizer, S. Granick, Nature **406**, 146 (2000).

[I.39] H. Shen, Y. Hu, W.M. Saltzman, Biophys. J. **91**, 639 (2006).

[I.40] T.T. Perkins, D.E. Smith, S. Chu, Science **276**, 2016 (1997).

[I.41] C.M. Schroeder, H.P. Babcock, E.S.G. Shaqfeh, S. Chu, Science **264**, 819 (1994).

[I.42] Ph. LeDuc, C. Haber, G. Bao, D. Wirtz, Nature **399**, 564 (1999).

[I.43] P.S. Doyle, B. Ladoux, J-L. Voivy, Phys. Rev. Lett. **84** (20), 4769 (2000).

[I.44] B. Ladoux, P.S.Doyle, Europhys. Lett. **52** (5), 511 (2000).

[I.45] S. Ferree, H.W. Blanch, Biophys. J. **85**, 2539 (2003).

[I.46] S. Ferree, H.W. Blanch, Biophys. J. **87**, 468 (2004).

[I.47] D. Stigter, C. Bustamante, Biophys. J. **75**, 1197 (1998).

[I.48] O.B. Bakajin, T.A.J. Duke, C.F. Chou, S.S. Chan, R.H. Austin, E.C. Cox, Phys. Rev. Lett. **80** (12), 2737 (1998).

[I.49] H.P. Spielmann, D.E. Wemmer, J.P. Jacobsen, Biochemistry **34**, 8542 (1995).

[I.50] F. Johansen, J.P. Jacobsen, J. Biomol. Struct. Dyn. 16, **205** (1998).

[I.51] W.H. Taylor, P.J. Hagerman, J. Mol. Biol. **212**, 363 (1990).

I.6. Manuscripts I

I.6.1. Activation Barrier for Single DNA Diffusion
from Direct Measurements of the Tracer Diffusion Coefficient

I.6.2. On the Energetics of a Single DNA Molecule

This is only the first draft of a manuscript entitled:

Activation Barrier for Single DNA Diffusion from Direct Measurements of the Tracer Diffusion Coefficient

Conrad Escher & Hans-Werner Fink

Institute of Physics, University of Zurich, Winterthurerstrasse 190, CH-8057, Switzerland

Molecular transport of bio-molecules in the liquid represents a fundamental issue related to the physics of biological systems. Mobility is a pre-requisite for subsequent interaction such as recognition and binding. The quantity describing such transport in microscopic systems is the diffusion coefficient. Within the last decade, tracking the motion of single DNA molecules in the liquid has become feasible by employing fluorescence video microscopy.

Here we present first direct measurements of the temperature dependent tracer diffusion coefficient by observing the random motion of a single DNA molecule. The molecules are stained and embedded in a sealed thin water film. With this, thermo dynamical equilibrium at different temperatures can be established. The DNA concentration is held sufficiently low to allow tracing an individual molecule reliably. The displacement of the centre of mass of the DNA random coil is monitored with time intervals of 30s between observations. According to $\langle x^2 \rangle = 2D\ t$, the mean square displacement reveals the diffusion coefficient. From the temperature dependence of the diffusion coefficient we compute the activation barrier for diffusion ; see Fig.1. (red curve).

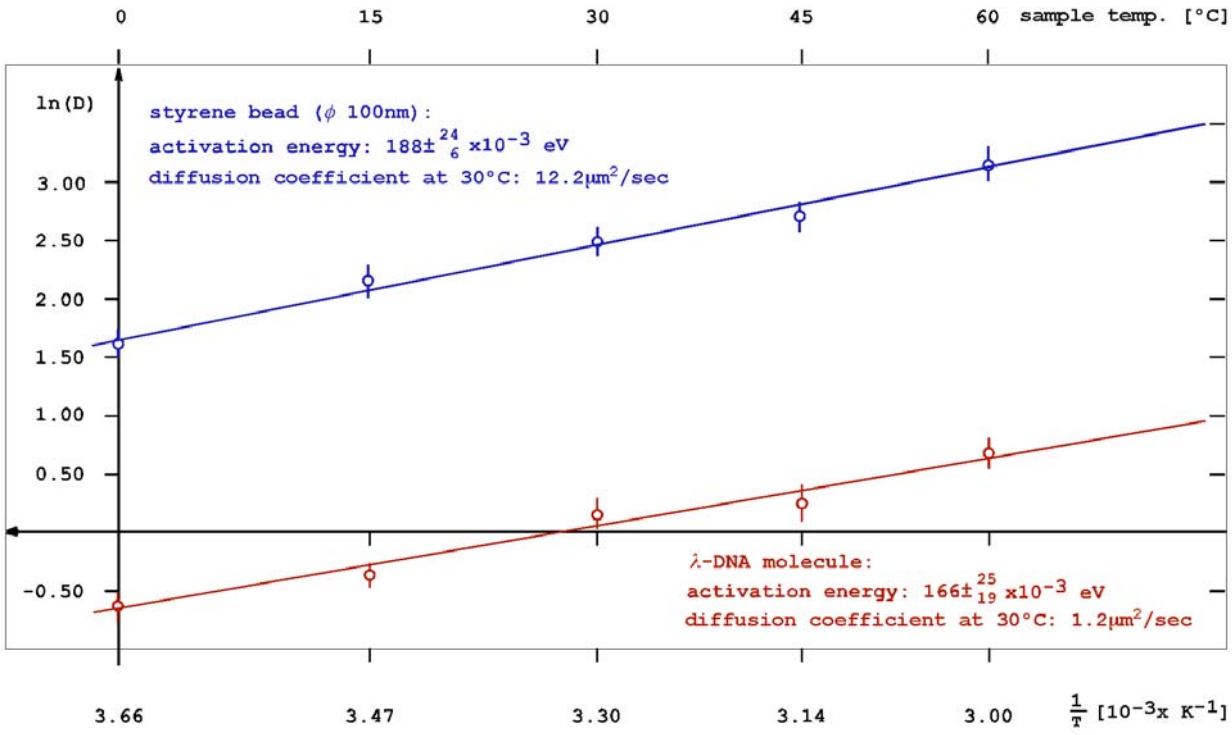

Fig. 1. Arrhenius plot for a single DNA diffusion experiment (red curve) and for a 50 nm radius latex sphere diffusion experiment (blue curve).

Since a DNA molecule is a semi flexible bio-polymer, it is not a priori clear how the displacement of the centre of mass actually proceeds. It seems however clear that the Brownian agitation of the solvent frequently leads to rearrangements of the molecule's configuration without displacing its centre of mass significantly. To evaluate this more quantitatively, we have also measured the diffusion of a rigid fluorescent sphere of 50nm radius unable to undergo shape changes upon statistical collisions with the solvent; see Fig. 1 (blue curve).

The mass of a 50nm radius latex sphere is about one order of magnitude bigger than that of a stained λ-DNA molecule. However, the diffusion coefficient is much larger while the barrier is only slightly increased compared to that of a DNA.

Currently, we investigate DNA molecules with twice the length of λ-DNA which have been designed for us by Eugen Ermantraut from Clondiag Chip Technologies® GmbH (Jena, Germany). The preliminary analysis of the data suggests interesting scaling behaviour in terms the DNA diffusion barrier.

On the Energetics of a Single DNA Molecule

Conrad Escher [a] and Hans-Werner Fink[b]

Physik Institut der Universität Zürich, Winterthurerstrasse 190, CH- 8057 Zürich, Switzerland

Abstract. Temperature dependent experiments with individual DNA molecules have been carried out using video fluorescence microscopy. Thermodynamical equilibrium has been established and the transition from the straight to the random coil configuration has been investigated for individual λ-DNA molecules in the liquid phase. The statistics of a total of 600 measurements with single molecules at 12 different temperatures reveal the existence of an activation barrier for the formation of the DNA random coil. Our findings provide the first quantitative data on the energetics governing the dynamics of a single DNA molecule.

PACS. 82.37.-j Single molecule kinetics - 87.14.Gg DNA, RNA - 87.15.-v Biomolecules: structure and physical properties - 87.15.He Dynamics and conformational changes - 82.35.Lr Physical properties of polymers

1 Introduction

The complexity of biological molecules associated with the fact that they operate at finite temperature is related to a significant entropy contribution towards the free energy in biological systems. The free energy landscape is thus of central significance; it determines the behavior of bio-molecules, such as proteins and DNA.

The DNA molecule is a highly flexible biopolymer. Its capability to assume a variety of configurations is essential for promoting its biological functions, like the packing in the nucleus of the cell and the molecular dynamics related to enzymatic reactions. Thus, an

[a] e-mail: escher@physik.unizh.ch
[b] e-mail: hwfink@physik.unizh.ch

insight into the free-energy landscape corresponding to the various configurations of the molecule is at the center of a basic understanding of its physics and chemistry. Apart from the molecules biological function, DNA is also an important object to test and further develop the foundations of polymer physics [1].

Theoretical models of the DNA follow Kuhn's pioneering work [2,3] in viewing the molecule as a chain made up of links of a defined persistence-length over which the molecule remains straight. For a freely joined chain it costs no energy to change the direction of all links in respect to each other. The molecule will thus assume a random coil equilibrium configuration at finite temperature. Its stability is due to the entropy term as the main contribution towards the minimum of the free energy. In contrast to the variety of possibilities to form a random coil, the straight configuration where all the links are aligned is the most unlikely one. It is hence associated with minimal entropy.

These two prominent configurations, the random coil and the straight configuration are depicted in Figure 1 together with a schematic free energy curve that governs the transition between the two states.

However, to measure free energies of a DNA molecule one has to consider that the molecule is embedded into a solvent which is part of the entire biological system and makes the situation somewhat more complex. Since the DNA is a poly-ion, the charged molecule is likely to attract and tightly bind water dipoles. The property of this water mantle as well as the viscosity of the solvent surrounding it will change with changing temperature. Furthermore, it is just as plausible to expect a temperature dependence of the persistence length. After all, the physical reality behind viewing the molecule as a chain of rigid links is the Brownian agitation of the solvent. The random collisions with the solvent molecules change with temperature and as a consequence, the persistence length should be temperature dependent. However, as the degree of influence of the effects discussed above are not accessible so far, temperature dependent experiments are needed to gain insight into the free energy landscape of a DNA. They shall present a basis to expand the current models of DNA towards questions of their energetics.

2 Experimental design

The ability to observe single molecules by means of video fluorescence microscopy, pioneered by Steven Chu, has made it possible to study the dynamics of single DNA molecules in liquids [4]. Our experiments have been performed by using such fluorescence video microscopy as exemplified by the two micrographs shown in Figure 1, namely that of a λ-DNA random coil as well as that of the same molecule straightened to its contour length of 16 μm. The question addressed here is how to derive direct information about the free energy of the system that governs the transition from the straight to the random coil state.

To actually derive quantitative information directly from statistical experiments on the energetics of single molecules, the experimental set-up must be such that thermal equilibrium conditions, free from disturbances by the observation process, are guaranteed at different temperatures. Furthermore, routine methods for anchoring the 16 μm long and 2 nm thick molecule at one end have to be available: first, to provide a proper distance reference, second, to straighten the molecule and third, to be able to derive sufficient statistics and obtain quantitative energy values. This has been achieved in collaboration with Clondiag Chip Technologies [5] that provided us with state of the art molecular biology techniques for binding a molecule to a silicon oxide substrate.

The experiments take place in a 10 μm thin water film in which stained λ-DNA of low concentration (5pM) is embedded. The film is carefully sealed to avoid evaporation and associated erratic liquid flow and thus perturbation of the equilibrium conditions, essential for deriving quantitative free energy data, is suppressed. A schematic of part of the apparatus is illustrated in Figure 2. The epoxidated silicon oxide sample binds streptavidin, which in turn provides an anchor for the DNA molecules that are biotinylated at one end. For straightening the λ-DNA to its contour length, an electric field of typically 15 V/cm is employed. The field is provided by two gold lines shadow evaporated onto the substrate.

2.1 Temperature calibration and control

A home build sample holder equipped with a peltier cooling element, a Pt-100 temperature sensor and a home build PID controller was used to adjust the sample temperature between -5°C and +50°C. Calibration of the sample temperature is done as follows. The temperature of the peltier element is adjusted to a fixed value by the PID controller. The temperature at the position where the scenario shall later take place is then calibrated versus the peltier stage temperature, the heat sink made up of the objective lens, the immersion oil drop and the temperature of the surrounding air. The intensity of the light through the objective lens onto the sample has been varied by several orders of magnitude to verify that the act of observation does not change the temperature at the place of observation.

2.2 Transition recording

Once the temperature calibration is carried out, the experiments are performed in the following manner. A search is made for a single DNA molecule that is bound at one end to the substrate. This is done by applying an electric field and looking for a straightened molecule. The unbound molecules are just drifting through the field of view towards the electrode at positive potential while the anchored molecules align due to the ionic current. Once a straightened molecule is selected, the electric field is switched to zero instantaneously by putting the two electrodes onto the same potential. Equilibrium of the liquid is thus provided immediately compared to the time scale that governs the molecular dynamics of the DNA. This can be verified by visual inspection of the stopping of the motion of unbound DNA molecules. Once this motion has stopped, it is evidence for thermodynamical equilibrium of the solvent in which the DNA then evolves towards the minimum of its free energy. With one particular molecule, typically 5 experiments of straightening and observing the progression towards the random coil configuration are performed. After having collected enough data, similar experiments are carried out at different temperatures.

3 Analysis of measured transition times

A total of 600 measurements at 12 different temperatures ranging from -5°C to +50°C spanning the range from freezing of the solvent to melting of DNA were evaluated. In Figure 3 the distribution of the observed transition times at three different temperatures are shown together with some sequences taken in the fluorescence video microscope. While the thermodynamically unlikely straight configuration is not observed under ordinary thermal conditions, it can be realized by applying an external electric field and, by switching off the field, the temporal evolution from the initial straight towards the state of minimum free energy can readily be measured as described above. In case of the presence of an activation barrier, the lifetime of this straight configuration, respectively the transition time for the re-formation of the random coil can be written as:

$$\tau = \tau_0 \exp (E_{rc}/kT) \qquad (1)$$

where E_{rc} denotes the activation free energy barrier for the formation of the random coil and the pre-factor τ_0 is associated with the molecular fluctuations of the solvent. As depicted in the Arrhenius plot in Figure 4, our data fit very well the description in equation (1) and as a result the formation of the DNA random coil is associated with an activation barrier of the order of ¼ eV.

4 Shape evolution of the molecule during transition

While the temperature dependence of the water viscosity between 0 and 50 °C is well known, data on the dependence of the persistence length with changing temperature are not available. However, a freely-joint chain subject to a laminar flow and fixed at one end to a substrate has theoretically been investigated in detail by Brochard-Wyart [6]. Once the laminar flow is stopped, the model predicts that the DNA assumes a “stem-flower” like shape during the evolution towards the equilibrium random coil configuration. We searched for such shape dependencies in our experiments. For this purpose we observed the transition of 32 μm long

DNA. For such a long molecule, despite the limited resolution of the optical microscope, it is possible to depict details of the evolution of the molecule's shape during the transition to the random coil. As evident from Figure 5, the molecule indeed assumes intermediate shapes that can be associated with a "stem-flower" like appearance as theoretically predicted by Brochard-Wyart.

5 Conclusion

For a single DNA molecule, embedded in a liquid of constant volume, the free energy can be written as: $F=U-T\cdot S$; where U denotes the internal energy of the molecule and is determined by the binding energy between the atoms that make up the molecule; T is the absolute temperature and S the entropy given by the Boltzmann relation $S=k\cdot \ln W$. The number of possible ways to generate a particular configuration of the DNA chain divided by all possible combinations to generate any configuration defines the probability W for this particular configuration and determines its entropy value.

Knowing that short DNA molecules can be viewed as rigid rods, it is conceivable that also in long molecules the stacking of the individual charged nucleotides is such that a straight configuration is energetically favorable and leads to a minimum of U. Apparently, at any experimentally accessible temperature between freezing the solvent and melting the molecule, the entropy term dominates and defines the absolute minimum of the free energy. Configurations in-between represent mixtures of both terms and add up to the barrier of about ¼ eV. While the existence of such free energy barrier is now established, conclusions about its origin will only become apparent after further experiments have been performed. Measuring the pair-distribution of the end to end separations of a single molecule under equilibrium conditions will reveal the free energies of the intermediate configurations as well as the absolute difference in free energy between the random coil and straight configuration. This will then complete the picture derived here and help to modify current theoretical models as well as to deepen the understanding of the molecules function.

We are grateful to Prof. Gert Ehrlich of the University of Illinois at Urbana-Champaign for his valuable comments on the manuscript and to Clondiag Chip Technologies for fruitful discussion and for providing their DNA anchoring technologies to us. The work was financially supported by the Swiss National Science Foundation (SNF).

References

1. P.-G. De Gennes, *Scaling Concepts in Polymer Physics* (Cornell University Press, Ithaca and London, 1979)
2. W. Kuhn, Kolloid-Zeitschrift **68**, 2 (1934)
3. W. Kuhn, H. Kuhn, Helv. Chim. Acta **26**, 1394 (1943)
4. R.H. Austin, J.P Brody, E.D. Cox, T. Duke, W. Volkmuth, Physics Today, 32 (February 1997)
5. Clondiag Chip Technologies® GmbH, Jena, Germany
6. F. Brochard-Wyart, Europhys. Lett. **30**, 387 (1995)

Figures

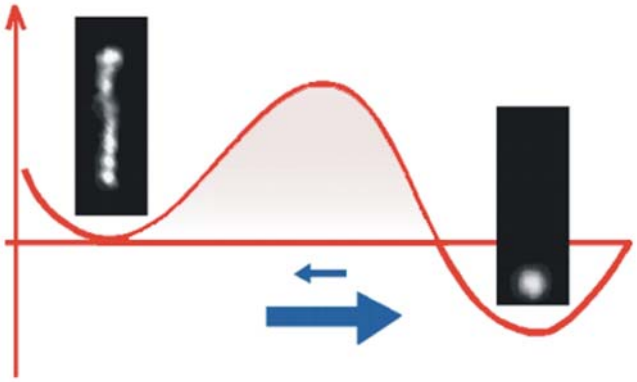

Fig. 1. Video fluorescence images taken of a single λ-DNA molecule in the liquid. Two prominent configurations, the straight as well as the random coil are shown. The red curve indicates an assumed free-energy variation in which the two configurations are separated by a barrier.

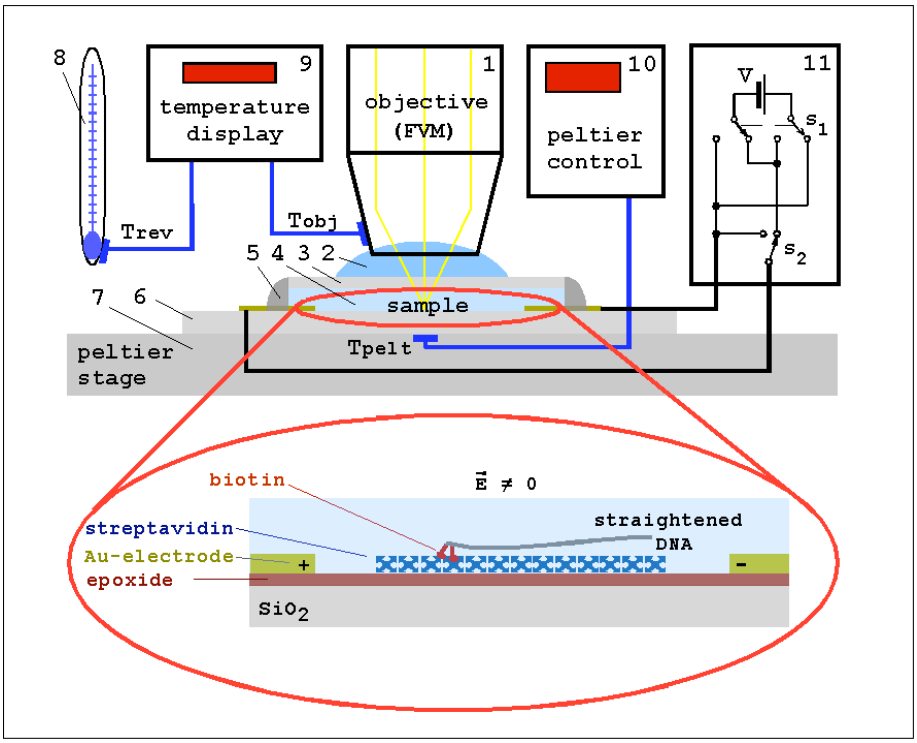

Fig. 2. Schematic of the set-up for measuring the energetics of single DNA molecules. Except for the objective lens, most of the optics are not shown here. The main parts of the set-up are: objective lens (1), oil drop (2), cover-slide (3), water-film in which the experiments

take place (4), seal to the water-film (5), epoxidated SiO_2 sample (6), peltier element (7), room temperature thermometer (8), temperature display (9), peltier PID controller (10), power-supply for the electric field (11) between the two gold electrodes. For determining the temperature at the place of the actual observation, a 4th temperature sensor (not shown here) is placed at the sample position prior to the experiment. Details of the temperature calibration are described in Section 2.1.

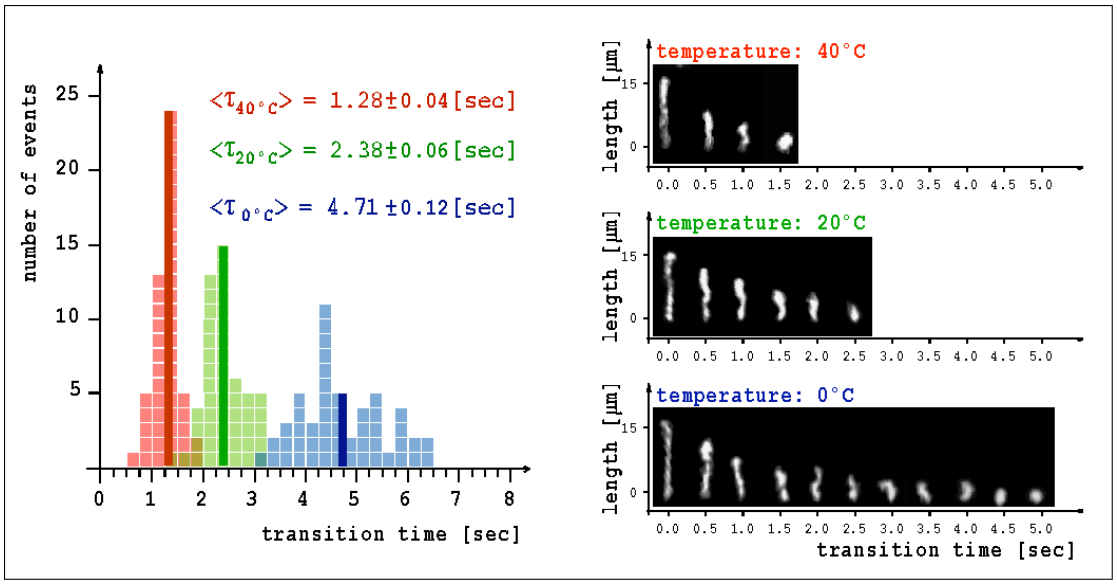

Fig. 3. Measurements of the transition time from the straight to the random coil DNA configuration. Right: Every 12th frame of the transition of a straight DNA towards the random coil is shown at 40, 20 and 0 °C. Left: The corresponding histograms of the distributions for the transition times and the average values are shown.

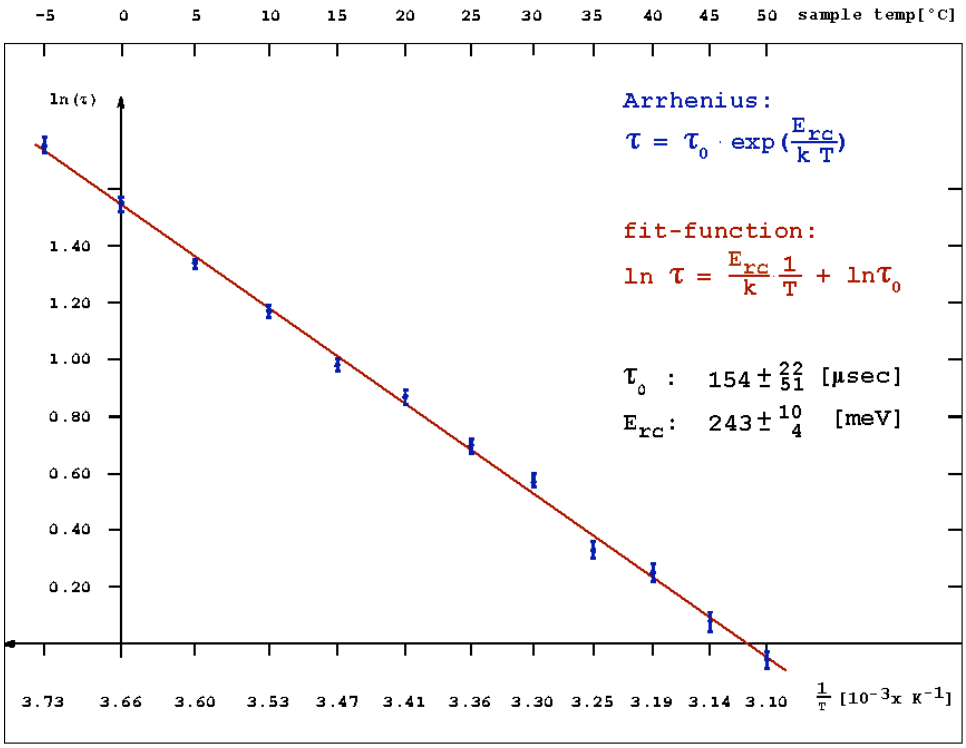

Fig. 4. Determination of the activation barrier height and pre-factor. According to equation (1), the data for the average transition times are represented in a semi-logarithmic plot. A least square fit to a linear dependence reveals the activation barrier E_{rc} and the pre-factor $\tau_{0.}$ The error bars reflect the statistical error of the average transition times (see also the raw data presented in Figure 3).

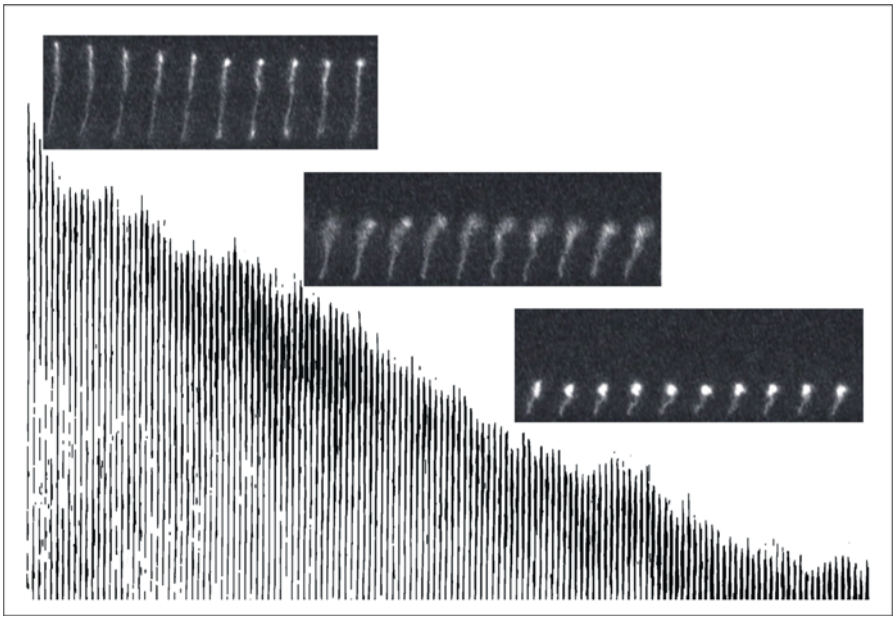

Fig. 5. Shape evolution during the transition towards the random coil. The three inlet sequences show a 32 μm long DNA molecule evolving towards the random coil at 20 °C. They contain 10 subsequent images out of a total of 138 observations and illustrate the evolution of the shape of the molecule in agreement with the prediction of the “stem-flower” model [6]. The histogram shows the evolution of the length of all 138 configurations during the transition time of 5.5 seconds after which the random coil equilibrium configuration is established.

I.7. Appendix I

I.7.1. Appendix I.1: Invited Review Article for *Physik in unserer Zeit*

I.7.2. Appendix I.2: DNA-Trap

I.7.1. Appendix I.1: Invited Review Article for *Physik in unserer Zeit*

submitted sept. 28th, 2006

Experimente mit einzelnen DNS-Molekülen

Hans-Werner Fink & Conrad Escher

Physik Institut der Universität Zürich, Winterthurerstrasse 190, CH-8057 Zürich, Schweiz

Desoxyribonukleinsäure (DNS), die Trägerin des genetischen Codes, ist ein Biopolymer mit fadenförmiger Gestalt. Die Länge kann - je nach Lebewesen, aus deren Zellen die DNS stammt - von einigen Mikrometern bis hin zu Millimetern und mehr reichen. Mit einer Dicke jedoch von nur 2 Nanometern (1Nanometer = 1nm = 10^{-9}m) gehört das DNS-Molekül auch zur Klasse der Objekte mit Nanometer-Dimensionen. Diese haben seit der Erfindung des Raster Tunnel Mikroskops und des daraufhin einsetzenden Booms der so genannten Nano-Technologie besonderes Interesse gefunden - nicht zuletzt, weil sich auf dieser Skala die Quantennatur physikalischer Phänomene direkt bemerkbar macht.
Trotzdem gibt es vergleichsweise wenige Arbeiten, die sich mit der Physik einzelner DNS-Moleküle beschäftigen. Der Grund liegt darin, dass solch ein einzelnes Molekül nicht gar so einfach zu handhaben ist. Im Gegensatz zu anderen mesoskopischen Objekten, wie Kohlenstoff-Nano-Röhrchen (carbon nanotubes) und weiteren anorganischen „Kleinst-Strukturen“, die man mit kommerziellen Elektronenmikroskopen abbilden und manipulieren kann, besteht bei einzelnen DNS-Molekülen nämlich die Schwierigkeit, sie routinemäßig sichtbar zu machen. Erst dieses Sichtbarmachen aber schafft die Voraussetzung, um kontrolliert an einzelnen Molekülen physikalische Experimente durchführen zu können.

An Fragestellungen im Zusammenhang mit diesem wichtigen „Molekül des Lebens“ mangelt es hingegen keinesfalls. Zum Beispiel: Ist die akzeptierte doppelhelikale Struktur der DNS die dominante oder nur die am besten beobachtbare und gibt es möglicherweise Übergänge zu anderen Strukturen, die mit bestimmten biologischen Funktionen verbunden sein könnten? Welche Größen bestimmen die Energetik einzelner DNS-Moleküle in ihrer natürlichen, wässrigen Umgebung? Und wie geht der Transport einzelner Moleküle - bestimmt durch charakteristische Diffusionszeiten – vonstatten? Antworten darauf bedeuteten mitunter wichtige Beiträge für ein grundlegendes physikalisches Verständnis der Wechselwirkung biologischer Systeme untereinander.
Über diese eher wissenschaftlichen Fragestellungen hinaus gibt es Perspektiven, wenn auch zur Zeit noch weitgehend spekulativen Charakters, die dahin zielen, dieses hochinteressante Molekül für Aufgaben einzusetzen, die über die ihm von der Natur zugedachten biologischen Funktionen hinausgehen. Ein entscheidender Aspekt dabei ist der Umstand, dass in den letzten Jahrzehnten molekularbiologische Methoden entwickelt worden sind, die es ermöglichen, in großen Mengen identische DNS-Moleküle definierter Länge und Sequenz zu produzieren. So ist es beispielsweise denkbar, DNS-Moleküle als feinste Leiterbahnen für

molekulare Elektronik zu verwenden. Vielleicht werden auch integrierte Schaltkreise, bestückt mit DNS-Transistoren, zukünftig Rechenaufgaben bewältigen.

Ob solche Ideen jemals in die Realität umgesetzt werden können, wird die Zukunft weisen müssen. Unabhängig davon jedoch, wie phantastisch diese Ideen sein mögen, müssten erst noch einige geeignete physikalische Methoden und Werkzeuge entwickelt werden, sollen solche Anstrengungen ernsthaft begonnen werden können.

Wir möchten in diesem Übersichtsartikel einige physikalische Methoden und Werkzeuge und damit verbundene Technologien beschreiben, die es erlauben, Fragen über die Beweglichkeit und Energetik individueller DNS-Moleküle anzugehen und die möglicherweise in der Zukunft zu einem besseren Verständnis über das Verhalten einzelner DNS in vivo verhelfen werden. Vielleicht wird die eine oder andere dieser Methoden auch ihren Beitrag zur Realisierung solch kühner Pläne wie dem einer „DNS-Elektronik“ leisten.

MODELLE ZUR GESTALT UND STRUKTUR DER DNS

Die wichtigsten Erkenntnisse, die zu unserem heutigen Bild eines einzelnen DNS-Moleküls geführt haben, sind in der Abbildung 1 zusammengefasst. Ein einzelnes, langes DNS-Molekül nimmt unter Gleichgewichtsbedingungen in flüssiger Umgebung die allermeiste Zeit eine sich laufend verändernde, verknäuelte Zufallskonfiguration (random coil) ein. Diese Erkenntnis geht zurück auf die Pionierarbeit von Werner Kuhn, in welcher er allgemein die Gestalt fadenförmiger Moleküle in Lösungen eingehend studiert [1]. In dieser wahrscheinlichsten, zufällig verknäuelten Form ist die freie Energie des Moleküls, gekoppelt an ein Wärmereservoir, minimiert. Entsprechend ist die Entropie des Systems bei dieser wahrscheinlichsten Konfiguration maximiert: Es gibt nämlich viel mehr Möglichkeiten aus einem langen, biegsamen Faden ein Knäuel zu formen, als etwa gestreckte oder nur wenig gekrümmte Anordnungen des gleichen Fadens herzustellen. In Abbildung 1a dient uns eine Nudel (Spaghetto) dazu, dieses Modell eines flexiblen DNS-Fadens zu illustrieren.

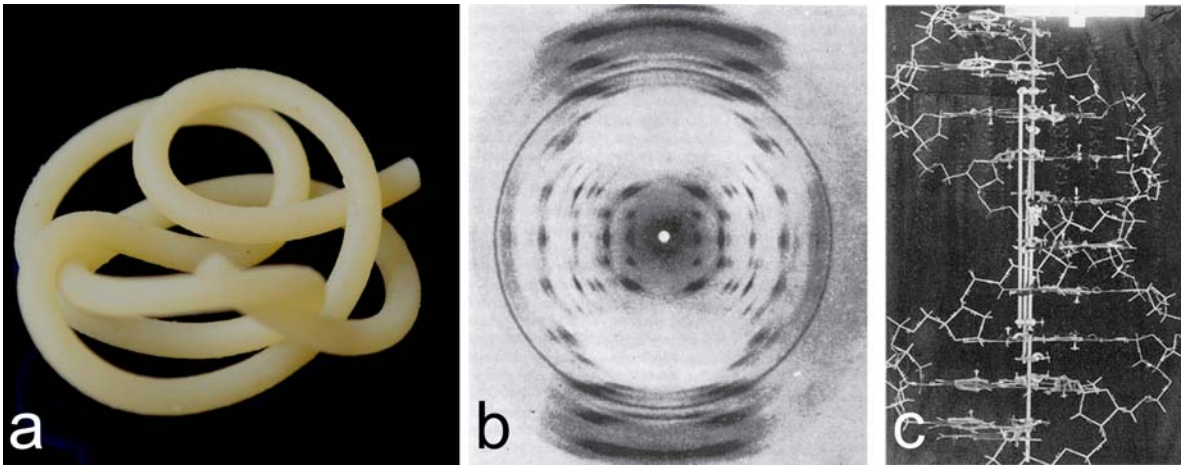

Abbildung 1: a) Modell eines einzelnen DNS-Moleküls, das in der flüssigen Phase die Form eines Knäuels annimmt (Spaghetto: 27mm lang, 2mm dick). b) Röntgenbeugungsmuster eines DNS-Kristalls, aufgenommen von R.Franklin. c) Die aus b) abgeleitete, berühmte Struktur der DNS-Doppelhelix, für deren Entdeckung J.Watson, F.Crick und M.Wilkins 1962 den Nobelpreis erhielten.

Das „Spaghetto-Modell“ zur Veranschaulichung eines einzelnen DNS-Moleküls ist für die weiter unten vorgestellten Experimente mit einzelnen λ-DNS-Molekülen[16] allerdings nur eine sehr grobe Näherung. Ein λ-DNS-Molekül hat einem Durchmesser von 2 Nanometer und eine Länge von 16 Mikrometern. Wir müssten uns somit einen 16 Meter langen Spaghetto (2mm dick) für die Abbildung 1a besorgen, um ein korrekt skaliertes Modell zu erhalten.

Ein weiterer historischer Meilenstein zum Erlangen eines grundlegenden Verständnisses des DNS-Moleküls ist in Abbildung 1b gezeigt, nämlich das von Rosalind Franklin [2] aufgenommene Röntgenbeugungsmuster eines DNS-Kristalls - das Beugungsmuster einer Vielzahl von Molekülen also, die zu einem mehr oder weniger periodischen Gesamten vereint worden sind. Bis heute gibt es leider keine Mikroskope, die einzelne DNS-Moleküle in wässriger Umgebung im Detail, wie etwa die Spaghetti in Abbildung 1a, darstellen könnten, geschweige denn in der Lage wären, die innere Struktur des Moleküls aufzulösen. Gelingt es jedoch, eine Vielzahl identischer Moleküle dazu zu bringen, eine periodische Anordnung über einen makroskopischen Bereich zu bilden, um dann Strahlung mit entsprechend kleiner Wellenlänge an diesem Kristall zu streuen, so kann die innere Struktur der einzelnen Moleküle aus dem Beugungsmuster „erraten“ werden. Die Bildung eines DNS-Kristalls und die Aufnahme von Beugungsmustern mit Röntgenstahlen ist Rosalind Franklin und Maurice Wilkins gelungen. Aus diesem Beugungsmuster haben es James Watson und Francis Crick [3] schließlich verstanden, die Anordnung der einzelnen Gruppen und damit aller Atome eines DNS-Moleküls der berühmten, doppelhelikalen Struktur zuzuordnen (siehe Abbildung 1c).

HEUTIGE TRENDS ZUR STRUKTURANALYSE AN EINZELNEN MOLEKÜLEN

Die wichtige Entdeckung der DNS-Doppelhelix beruht wie gesagt auf Streuexperimenten an Kristallen und zwar unter Verwendung von Röntgenstrahlen mit Wellenlängen im Ångström-Bereich (1Ångström = 1Å = 0.1nm = 10^{-10}m). Da Röntgenstrahlen bei biologischen Systemen zu erheblichen Strahlenschäden führen, sind Streuexperimente an makroskopischen Proben insofern von Vorteil, als genügend Signal akkumuliert werden kann, bevor ein Grossteil der Moleküle im Kristall zerstört ist. Die Methode der Röntgenbeugung an Kristallen zur Strukturanalyse einzelner Moleküle birgt aber auch gravierende Nachteile. Zum einen muss man die Moleküle dazu bringen Kristalle zu bilden, ohne dass dabei die Struktur des einzelnen Moleküls verändert wird. Das ist oft nicht einfach, da im Gegensatz zu vielen anorganischen Materialien die Bildung von Kristallen für biologische Systeme kein natürlicher Prozess ist, sondern nur durch äußeren Zwang erreicht werden kann. Hinzu kommt, dass ein Beugungsmuster wie in Abbildung 1b nicht auf direktem Wege zu einer eindeutigen Struktur des zu Grunde liegenden Moleküls führt. Es braucht zusätzliche Information, ein Modell oder Intuition um letztlich auf die richtige Struktur schließen zu können. Diese Limitierung der Röntgenbeugung an Kristallen ist mit dem Begriff des „Phasen-Problems“ verbunden: Da die Phase bei der Streuung an einem Kristall nicht aufgezeichnet wird - nicht aufgezeichnet werden kann, da es keine phasenempfindlichen Detektoren gibt - ist die Objektstreuwelle nicht eindeutig bestimmbar.

Die wohl berühmteste Lösung besagten Phasenproblems hat Dennis Gabor [4] mit der Erfindung der Holografie vorgestellt. Dabei wird die Phase der Objektstreuwelle mit einer Referenzwelle zur Interferenz gebracht, was einer Bestimmung der Phase der Objektwelle gleichkommt. Zum Beispiel ist überall dort auf dem Detektor wo Interferenz-Maxima durch konstruktive Interferenz auftreten, die Phase der Objektwelle gleich derjenigen der

[16] λ-DNS bezeichnet die DNS des so genannten λ-Bakteriophagen. Dies ist ein Virus, der das Bakterium E. coli zum Wirt hat.

Referenzwelle. Das so gebildete Hologramm enthält demnach die vollständige Information über das Objekt bzw. dessen Streuwelle, beschrieben durch Amplitude **und** Phase, sodass durch numerische Rekonstruktion schließlich auf die Struktur des Objektes geschlossen werden kann.

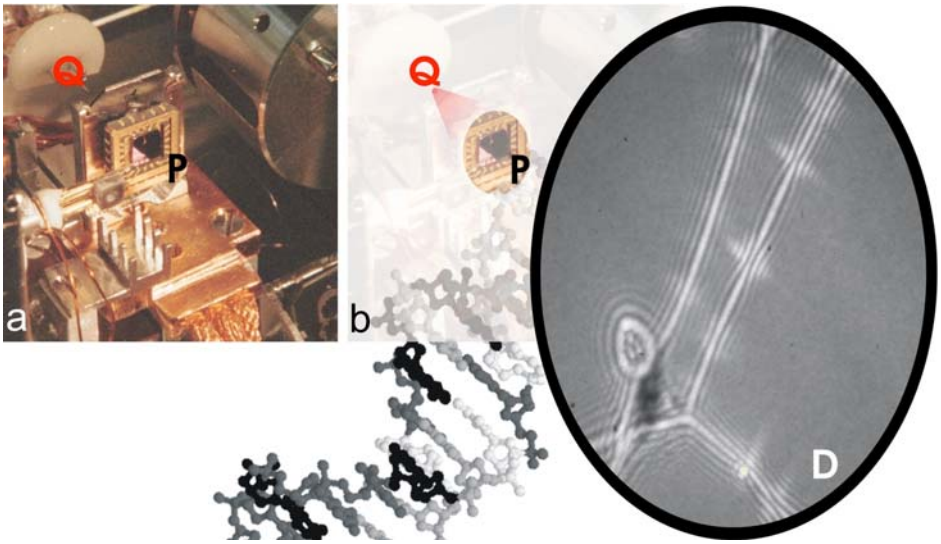

Abbildung 2: Zur Holografie mit langsamen Elektronen. a) Einblick in eine Apparatur zur Elektronenholografie. Eine Quelle (Q) emittiert kohärente Elektronen. In einem Abstand der Größenordnung eines Mikrometers befindet sich die Probe (P); in diesem Fall DNS Moleküle, die freitragend über Löcher einer geeigneten Mikrostruktur gespannt worden sind. b) Die schematische Darstellung betont nochmals Punktquelle und Probe und zeigt zudem ein Hologramm eines DNS-Netzwerkes, das auf einem etwa 10cm hinter Quelle und Probe platzierten Detektor (D) mit hoher Vergrößerung aufgezeichnet wird.

Somit stellt die Holografie eine mögliche zukünftige Methode der Strukturbiologie an einzelnen Molekülen dar. Sie löst das Phasenproblem und die Notwendigkeit der Kristallbildung wird hinfällig. Leider jedoch ist die Holografie zurzeit nur eine prinzipielle oder konzeptionelle Lösung; für die praktische Umsetzung sind noch zahlreiche Probleme zu bewältigen. Zum einen ist kohärente Strahlung im Wellenlängenbereich weniger Ångström erforderlich, zum anderen eine Lösung für das Problem der Strahlenschäden, welche bei einem notwendigen Streu-Signal von nur einem einzigen Molekül naturgemäß schneller ihre Wirkung zeigen als bei einem großen Kristall.

Im Falle von Röntgenstrahlung stehen mit den mittlerweile weltweit verbreiteten Synchrotrons[17] kohärente Quellen in großer Zahl zur Verfügung. Holografie an einzelnen Molekülen mit Synchrotron-Strahlung ist jedoch wegen der genannten Strahlenschäden nicht möglich; ein einzelnes Molekül wäre vollständig zerstört, lange bevor auf dem Detektor ein Hologramm mit brauchbarem Signal/Rausch-Verhältnis erfasst wäre, um daraus die Objektwellenfunktion, bzw. die Struktur des einzelnen Moleküls zu rekonstruieren.

Ein allfälliger zukünftiger Weg vorbei an dieser Schwierigkeit weist der so genannte „Free Electron Laser“, der zwar Investitionen in Milliardenhöhe brauchen wird, dafür aber eine helle Zukunft für Strukturaufklärung an einzelnen biologischen Molekülen verspricht. Die Idee dabei ist einfach: Hinsichtlich eines brauchbaren Signal/Rausch-Verhältnisses wird ein einzelnes Molekül mit ausreichend vielen Röntgenquanten konfrontiert,

[17] In einem Synchrotron wird ein Elektronenstrahl auf einer Kreisbahn gehalten, was einer beschleunigten Bewegung geladener Teilchen entspricht. Dies hat die Erzeugung intensiver gebündelter elektromagnetischer Strahlung im Röntgenbereich zur Folge.

jedoch nur während einer extrem kurzen Dauer; es handelt sich dabei der Größenordnung nach um 10^{12} Photonen in einem Puls von nur 10 Femtosekunden (1Femtosekunde = 1fs = 10^{-15}s). So ist auf Grund der Massenträgheit der einzelnen Atome des Moleküls der strukturaufklärende, elastische Streuprozess passiert, bevor die Probe ihrer unvermeidbaren Zerstörung hat nachkommen können und die Information über die intakte Molekülstruktur kann auf einem Detektor festgehalten werden.

Eine alternative Holographie-Methode zur Strukturbiologie an einzelnen Molekülen ist die Holographie mit langsamen Elektronen. Sie benutzt ebenfalls kohärente Strahlung im Ångström-Wellenlängenbereich und ist somit bezüglich Auflösungsvermögen vergleichbar mit Röntgenstahl-Holographie. Jedoch ist ihr eine weitaus harmlosere Art der Wechselwirkung mit biologischen Systemen eigen. Elektronen mit Energien zwischen 30 und 300eV, die von einer atomar kleinen Quelle erzeugt werden, stellen eine Kugelwelle dar, die auf dem Weg zu einem entfernten Detektor mit einem einzelnen Molekül in Wechselwirkung tritt. Die vom Molekül elastisch gestreute Objektwelle interferiert mit dem ungestreuten Teil der Kugelwelle und bildet so auf dem Detektor das Hologramm, in dem sowohl die Amplitude der Objektwelle als auch deren Phase festgehalten sind. Wenn auch die Details der inneren, atomaren Struktur bislang verborgen geblieben sind, gelingt es so, einzelne, freitragend über Löcher gestreckte DNS-Moleküle als fadenförmige Objekte mit 2nm Durchmesser abzubilden [5]. Das in der Abbildung 2c gezeigte Hologramm kann - ohne detektierbare Strahlenschäden an den Molekülen - über Stunden beobachtet werden.

Mit einer Wellenlänge der kohärenten Elektronen im Ångström-Bereich, neuartigen Detektoren für langsame Elektronen mit höherer Dynamik und weniger Rauschen und der Berücksichtigung der Vorwärts-Streuung von langsamen Elektronen besteht berechtigte Hoffnung, dass die Holografie mit niederenergetischen Elektronen zu einer tauglichen Methode der Strukturbiologie an einzelnen Molekülen reifen wird.

EINZEL-MOLEKÜL EXPERIMENTE IN DER FLÜSSIGEN PHASE

Neben der Frage nach der inneren Struktur einzelner Moleküle, die vielleicht in Zukunft mit Hilfe kohärenter Röntgenstrahl-Pulse oder langsamer Elektronen geklärt werden kann, ist das Verhalten einzelner DNS-Moleküle in ihrer natürlichen Umgebung, also in wässriger Lösung, von fundamentalem Interesse. Einerseits ist das Verständnis von Kinetik und Dynamik eines einzelnen DNS-Moleküls Voraussetzung, um dessen Verhalten in komplexeren biologischen Systemen zu verstehen, anderseits kann man allgemeiner das DNS-Molekül als ein Testobjekt für moderne Modelle und Theorien zur Polymerphysik betrachten. Kenntnisse der Eigenschaften einzelner DNS-Moleküle haben somit neben der biologischen Relevanz auch einen direkten Bezug zu den Grundlagen der Polymer-Physik ganz allgemein. Untersuchungen von Objekten in wässriger Umgebung werden vorwiegend unter dem Lichtmikroskop vorgenommen. Auf Grund seiner Auflösungsbegrenzung von etwa 500nm scheint dieses zum Studium einzelner DNS-Moleküle mit einem Durchmesser von nur 2nm aber zunächst ungeeignet. Die Pionierarbeiten von Steven Chu jedoch haben gezeigt, dass mit Hilfe der so genannten Fluoreszenz-Mikroskopie, einer speziellen Form der Lichtmikroskopie, sehr wohl einzelne DNS-Moleküle in der Flüssigkeit studiert werden können [6]. Dabei wird das Molekül vorgängig mit einem Fluoreszenzfarbstoff versehen, sodass durch Anregung mit Licht geeigneter Frequenz das Molekül anschließend zur Fluoreszenz gebracht und somit sichtbar gemacht werden kann (siehe Abbildung 3). Wenngleich dabei natürlich die innere Struktur verborgen bleibt, kann zumindest der Aufenthaltsort bestimmt, bzw. die Kinetik des Moleküls beobachtet werden. Darüber hinaus macht es die Methode möglich, die globale Gestalt einzelner, fadenförmiger

Moleküle in der flüssigen Phase, sowie allfällige Übergänge zwischen verschiedenen Konfigurationen zu studieren.

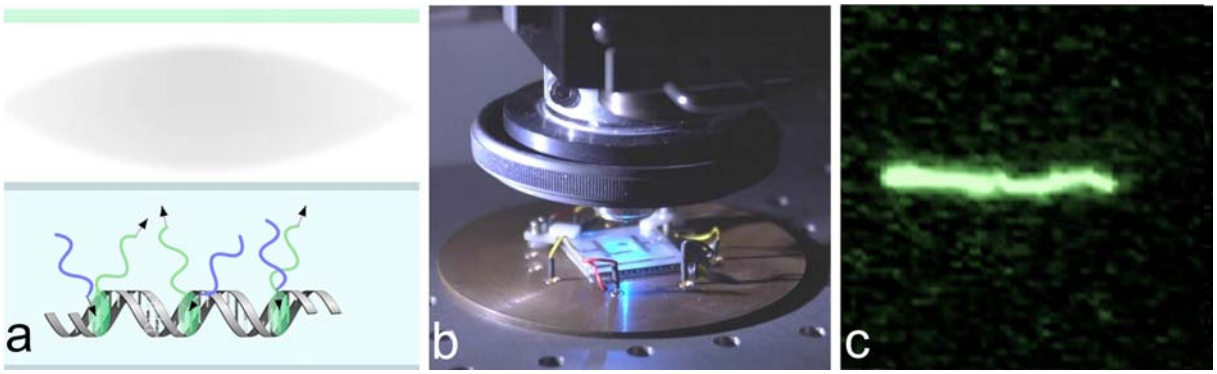

Abbildung 3: Fluoreszenz-Mikroskop um Bewegung und Gestalt einzelner DNS-Moleküle in der flüssigen Phase zu studieren. a) Schematische Darstellung der wesentlichen Elemente der Fluoreszenz-Mikroskopie. Die DNS-Moleküle mit eingebautem Farbstoff befindet sich in einem dünnen Wasserfilm. Ein optisches System (Linsen und Filter) sorgt dafür, dass nur das vom Molekül ausgesandte Licht zu einem empfindlichen CCD Chip gelangt, während das Anregungslicht blockiert wird. b) Fotografie einer Probe unter dem Fluoreszenz-Mikroskop. c) Einzelnes λ-DNS-Molekül, das in einem elektrischen Feld auf seine Gesamtlänge von 16μm gestreckt ist.

Folgende Experimente spielen sich in einem nur 8 Mikrometer dicken Wasserfilm im thermodynamischen Gleichgewicht ab, der vorsichtig nach außen abgeschlossen und dadurch frei von Temperatur- und Strömungs-Gradienten ist. Untersucht werden Aspekte der Kinetik bzw. der Energetik besagter λ-DNS-Moleküle mit einer Länge von 16 Mirometern.

DIFFUSION EINZELNER DNS-MOLEKÜLE

Die Beweglichkeit von mikroskopischen, biologischen Objekten ist eine fundamentale Größe im Zusammenhang mit dem zeitlichen Reaktionsablauf biologischer Prozesse. Auf mikroskopischer Skala wird die Beweglichkeit solcher Objekte durch den Diffusionskoeffizienten charakterisiert. Albert Einstein hat uns im Zusammenhang mit seiner mikroskopischen Deutung des statistischen Charakters der Physik der Wärme die Beschreibung des Zufallsweges eines mikroskopischen Objekts in einer Flüssigkeit geliefert. Demnach gilt für ein Molekül, welches den statistischen Stößen von Wassermolekülen ausgesetzt ist, also einen Zufallsweg beschreibt, folgendes: Bezüglich seines ursprünglichen Aufenthaltsortes wächst die mittlere quadratische Verschiebung $<\Delta x^2>$ des Moleküls proportional mit der Zeit t. Die Proportionalitätskonstante wird Diffusionskoeffizient D genannt. Auf einer Oberfläche oder in einem dünnen Film, also in zwei Dimensionen, ergibt sich:

$<\Delta x^2> = 2D \cdot t.$

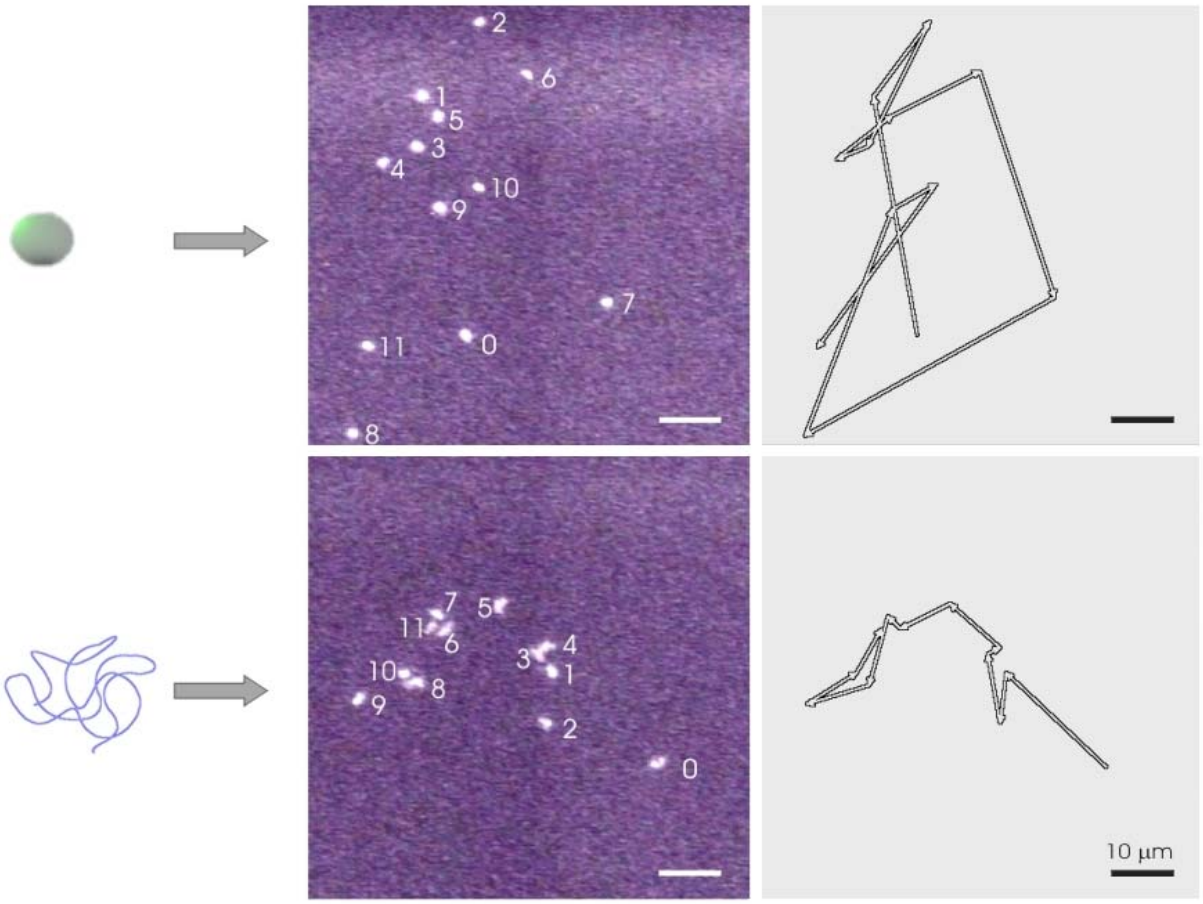

Abbildung 4: Messung des Diffusionskoeffizienten aus der mittleren quadratischen Verschiebung einer Latex-Kugel mit einem Radius von 50nm (oben) und eines einzelnen DNS-Moleküls (unten). Durch Überlagerung von 12 Fluoreszenz-Mikroskop Bildern sind rechts in grau die ersten 11 Schritte der Zufallswege dieser beiden Objekte gezeigt. Die Zeitintervalle zwischen aufeinander folgenden Beobachtungen betragen 30s.

Die Abbildung 4 zeigt die Durchführung eines solchen Diffusionsexperiments. Durch direkte Messung der mittleren quadratischen Verschiebung eines Objektes nach bestimmten Zeitintervallen wird der Diffusionskoeffizient bestimmt, indem genannte Proportionalität zur Anwendung kommt. Dabei wird der Diffusionskoeffizient einer Latex-Kugel mit 50nm Radius und derjenige eines einzelnen λ-DNS-Moleküls gemessen und verglichen. Der obere Teil der Abbildung zeigt einen kleinen Ausschnitt aus dem Zufallsweg der Latex-Kugel, der untere Teil zeigt denjenigen des λ-DNS-Moleküls. Der Ort der Objekte (Startpunkt ist mit „0“ markiert) wurde nach jeweils 30 Sekunden markiert. Die so erhaltenen Zufallswege sind im rechten Teil der Abbildung skizziert. Insgesamt wurden bei diesem Experiment je 50 Beobachtungen bei 5 verschiedenen Temperaturen durchgeführt, um statistisch relevante Daten zu gewinnen. Die Latex-Kugel mit 50nm Radius besitzt etwa die 8-fache Masse des DNS-Moleküls. Trotz der größeren Masse sind die Diffusionswege der Kugel im Mittel deutlich länger als diejenigen des Moleküls (vgl. Abb. 4). Offensichtlich hat die Flexibilität, also die hohe Anzahl innerer Freiheitsgrade des Moleküls einen entscheidenden Einfluss auf dessen Diffusionsgeschwindigkeit. Das Molekül als ganzes, bzw. sein Schwerpunkt, lässt sich durch die statistischen Impulsüberträge der Wassermoleküle (bei gleicher Temperatur) deutlich langsamer durch die Flüssigkeit schubsen als ein starrer Körper vergleichbarer Masse. Weitere Experimente mit DNS-Molekülen verschiedener

Längen, sowie der Vergleich mit Simulationen, werden Aufschluss darüber geben, wie gut bestehende Theorien der Polymerphysik die Natur zu beschreiben verstehen.

ZUR ENERGETIK EINZELNER DNS-MOLEKÜLE

Die diskutierten Experimente zeigen, dass ein einzelnes DNS-Molekül fast ausschließlich in der zufällig verknäuelten Konfiguration beobachtet wird. Das liegt daran, dass wir nur einige wenige hundert Beobachtungen auswerten und daher die Wahrscheinlichkeit, das Molekül wenigstens ab und zu einmal in einer Konfiguration anzutreffen, die einer größeren freien Energie entspricht, sehr unwahrscheinlich ist. Hätten wir jedoch die Zeit ein Molekül so lange beobachten zu können, bis es uns alle seine möglichen Konfigurationen offenbarte, entdeckten wir immer mal wieder auch eine weniger verknäuelte Konfiguration höherer freier Energie. Sämtliche beobachteten Konfigurationen, nach welchen klassifiziert werden könnte, ergäben schließlich die Topographie der „Freie-Energie-Landschaft“ eines DNS-Moleküls in der Flüssigkeit. Aus Mangel an Zeit[18] müssen wir uns zunächst mit bescheideneren Experimenten zufrieden geben. Wir stellen uns also die einfache Frage nach dem Übergang eines Moleküls von der Konfiguration höchster freier Energie, nämlich der vollständig gestreckten Konfiguration, zu der energetisch niedrigsten und daher am häufigsten beobachteten „Knäuel-Konfiguration“. Da erstere statistisch äußert unwahrscheinlich ist, wir demzufolge sehr lange abwarten bräuchten, um sie auch nur einmal zu beobachten, ist es vernünftiger, die gestreckte Konfiguration durch geeignete äußere Bedingungen hervorzurufen: Moderne molekularbiologische Methoden erlauben es, einzelne Moleküle mit nur einem Ende aufs Substrat zu fixieren[19]. Mit Hilfe zweier Metall-Elektroden lassen sich die verankerten Moleküle im elektrischen Feld strecken, sobald über die Elektroden eine Spannung angelegt wird. Abruptes Abschalten der Spannung schafft thermodynamische Gleichgewichtsbedingungen und ermöglicht so die Beobachtung des Überganges von der gestreckten Konfiguration des Moleküls zur energetisch bevorzugten. Ein solches Experiment ist in Abbildung 5 gezeigt. Die Bestimmung der Zeiten zur Wiederherstellung der „Knäuel-Konfiguration“, gemessen bei verschiedenen Temperaturen, erlaubt es, Informationen über die Energetik einzelner DNS-Moleküle in Bezug auf besagten Übergang zu gewinnen.

[18] Neben den enormen Datenmengen gäbe es auch noch weitere technische Probleme, wie zum Beispiel das „Ausbleichen“ der Fluoreszenz-Farbstoffe.

[19] Das Siliziumdioxid-Substrat wird mit einem geeigneten Protein (Streptavidin) beschichtet (Clondiag Chip Technologies® GmbH, Jena), woran das vorgängig biotinylierte Ende des DNS-Moleküls spezifisch bindet.

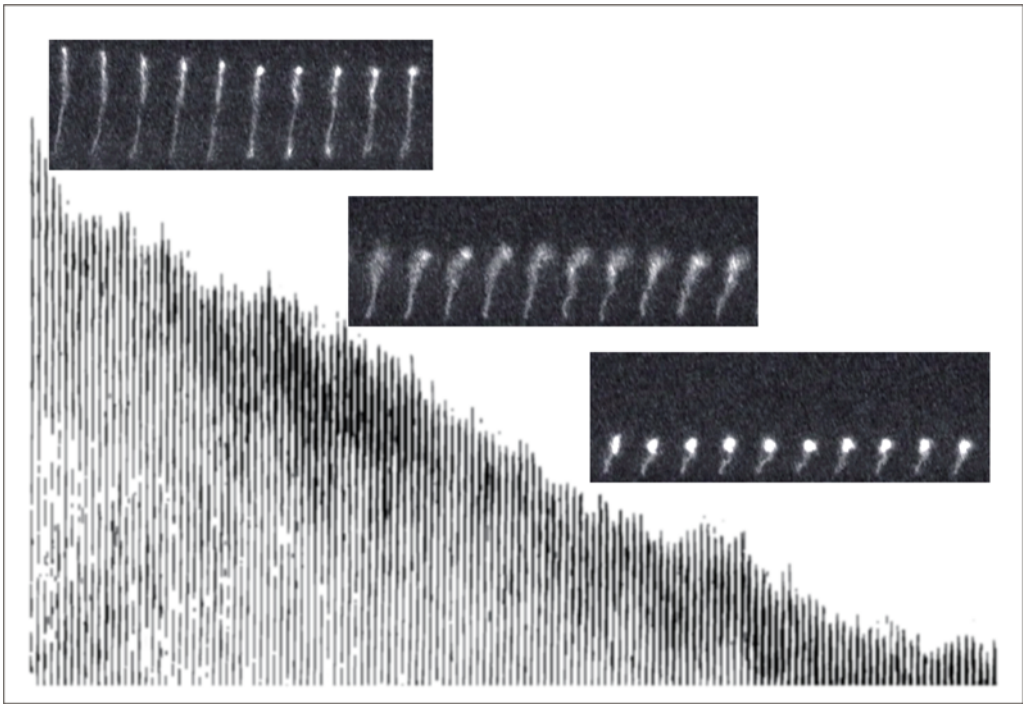

Abbildung 5: Zur Energetik eines einzelnen DNS-Moleküls. Der Übergang von der gestreckten zu der „Knäuel-Konfiguration“ wird mit Videofrequenz beobachtet. Das Histogramm illustriert die zeitliche Entwicklung der Distanz zwischen dem freien Ende des Moleküls und seinem Ankerpunkt. Zur Illustration der Kinetik dieses Übergangs sind einige Bildsequenzen eingefügt.

Abschließend möchten wir noch einmal zu den, in der Einleitung erwähnten, großen Visionen mit kleinen Molekülen zurückkommen. Das Experiment zur Energetik hat auch gezeigt, dass einzelne DNS-Moleküle mit Siliziumdioxid-Substraten und somit also auch mit Silizium-Strukturen verbunden werden können. Es scheint nahe liegend, als nächstes die Moleküle auf einem Silizium-Chip mit elektrischen Kontakten zu versehen und damit Schaltfunktionen zu realisieren. Durch selbständiges Anlagern der Moleküle an die Kontakte (self assembly) schließlich könnten sich diese Schaltfunktionen von sich aus zu komplexen integrierten Schaltkreisen zusammenfügen. Dies allerdings führt nun wohl - aus unserer Zeit heraus - in die *„Physik in unserer Zukunft“*.

Danksagung

Die Arbeiten unter dem Titel „Einzel-Molekül Experimente in der flüssigen Phase“ wurden vom Schweizerischen Nationalfonds zur Förderung der Wissenschaftlichen Forschung (SNF) unterstützt.

Literatur

[1] W. Kuhn, Kolloid-Zeitschrift **1934**, 68, 2.

[2] R. Franklin, R.G. Gosling, Nature **1953,** 171, 740.

[3] J.D. Watson, F.H.C Crick, *Nature* **1953,** 171, 737.

[4] D. Gabor, Nature **1948**, 161, 777.

[5] H.-W. Fink, H. Schmid, E. Ermantraut, T. Schulz. J. Opt. Soc. Am. **1997**, 14, 2168.

[6] R.H. Austin, J.P. Brody, E.D. Cox, T. Duke, W. Volkmuth, Physics Today, Feb. **1997,** 32.

I.7.2. Appendix I.2: DNA-Trap

The ability to specifically anchor DNA molecules to some counter part, such as glass substrates, fibres and micro beads, has opened a wide range of possibilities for investigations on individual molecules; see paragraph I.2.1 and I.2.2. As mentioned there, the findings concerning electrical conductivity of DNA are controversial and further experiments are needed. Related to this, an ongoing project is presented in the following.

A "DNA-trap" has been developed to try and deposit an individual DNA molecule between two electrodes. The skeletal structure is given by two gold electrodes separate by a gap of *1µm* on a *Si/SiON* substrate[20]; see fig.I.7.

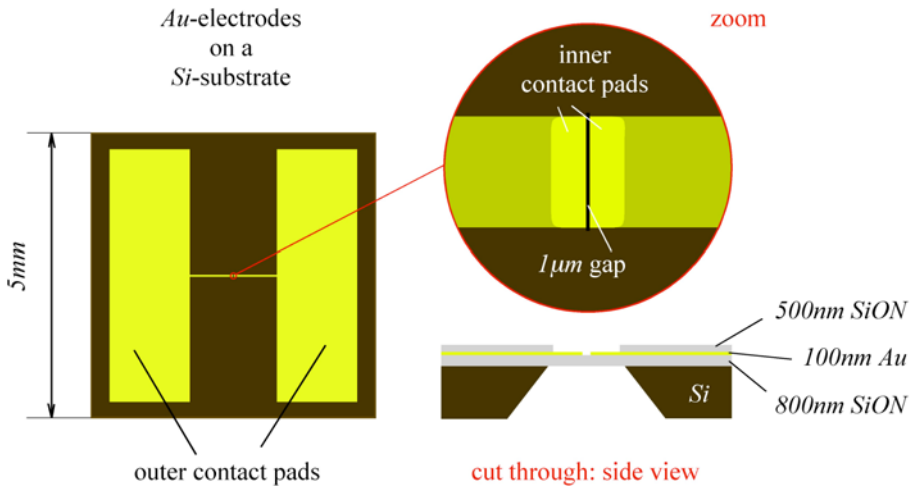

fig.I.7

The centre of the substrate consists of a thin membrane (*800nm*) and apart from the contact pads the electrodes are insulated with a fine coat of *SiON* (*500nm*).

In a first step two holes (gap holes) are drilled in the gap between the electrodes through the membrane with a focussed ion beam (FIB); see fig.I.8. Looking at the membrane now from the bottom the position of the gap can be identified by these gap holes; see fig.I.9a. Next, two more holes (trap holes) of an appropriate diameter are drilled through the membrane from the bottom on either side of the gap at a certain distance from each other; see fig.I.9b. (To minimize abrasion of the electrodes by the FIB, as many milling steps as possible are accomplished from the bottom.)

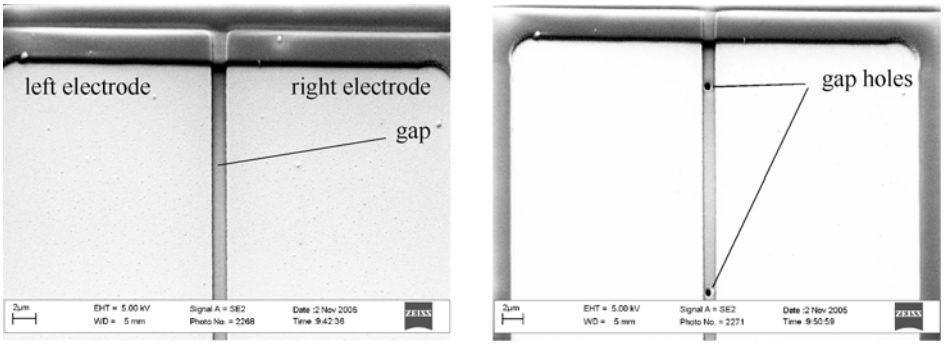

a) b)

fig.I.8

[20] The structure is manufactured photo lithographically at *Clondiag Chip Technologies® GmbH* in Jena (Germany).

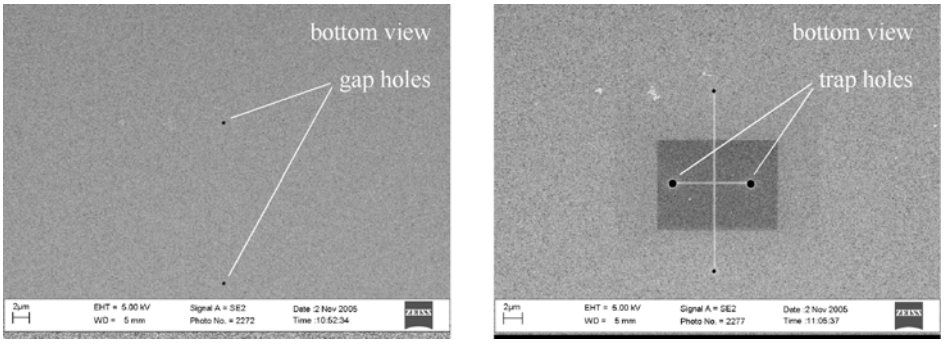

a) b)

fig.I.9

Then a droplet of streptavidin coated styrene beads (diameter: *1μm*) in aqueous solution is applied onto the sample. The diameter of the micro beads is slightly bigger than the diameter of the holes, so that careful rinsing with water removes all beads again except the ones sticking on the holes; see fig.I.10.

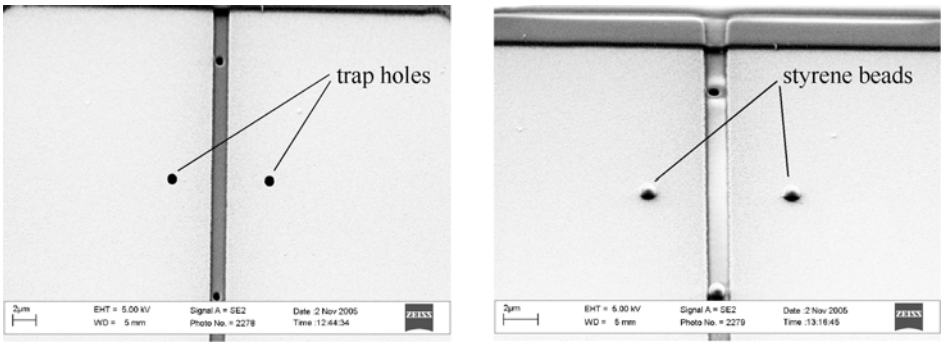

a) b)

fig.I.10

Finally, one last hole (central hole) is drilled from the bottom between the beads trough the gap; see fig.I.11a. (This last step is needed only if succeeding investigations in the Low Energy Electron Point Source (LEEPS) microscope are considered.)

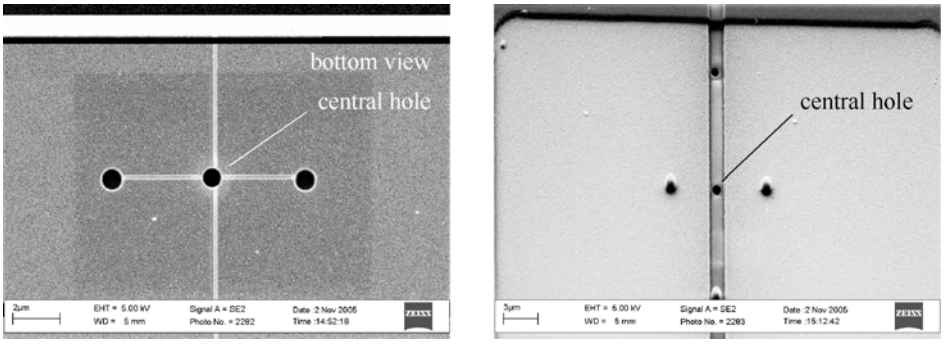

a) b)

fig.I.11

On a structure like the one shown in fig.I.11b it should be possible to trap an individual DNA molecule between the electrodes (possibly freestanding over the central hole). Therefore the DNA needs to be biotinylated[21] at both ends, stained and finally be applied in appropriate concentration onto the "trap". By the aid of external electrodes

[21] Biotin provides a strong anchor to streptavidin and thus to the micro beads; see chapter I.2.

the molecules can be driven electrophoretically over the bead/gap structure visually controlled under the fluorescence microscope. Once the one end of a DNA molecule anchors to one of the beads the polarity of the external electrodes is set accordingly, so that the molecule is combed towards the second bead. If the distance between the beads is chosen appropriately, the free end of the molecule should easily bind to the opposite bead. Trapped like this between the central electrodes the *I/V*-characteristics of the molecule in the liquid phase could be measured at various temperatures. Moreover, careful drying of the sample might leave the molecule intact over the central hole and thus ready for further investigation under vacuum in the LEEPS microscope. After having collected enough experience in trapping individual DNA molecules, also “blind” trapping with unstained DNA might be approached.

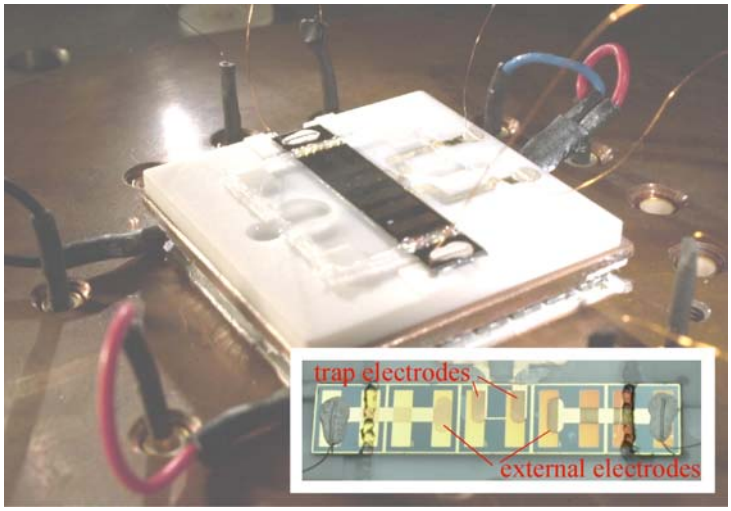

fig.I.12

Fig.I.12 shows a DNA-trap on a Peltier cooling stage electrically contacted and ready to snap.

Section II

On the Dynamics of the Conduction Mechanism and Field Ion Emission from a Solid Electrolyte

II.0. Introduction to Section II

Solid state ionics, a term in analogy to *solid state electronics*, denotes a fairly new field of research. Up to the 1960s mainly electron conducting materials have been known. In particular semiconductors were studied extensively at that time since the transistor had been invented in 1957. The few ion-conducting devices were liquid electrolyte based (e.g. aqueous batteries) and thus often inconvenient due to their bulky size and limited temperature range of operation. The early ion-conducting solids such as alkali halides and silver halides are very poor conductors ($\sigma \approx 10^{-7}$-10^{-12} *S/cm*). However, by now there is a great number of fast ion-conducting solids known with various mobile ion species such as H^+, Li^+, Na^+, K^+, Ag^+, Cu^+, F^-, O^{-2} and ion conductivities up to 10^{-1}*S/cm* at room temperature [II.1]. The solids exhibiting high ionic conductivity are termed *solid electrolytes*[22]. Due to the possibility of miniaturisation and their utility over a wide range of temperatures, in particular below *0°C* or above *100°C* (i.e. where devices with aqueous electrolytes normally cease to work) solid electrolytes have an immense technological potential (e.g. sensors, memory devices, fuel cells etc.).

II.1. The Classification of Solid Electrolytes

There are solid electrolytes with different microstructures and physical properties. According to this, they are subdivided into four classes:

a) Framework crystalline materials: These solid electrolytes consist of a rigid crystalline skeleton and more or less mobile ions and are further divided in *soft-* and *hard-framework crystals* respectively.

b) Amorphous-glassy electrolytes: Ionic glasses are network glasses. They consist 1st of a "network former" also referred to as oxide glass former (e.g. SiO_2, MoO_3, $AgPO_3$ etc.), 2nd of a "network modifier" (mainly alkali oxides such as Na_2O, K_20, Li_2O, etc.) that opens up the glass structure so the alkali ions involved are more or less mobile and can diffuse through the glassy network and/or 3rd a dopant (halide) salt (e.g. *AgI*). Upon doping the glass expands and the conductivity can be increased drastically by the dopant metal ions.

c) Composite electrolytes[23]: These are multiphase solid systems in which submicron-size particles of insulating and chemically inert materials called "second phase dispersoids" are dispersed into a moderate-ionic conducting solid called "first phase host matrix" leading to conductivity enhancement of up to three orders of magnitude compared with the initial host matrix. According to the nature of the host matrix and the dispersoid, these systems are subdivided in *crystal-crystal*, *crystal-glass*, *glass-polymer composites* etc.

d) Polymer electrolytes: This is the newest class of solid ionic materials formed by complexing polar polymers such as *polyethylene oxide* (*PEO*), *polyphenylene oxide* (*PPO*) or *polyethylene glycol* (*PEG*) with ionic salts. So far solid polymer electrolytes still have a relatively poor ionic conductivity but their good thin film forming properties and mechanical flexibility are some of the advantages that are promising for future applications.

[22] Solid electrolytes are also referred to as *super ionic solids*, *hyper ionic solids* or *fast ion conductors*.
[23] Also referred to as *heterogeneously doped materials* or *dispersed solid electrolytes*.

II.2. Theoretical Models

Various theoretical models, based on different structural and non-structural factors, have been suggested to explain the fast ion conduction in solid electrolytes. Yet, no unified theory exists that can explain all the essential common features of different solid electrolyte systems.

For the crystalline systems relatively simple *single-particle hopping* and *continuous diffusion models* based on the random hopping motion of mobile ions have been developed first [II.2]. However, these models cannot account for many-body effects like correlation effects in the diffusion process or structural short-range order interaction. For that purpose several *lattice-gas models* have been developed [II.3- II.8]. Moreover, to describe the ion dynamics in solid electrolytes the *free-ion model* [II.9], the *jump-diffusion model* [II.10], the *jump-relaxation model* [II.11] etc. have been proposed.

Based on some of these models more sophisticated theories had to be developed for the class of the amorphous-glassy electrolytes. From a microscopic point of view the physics of ionic glasses are much more complex than the ones of the crystalline-polycrystalline solid electrolytes. In ionic glasses there is on the one hand a disordered network structure that exhibits no long-range but short-to-medium-range order and interacts with the mobile ions. On the other hand the mobile ions themselves may interact with each other by long-range Coulomb forces. Moreover, the dynamics of the glass formation may be governed by the mobile ions.

There is the *A-S model* [II.12] assuming that the activation energy for ion migration is the sum of the electrostatic binding energy and the strain energy caused by the deformation of the network due to ion movement. In this model the mobility of the ions and consequently the conductivity increases with increasing temperature rather than mobile ion concentration. This aspect has been supported experimentally by neutron scattering studies [II.13].

Another model is called the *decoupling-index model* [II.14]. This model is concerned with the observation that in highly conductive glasses, below the glass transition temperature T_g[24], ion transport is decoupled from structural dynamics. The decoupling index $R_\tau = \tau_s / \tau_o$ is introduced, τ_s is the structural relaxation time and τ_o is associated to the electrical relaxation of the solid electrolyte. This index is a measure for how much the electrical process decouples from the viscous process as a function of temperature and may be of the order of 10^{12}.

In order to explain the observation of the correlation between the conductivity at T_g and the activation energy for ion migration the continuous random network model was modified to become the *cluster-bypass model* [II.15]. According to the model, preferred partial conduction pathways for ion migration are provided by residual liquid around ordered clusters. The residual liquid accounts for the high conductivity at T_g and the larger decoupling index R_τ. The model elucidates various transport phenomena in *AgI*-based glasses and also the mixed-alkali effect[25]. However, it cannot explain cluster formation in a wide range of glassy solid electrolyte materials.

Based on the experimental evidence that cations in glass create and maintain their characteristic environments the *dynamic-structure model* has been proposed [II.16]. The three assumptions: i) the glass structure is not completely frozen until far below T_g, ii) the mobile cations are actively determining the glass structure and iii) the transport is a hopping process, lead to the perception of fluctuating pathways within a dynamically determined structure and give rise to relaxation and site memory effects. This model not only explains

[24] The glass transition temperature T_g is defined as the temperature where the dynamic viscosity of the glass is 10^{13} *poise*. (The viscosity of water is of the order of 10^{-2}, the one for honey about 10^4 *poise*. *1poise = 1P = 0.1 Pa s*.)

[25] The mixed-alkali effect occurs in several vitreous solid electrolytes and terms a class of anomalies that is considered to play a central role for understanding the conduction mechanism in solid electrolytes; see chapter II.3.

quantitatively the occurrence of the mixed alkali effect, but also the anomalous scaling law of *ac*-conductivity in single alkali glasses[26]. However, the existence of site relaxation, memory effects and their influence on the ion transport and the local structural relaxation need more corroboration.

But also to understand the ion transport mechanism in composite electrolyte systems several phenomenological models have been proposed[27] [II.17- II.25]. Yet, no single unified model exists to explain consistently various experimental findings on different composite electrolyte systems. However, the central feature appears to be the existence of a space-charge region at the interface between the host matrix and the dispersoids.

Finally also onto ion conduction mechanism in solid polymer electrolytes a few propositions have been made [II.26, II.27], but there are no approved theories available so far.

II.3. The Amorphous-Glassy Electrolytes

The experiments presented in the manuscripts have been carried out with a solid electrolyte from the class of the amorphous-glassy electrolytes. Therefore some of the most important previous findings concerning this class of solid electrolytes and for which any unified model will have to account shall be introduced.

For glass in general holds: The glassy state is obtained from the melt by cooling sufficiently rapidly. At the melting temperature T_m the liquid does not reach the thermodynamically stable crystalline state but is transformed to an under cooled liquid and at still lower temperatures to glass. During cooling the viscosity increases strongly. While the under cooled liquid is cooled down, its structure changes continuously. These changes in structure are associated with a characteristic relaxation time τ. At the glass transition temperature T_g the relaxation time is of the order of minutes or hours. At lower temperatures the characteristic relaxation time τ increases to the order of days and years and the global structure is frozen in.

In single modified ionic glasses the *dc*-conductivity increases drastically with the modifier content [II.28]. The *dc*-conductivity exhibits a power law dependence on the modifier content and the activation energy decreases logarithmically with the modifier content.

Doping glasses with metal halide salts also increases the *dc*-conductivity σ drastically but also expands the glass. It was found that the increase in the conductivity is related to the increase in volume by a cubic power law [II.29, II.30]:

$$\sigma(x)/\sigma(0) \propto [(V_d - V_u)/V_u]^3 \qquad x = 0.1...0.6$$

eqn.II.1

V_u and V_d is the un-doped and the doped volume respectively and x is the mole fraction of the dopant salt.

In highly conducting *AgI*-doped glasses the conductivity behaviour deviates from the well-known Arrhenius behaviour even below T_g [II.31- II.33], but the effect can be eliminated in certain cases by carefully annealing the glass [II.34]. This deviation is most pronounced for the fastest ionic conductors and disappears for normal ion conducting glasses [II.35].

A puzzling phenomenon emerges in the *ac*-conductivity of single modified and doped glasses. The conductivity was found to obey a simple scaling law [II.36]. Once the average *dc* mobility of the ions is determined the entire

[26] It has been discovered that in single alkali glasses the *ac*-conductivity scales with the content of the network modifier and the *dc*-mobility according to a strikingly simple law; see chapter II.3.

[27] There are several *space-charge models*: There is the *adsorbtion/desorbtion model*, the *resistor-network model*, the *percolation model* and the *morphological model* to mention only some.

ac-spectrum up to *MHz* is known. It seems that the scaling function is universal and does hardly depend on the glass in question. The same scaling function seems even to apply to glass-forming super cooled ionic melts where the motion of the ions is fully coupled to the process of viscous flow.

The most fascinating phenomena occur in glasses where two types of mobile ions are present. Several properties of these glasses depend highly on the ratio of the conducting ions. The collection of these phenomena is referred to as "mixed alkali effect" and is believed to play a key role for the understanding of the conduction mechanism in solid electrolytes and therefore still studied extensively [II.37]. For example internal friction measurements with $(Li_2O)_{(1-x)}(Na_2O)_x\ 3SiO_2$ show that the temperature dependence of the friction changes clearly when Li^+ ions are replaced by Na^+ ions, already when $x=0$ is enhanced to $x=0.005$ [II.38]. But also the conductivity is governed by the mixed alkali effect [II.39, II.40]. The conductivity $\sigma(x)$ runs through a deep minimum (at $x=0.5$) when Li^+ ions are replaced by Na^+ ions while for $x=0$ and $x=1$ the conductivity is the same. The effect is most pronounced at low temperatures and frequencies. Even more striking is the influence of the mixed alkali effect on the diffusion of the individual cations [II.41]. When one type of alkali ion is replaced by one of the other type, the diffusion coefficient of the former continuously decreases while the coefficient of the latter increases. At a particular ion type ratio the two constituents have the same mobility and this ratio is close to the one at lowest ionic conductivity.

II.4. The Field Emission Microscope

The investigations on the solid electrolyte presented in this thesis have all been carried out in the field emission microscope (FEM). Thus, its mode of operation is briefly explained in the following.

Field emission microscopy is closely related to field ion microscopy [II.42, II.43]. While the latter allows to image metal surfaces atomically resolved and also to manipulate the surfaces (field evaporation), the former is typically used to determine the work function for electrons from different crystallographic planes of different metals and to study the influence of ad-atoms on the work function. But it can also be used to study dynamical processes such as diffusion of ad-atoms on a metal surface, not atomically resolved though [II.44]. Basically the FEM consists of a sharp tip (sample), a multi channel plate (MCP) for signal amplification placed a few centimetres opposite of the tip and a detector; all placed in a vacuum chamber; see fig.II.1a.

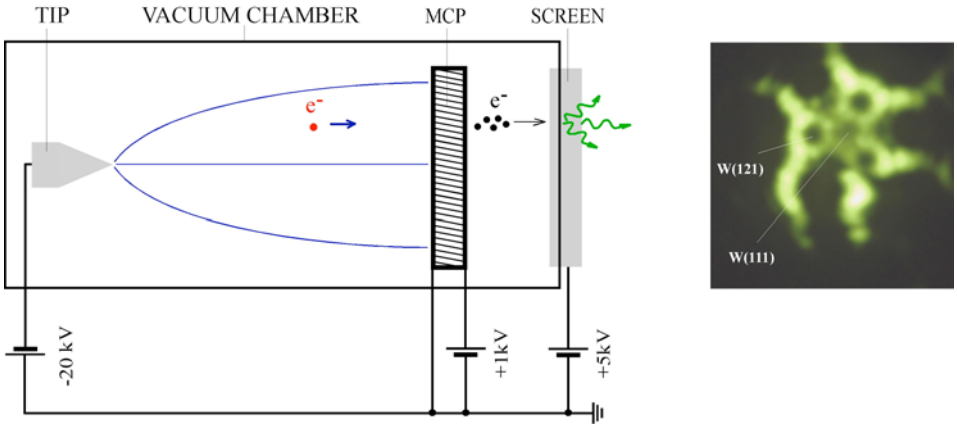

a) b) fig.II.1

In case of electron emission out of a metal tip, the tip is set on negative potential. Due to the strong potential gradient superposed on the work function barrier the electrons from the Fermi edge of the tip can tunnel through the reduced barrier into the vacuum. Once free, the electron is accelerated towards the MCP and evokes an electron shower. Hereupon the amplified electronic signal is accelerated towards the phosphorous screen where it is finally detected as a light signal. In fig.II.1b) a typical field emission pattern of a metal tip (e.g. *W(111)*) is depicted. Some areas are darker than others indicating different values for the work function Φ for different crystallographic planes. These facets are bordered with very bright areas stemming from the step edges in between. Here the field is locally enhanced due to a smaller radius of curvature leading to a higher electric field and emission current consequently. The electron emission via tunnelling is often referred to as cold emission and occurs at field strengths of typically $10^9 V/m$. In addition the emission sometimes is thermally assisted and electrons from the Fermi edge may overcome the barrier instead of tunnelling through (Schottky emission). The tunnelling probability in one dimension as a function of the particles potential energy V and its kinetic energy E is given by:

$$P(E,V) = f(E,V)\exp[-2(2m/\hbar)^{1/2}\int_0^L (V-E)^{1/2}dx]$$

eqn.II.2

Here L is the barrier length, m is the mass of the particle and f is an insensitive function of E and V. In fig.II.2 the one dimensional energy diagram for electrons at the metal-vacuum interface is depicted: fig.II.2a) shows the situation without external field, fig.II.2b) shows how the potential barrier is deformed under the influence of an external electric field of strength F. According to eqn.II.2 electrons with energies close to the Fermi energy E_F have a certain probability to leave the metal.

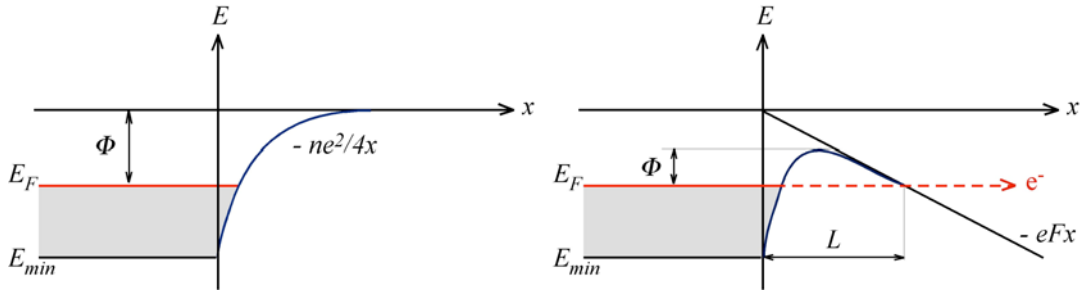

a) b) fig.II.2

For the tunnel current density *i(Φ,F)* the following equation (*Fowler-Nordheim equation*) holds [II.45]:

$$i = A\left(\frac{(E_F/\Phi)^{1/2}}{E_F+\Phi}\right)F^2\exp\left(\frac{-B\Phi^{3/2}}{F}\right) \qquad \text{where: } A = e^3/2\pi\hbar,\quad B = \sqrt{m}/2\pi\hbar e$$

eqn.II.3

Here e is the elementary charge and m is the tunnelling particle mass.

In principle, above relations also hold for positively charged particles. Of course, for emission of positive ions the tip ought to be set on positive potential accordingly. But in contrast to the emission of electrons the tunnel probability for massive ions is negligibly small; see eqn.II.3. Nevertheless, the potential barrier height can be reduced significantly by a high electric field at the tip apex, allowing ions to overcome the barrier more easily; see fig.II.2. From a physical point of view ion emission can be looked at as a field evaporation process. To achieve reasonable emission currents, i.e. to get more ions to overcome the potential barrier into vacuum the source can either be heated up (e.g. liquid Ga^+ ion source) [II.46] or else the tip must provide free ionic charge carriers with a sufficiently small work function, as may be the case for a solid electrolyte, to allow ion emission at room temperature.

II.5. Introduction to the Presented Experiments with Solid Electrolytes

The experiments discussed in the following manuscripts address questions concerning the conduction mechanism of $(AgI)(AgPO_3)$ and its applicability as a solid Ag^+ ion source.

Systems of the formula $(AgY)(AgPO_3)$ were $Y = Cl, Br, I$, generally are good ionic conductors. The conductivity σ is associated with Ag^+ ion movement increasing with the halogen ion size and reaches values of the order of 10^{-4}, 10^{-3} and $10^{-2} S/cm$ respectively [II.47]. The activation energy for the Ag^+ ions is of the order of $5.4eV$ [II.48]. The conductivity of $(AgI)_x(AgPO_3)_{1-x}$ is highly dependent on the molar fraction x of AgI [II.49, II.50]. The conductivity is believed to be mainly due to diffusion of Ag^+ ions within pathways of AgI, whereas the $AgPO_3$ is a relatively low conducting amorphous matrix. In fact, for pure $AgPO_3$ (i.e. $x=0$) the conductivity σ is of the order of $10^{-7} S/cm$ at $298K$ and increases to $10^{-2} S/cm$ for $x=0.6$ following a power law. For $x > 0.6$ the mixture does not readily form a glass and becomes unstable. More recently, neutron and x-ray diffraction measurements have shown that conductivity increases due to an increase of the free volume for Ag^+ motion with x and the glass forming is limited due to decreasing ionic cross-linking of the phosphate network [II.51]. This network has been found to have an approximate periodicity of $10Å$ and a correlation length of $25Å$ [II.52].

The experiments presented here have been carried out in the FEM using $(AgI)_{0.5}(AgPO_3)_{0.5}$. As it turned out $(AgI)_{0.5}(AgPO_3)_{0.5}$ can be shaped into sharp tips and hence can serve as a stable field ion emission source with fairly high emission currents. The recorded field ion emission patterns allow direct observation of the conduction dynamics in solid electrolytes on a microscopic scale and hopefully help to further elucidate the conduction mechanism in solid electrolytes.

II.6. Reference List II

[II.1] R.C. Agrawal, R.K. Gupta, J. Mat. Sci. **34**, 1131 (1999).

[II.2] P. Brinkmann, *Recent Advances in Fast Ion Conducting Materials and Devices*, World Scientific, Singapore, 11 (1990).

[II.3] G.D. Mahan, Phys. Rev. B **14**, 780 (1976).

[II.4] W. Dieterich, Solid State Ionics **5**, 21 (1981).

[II.5] H. Sato, Solid State Ionics **40/41**, 725 (1990).

[II.6] Ph. Maass, J. Petersen, A. Bunde, W. Dieterich, Phys. Rev. Lett. **66**, 52 (1991).

[II.7] H. Sato, T. Ishikawa, K. Funke, Solid State Ionics **53-56**, 907 (1992).

[II.8] K. Funke, Prog.Solid State Chem. **22**, 111 (1993).

[II.9] M.J. Rice, W.L. Roth, J. Solid State Chem. **4**, 294 (1972).

[II.10] B.A. Huberman, P.N. Sen, Phys. Rev. Lett. **33**, 1379 (1974).

[II.11] K. Funke, Solid State Ionics **18-19**, 183 (1985).

[II.12] O.L. Anderson, D.A. Stuart, J. Amer. Ceram. Soc. **37,** 573 (1954).

[II.13] M. Tachez, R. Mercier, J.P. Malugani, A.J. Dianoux, Solid State Ionics **20**, 93 (1984).

[II.14] C.A. Angell, Solid State Ionics **9/10**, 3 (1983).

[II.15] M.D. Ingram, M.A. Mackenzie, W. Müller, M. Torge, Solid State Ionics **40/41**, 671 (1990).

[II.16] Ph. Maass, A. Bunde, M.D. Ingram, Phys. Rev. Lett. **68**, 3064 (1992).

[II.17] K.L. Kliewer, J. Phys. Chem. Solids **27**, 705 (1966).

[II.18] T. Jow, B. Wagner Jr, J. Electrchem. Soc. **126**, 1963 (1979).

[II.19] A.M. Stoneham, E. Wade, J.A. Kilner, Mater. Res. Bull. **14**. 661 (1979).

[II.20] S. Pack, Electrochemical Society Meeting, Los Angeles, Abstract No. 133 (1979).

[II.21] J. Maier, *Superionic Solids and Solid Electrolytes – Recent Trends*, Academic Press, New York, 137 (1989).

[II.22] U. Lauer, J. Maier, Solid State Ionics **51**, 209 (1992).

[II.23] N.J. Dudney, J. Amer. Ceram. Soc. **68**, 538 (1985).

[II.24] A. Bunde, W. Dieterich, E. Roman, Phys. Rev. Lett. **55,** 5 (1985).

[II.25] N.F. Uvarov, P. Isupov, V. Sharma, A.K. Shukla, Solid State Ionics **51**, 41 (1992).

[II.26] M.G. Maclin, C.A. Angell, Solid State Ionics **53-56**, 1027 (1992).

[II.27] S.D. Druger, M.A. Ratner, A. Nitzan, Solid State Ionics **18/19**, 106 (1986).

[II.28] S.W. Martin, Solid State Ionics **18/19**, 472 (1986).

[II.29] J. Swenson, L. Börjesson, Phys. Rev. Lett. **77**, 3569 (1996).

[II.30] J. Swenson, R.L. McGreevy, L. Börjesson, J.D. Wicks, Solid State Ionics **105**, 55 (1998).

[II.31] R.J. Grant, M.D. Ingram, L.D.S. Turner, C.A. Vincent, J. Phys. Chem. **82**, 2838 (1978).

[II.32] A. Magistris, G. Chiodelli, Electrochim. Acta **26**, 1241 (1981).

[II.33] C.J. Kawamura, M. Shimaji, J. Non-Christ. Solids **88**, 2811 (1986).

[II.34] M.D. Ingram, C.A. Vincent, A.R. Wandless, J. Non-Christ. Solids **53**, 73 (1982).

[II.35] J. Kincs, S.W. Martin, Phys. Rev. Lett. **76**, 70 (1996).

[II.36] B. Roling, A. Happe, K. Funke, M.D. Ingram, Phys. Rev. Lett. **78**, 2160 (1997).

[II.37] R. Peibst, St. Schott, Ph. Maass, Phys. Rev. Lett. **95**, 115901 (2005).

[II.38] J.E. Shelby, D.E. Day, J. Amer. Ceram. Soc. **52**, 169 (1969).

[II.39] G. Gehlhoff, M. Thomas, Z. Techn. Phys. **6**, 544 (1925).

[II.40] M. Tomozawa, M. Yoshiyagawa, Glastech. Ber. **56**, 939 (1983).

[II.41] D.E. Day, J. Non-Christ. Solids **21**, 343 (1976).

[II.42] E.W Müller, Field Desorbtion, Phys. Rev. **102**, 618 (1956).

[II.43] E.W. Müller, T.T. Tsong, *Field Ion Microscopy, Field Ionisation and Field evaporation.* Progress in Surface Science. Braunschweig, Pergamon Press, Vol.4, Pt.1 (1973).

[II.44] R. Gomer, *Field Emission and Field Ionisation.* Cambridge, Harvard University Press (1961)

[II.45] R.H. Fowler, L.W. Nordheim, Proc. Roy. Soc. (London), A **119**, 173 (1928).

[II.46] J. Orloff, M. Utlaut, L. Swanson, *High Resolution Focused Ion Beams - FIB and Its Applications*, Kluwer Academic/Plenum Publishers, New York (2003).

[II.47] J.P. Malugani, A. Wasniewski, M. Doreau, G. Robert, A. Al Rikabi, Mat. Res. Bull. **13**, 427 (1978).

[II.48] M. Tachez, R. Mercier, J.P. Malugani, A.J. Dianoux, Solid State Ionics **18&19**, 372 (1986).

[II.49] M. Magnion, G.P. Johari, Phys. Rev. B **36** (16), 8845 (1987).

[II.50] P. Mustarelli, C. Tomasi, A. Magistris, Phys. Rev. B **63** (14), 144203 (2001).

[II.51] J.D. Wicks, L. Börjesson, G. Bushnell-Wye, W.S. Howells, R.L. McGreevy, Phys. Rev. Lett. **74** (5), 726 (1995).

[II.52] E. Kartini, M.F. Collins, T. Priyanto, M. Yusuf, N. Indayaningsih, E.C. Svensson, S.J. Kennedy, Phys. Rev. B **61** (2), 1036 (2000).

II.7. Manuscripts II

II.7.1. Vaccum Ion Emission from Solid Electrolytes:
An Alternative Source for Focused Ion Beams

II.7.2. Direct Evidence for Conduction Pathways in a Solid Electrolyte

Vacuum ion emission from solid electrolytes: An alternative source for focused ion beams

Conrad Escher, Sandra Thomann, Cornel Andreoli, and Hans-Werner Fink[a)]
Physik Institut der Universität Zürich, Winterhurerstrasse 190, CH-8057 Zürich, Switzerland

Julien Toquant and Dieter W. Pohl
Physik Institut der Universität Basel, Klingelbergstrasse 82, CH-4056 Basel, Switzerland

(Received 12 April 2006; accepted 13 June 2006; published online 4 August 2006)

A bright ion source based on the solid electrolyte $(AgI)_{0.5}(AgPO_3)_{0.5}$ has been developed. The solid electrolyte source provides stable currents of Ag^+ in the microampere regime that make it suitable for focused ion beam applications. Similar conditions are expected for different solid electrolyte materials and their corresponding ions. This opens a broad field of applications in structuring and modifying devices on a nanometer scale using focused ion beams. © *2006 American Institute of Physics*. [DOI: 10.1063/1.2264092]

Focused ion beams play a vital role in structuring devices on the nanometer scale.[1] A prerequisite for the generation of such focused ion beams are ion sources with a high degree of confinement and brightness as well as stability in continuous operation. This excludes volume plasma sources due to their lack of confinement as well as gas field ionization sources due to their limited brightness. So far, the only source that has been satisfying these three requirements routinely is the liquid gallium ion source[1] with emission currents in the microampere regime.

The operating principle of the liquid gallium source is based on a tungsten tip coated with liquid gallium. By means of an electric field, a delicate balance of surface tension and electrostatic forces forms a cone of gallium at the apex of the tip. The pointed cone is required to confine the extraction field to a small source region. The loss of ions is compensated by diffusion from a liquid metal reservoir, which enables continuous operation. Ga^+ ion beams can be focused to diameters down to about 5 nm, a limit imposed by the broad energy spread of the ions leading to considerable chromatic aberrations inherent to electrostatic ion lenses.[1]

In a good solid electrolyte the mobile ions can move almost as freely as in a liquid.[2] If the solid electrolyte was given the shape of a sharp tip and contacted to a reservoir of bulk metal, ions of the mobile species might be field emitted from the apex and replenished from the reservoir [Fig. 1(a)]. The nonmobile constituents of the material, however, would serve as a rigid frame that fixes the shape of the tip.

Out of the large number of known solid electrolytes, amorphous $(AgI)_{0.5}(AgPO_3)_{0.5}$ was chosen for our investigation. Its room temperature conductivity is one of the largest known ($\sigma \approx 10^{-2}$ S/cm at 25 °C),[3,4] its fabrication is easy, and, as it turned out, it can readily be shaped into a sharp tip, as shown in Figs. 1(b)–1(d). All tested tip geometries provide sufficiently high electric fields at the apex to allow ion emission into vacuum. The data presented here were generated with the micropipette filled structures, as shown in Fig. 1(c). They provide most stable and long term ion emission. Glass micropipettes are readily available with openings in the submicron regime. The pulverized solid electrolyte is filled into the pipette and heated to the melting temperature. The molten electrolyte has excellent wetting properties to glass. As a result, it moves towards the very end of the pipette, where it forms the desirable shape of a spherical calotte. Contacting the tip to a silver wire or fixing it with silver paste to the source holder provides a silver reservoir required for continuous operation.

For investigating the emission properties of such ion sources, a field ion microscope (FIM) is employed.[5] When the solid electrolyte tip is put on high potential with respect to a microchannel plate (MCP), Ag^+ ions are field emitted from the solid electrolyte and accelerated onto the MCP.

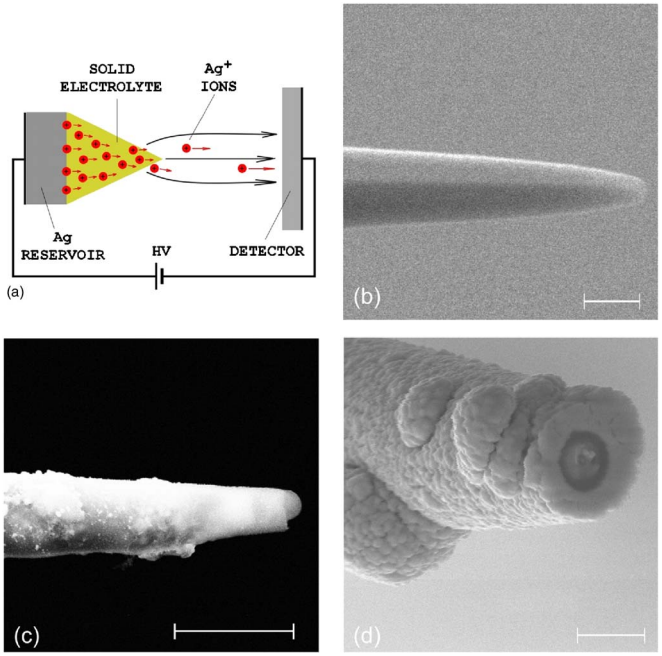

FIG. 1. (Color online) Schematic of the solid electrolyte ion source and realizations of it. (a) Principle of the solid electrolyte ion beam source. Different fabrication methods have been explored, ending up with sharply pointed tips. (b) Shaping of a tip by drawing a heated fiber of the solid electrolyte material. (c) Filling the solid electrolyte material into a glass capillary. (d) Evaporating silver onto the glass capillary followed by using a focused ion beam to cut off the very end of the tip. Although this structure is more complicated to fabricate, it has the advantage of the silver reservoir being in immediate contact to the emitting region of the solid electrolyte. The bars in the scanning electron micrographs correspond to 1 μm.

[a)]Electronic mail: hwfink@physik.unizh.ch

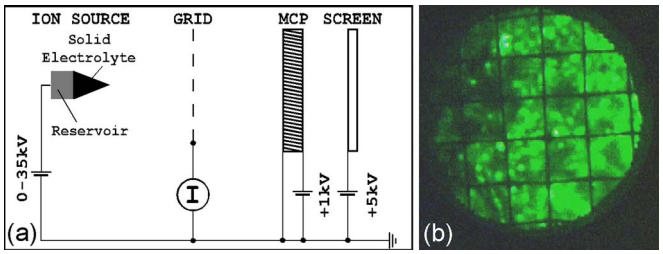

FIG. 2. (Color online) Schematic setup and field ion pattern. (a) The silver ions are field emitted from the tip and accelerated towards the MCP screen detector from which the ion emission pattern is recorded with a video camera. A grid placed in the path of the ion beam is used to measure a certain fraction of the current. (b) A field ion pattern as observed at the MCP screen detector.

There they provoke an electron avalanche, which is finally transferred into a light spot on a phosphorous screen. As the detector is approximately 10 cm away from the source, a highly magnified image of the emission sites at the tip apex is observed on the screen and recorded by a video camera. It is seen that the emission occurs in little spots representing the ends of migration channels.[6] A grid between the source and the detector is incorporated into the FIM [Fig. 2(a)]. It enables us to measure the ion current while *in situ* observing the dynamics of the emission patterns on the screen [Fig. 2(b)]. Since the grid blocks just 5% of the beam, only a fractional current is measured. However, when scaling it up to the total beam current, it agrees well with an independent measurement using a Faraday cup to capture the entire beam.

The maximum current amounts to almost 1 μA, as shown in Fig. 3(a). The plot of Fig. 3(b) indicates that the emission currents are well reproduced with changing voltages applied to the source. Moreover, long term stability of the source current has been monitored during operation for a few days. It appears conceivable that the lifetime of the source is essentially limited by the volume of the silver reservoir. The plot in Fig. 3(c) shows the time dependence of the current for the first 20 min of operation. Except for the first few minutes the emission current from the solid ion source proves to be very stable.

The findings presented above, considering the large number of known solid electrolyte materials, open up the possibility for generating ion beams from a variety of chemical elements.[7] Focused ion beam tools can profit from the use of Ag^+ ions (or Cu^+) where implantation of Ga is to be avoided. Possibly, even direct conductor path writing with linewidths of just a few nanometers might be envisioned. Other advantages of the solid electrolyte source compared to the liquid metal ion source might be higher mechanical stability, smaller energy spread, and, as a result, better ion optical performance. Last but not the least, the extension to solid electrolytes with conducting species different from metals will open up possibilities for alternative focused ion beam applications, such as etching with reactive ions such as F^-, O^{2-}, and H^+ and, relevant for integrated optics devices, doping with rare earth ions.

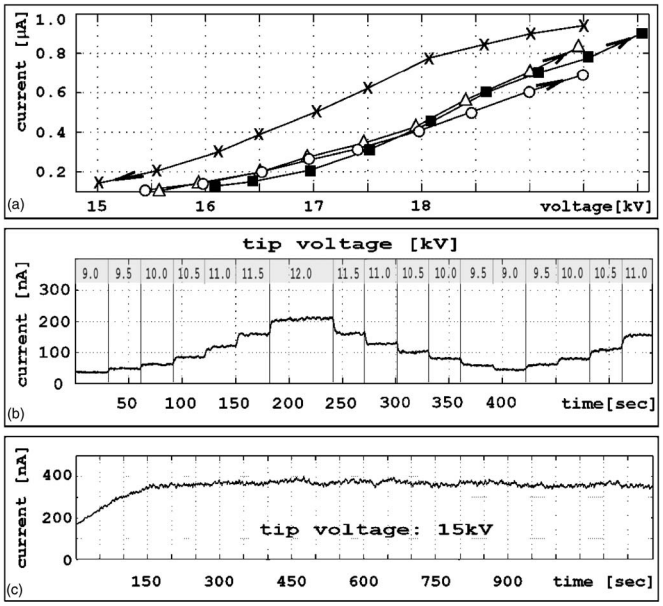

FIG. 3. Ion current measurements. (a) Four current-voltage characteristics. The data marked with circles, triangles, and squares are taken as the voltage gradually increased from 15 to 20 kV, whereas the data marked with crosses are taken as the voltage decreased from 20 to 15 kV. A slight hysteresis is apparent. (b) The current vs time response of a silver ion source to various bias voltages between 9 and 12 kV shows rather stable behavior. (c) The first 20 min of a long term current measurement at constant voltage is depicted.

Part of the work [by two of the authors (J.T. and D.W.P.)] was financially supported by the National Center of Competence in Research (NCCR) Nanoscale Science being part of the Swiss National Science Foundation (SNF).

[1] J. Orloff, M. Utlaut, and L. Swanson, *High Resolution Focused Ion Beams: FIB and Applications* (Kluwer Academic, Dordrecht/Plenum, New York, 2003).
[2] C. A. Angell, Annu. Rev. Phys. Chem. **43**, 693 (1992).
[3] J. P. Malugani, A. Wasniewski, M. Doreau, G. Robert, and A. Al Rikabi, Mater. Res. Bull. **13**, 427 (1978).
[4] P. Mustarelli, C. Tomasi, and A. Magistris, Phys. Rev. B **63**, 144203 (2001).
[5] E. W. Mueller and T. T. Tsong, *Field Ion Microscopy: Principles and Applications* (Elsevier, New York, 1969).
[6] C. Escher, T. Latychevskaia, H.-W. Fink, and D. W. Pohl, Phys. Rev. Lett. (to be published).
[7] R. C. Agrawal and R. K. Gupta, J. Mater. Sci. **34**, 1131 (1999).

Direct Evidence for Conduction Pathways in a Solid Electrolyte

Conrad Escher, Tatiana Latychevskaia, and Hans-Werner Fink
Physik Institut der Universität Zürich, Winterhurerstrasse 190, CH-8057 Zürich, Switzerland

Dieter W. Pohl
Physik Institut der Universität Basel, Klingelbergstrasse 82, CH-4056 Basel, Switzerland

(Received 31 January 2006; revised manuscript received 20 March 2006; published 26 September 2006)

The emission of silver ions from the apex of an amorphous electrolyte tip has been investigated by field ion microscopy. The ion emission patterns show discrete nanometer-sized spots. We present evidence that they represent the termination of bulk ion conduction pathways at the solid-vacuum interface. The analysis of the signals from individual emission sites suggests the existence of a network of such pathways in the solid. Auto- and cross-correlation measurements of the currents from individual sites provide quantitative information on the microscopic dynamics of charge transport in solid electrolytes as well as on the lateral extent of the pathway network.

DOI: 10.1103/PhysRevLett.97.136601 PACS numbers: 72.80.−r, 66.10.Ed, 68.37.Vj, 79.70.+q

In a good solid electrolyte, the mobile ions can move almost as freely as in a liquid. The resulting dc and ac conduction in solid state devices of the type shown in Fig. 1(a) has been studied extensively [1,2]. However, details about the microscopic conduction mechanism in solid-electrolyte conductors are experimentally not directly accessible. If, on the other hand, the solid electrolyte is given the shape of a sharp tip, set on high potential with respect to some counter electrode, ions of the mobile species may be field emitted and detected on a screen of a field ion microscope [3]. This opens up the possibility to measure the emission current [4] and to observe the emission dynamics. In this way, direct insight into the conduction mechanism can be obtained. Here we report such an experiment with a source made of amorphous (a-) $(AgI)_{0.5}(AgPO_3)_{0.5}$.

The solid electrolyte was prepared according to the recipe of Malugani *et al.* [5]. Shaping the material into sharp tips with radii of the order of 200 nm has been realized in different ways [4]. The data described below have been obtained with sources produced according to the following method. Powder of the solid electrolyte is filled into a standard glass micropipette and heated to about 150 °C for a few minutes. Being a polar glass, a-$(AgI)_{0.5} \times (AgPO_3)_{0.5}$ wets the glass of the pipette all the way through, ending in a bulge of less than 100 nm radius at the opening of the narrow side.

The room temperature conductivity of a-$(AgI)_{0.5} \times (AgPO_3)_{0.5}$ is one of the largest known ($\sigma \approx 10^{-2}$ S/cm at 25 °C) [5,6]. Contacting the tip to a silver wire or fixing it with silver paste to the source holder provides a silver reservoir, which is required for continuous operation [4]. The solid-electrolyte tip is incorporated in a field ion microscope [Fig. 1(b)].

When a high voltage is applied between the tip and detector, Ag^+ ions are field emitted from the solid electrolyte and accelerated onto the detector. The ion emission signal is finally transferred into a light signal on a fluorescent screen as shown in Fig. 1(c). A highly magnified image of the emission sites at the tip apex is observed, and the dynamics of the emission patterns on the screen are recorded by a video camera [7]. With this technique, we address the question of the conduction mechanism in amorphous electrolytes.

Theory predicts that the mobile ions move in conduction "pathways" [5,6,8–15], but experimental evidence has been indirect only. In amorphous $(AgI)_x(AgPO_3)_{1-x}$, with $x \approx 0.5$, chosen for our investigation, it is believed that the pathways are made up of the highly conductive AgI or its Ag^+ ions, which squeeze between the glass-forming, less conductive $AgPO_3$ chains. This expands the glass network, which might explain the existence of a "first sharp diffraction peak" in the neutron diffraction spectrum at unusually small momentum transfer [13–17]. Above concentrations $x \approx 0.3$, clusterlike regions percolate into extended channels [6,8,9]. This allows hopping of Ag^+ through the whole solid electrolyte. Extended numerical simulations of the atomic arrangement in the ionic glass

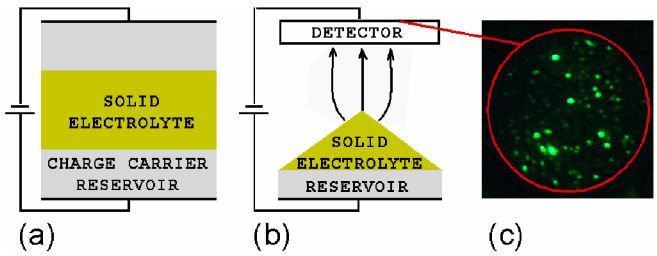

FIG. 1 (color online). Schematic setups to measure ion conduction properties. (a) Electrolytic cell: time-resolved measurements on a macroscopic scale. (b) Field ion microscope with a solid electrolyte as the source: time- and spatially resolved measurements of a microscopic area. (c) The ion emission signal from an $(AgI)_{0.5}(AgPO_3)_{0.5}$ tip, recorded with a video camera.

structure confirm this picture [8,11]. Especially the mixed alkali effect, which plays a key role in understanding ion transport in solid-electrolyte glasses, leads to more refined models, taking the dynamics of the network structure into account [10,18–20]. The latter is slow in comparison to the hopping dynamics of the ions; the network structure thus persists for some time after an ion has hopped to the next site. This leaves a trace for more ions to follow its path.

We shall first describe experimental observations consistent with the model outlined above. Thereafter, we present quantitative data that provide direct experimental evidence for the existence of ion conduction pathways. As apparent from Fig. 1(c), the emission does not originate from a single, large spot as one might have expected for a tip surface that is completely smooth in the electron microscope [4]. Instead, it consists of a number of bright spots as small as 3 nm in diameter. Upon cooling with liquid nitrogen, the number of emission sites decreases while the intensities of the remaining sites stabilize (Fig. 2). In view of the conduction pathway model, it appears plausible that the hopping dynamics slows down when the electrolyte is cooled. But also the dynamics of the surrounding network structure is reduced. As a possible consequence, only the most pronounced pathways remain active. This would explain our observations at reduced temperature [21].

However, the most direct indication for ion emission from individual end points of conduction pathways, sketched in Fig. 3(a), are the emission patterns. The individual spots fluctuate between apparently random positions [7]. A superposition of 3000 consecutive emission patterns, equivalent to an integration over 2 minutes, however, shows that they actually fluctuate between discrete positions [or else they would smear homogeneously over the entire surface, Fig. 3(b)]. Given this distinct spatial distribution of emission sites, the observed fluctuations in the overall ion signal must be due to fluctuations of the current from individual sites. It is interesting to note that the emission current from an $(AgI)_{0.5}(AgPO_3)_{0.5}$ tip needs a few minutes to build up, and hysteresis in the I/V characteristics is observed [4].

The time dependence of the individual microscopic currents should provide insight into the dynamics of charge transport within individual pathways. To explore this, we measured the intensity autocorrelation function for 14 individual spots. The current versus time signal has been evaluated by monitoring the relative detector intensities of individual spots. For each spot, the autocorrelation function f has been computed according to:

$$f(\Delta t) = \frac{1}{N-\Delta t}\sum_{t=0}^{N-\Delta t}\frac{(I(t)-\bar{I})(I(t+\Delta t)-\bar{I})}{(I(t)-\bar{I})^2}, \qquad (1)$$

where $I(t)$ is the intensity at time t, $\bar{I}$ represents the mean intensity, $N+1$ is the number of data points $t = 0, \ldots, N$,

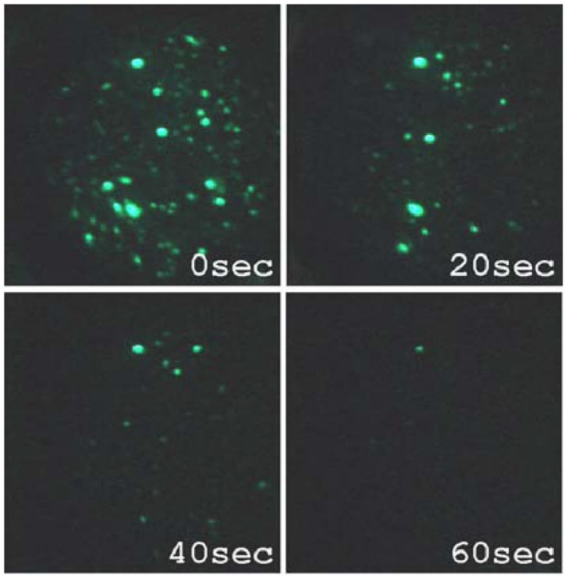

FIG. 2 (color online). Qualitative observation of the temperature dependence of the ion conductivity. The sequence shows the decay of the emission spot intensities at constant voltage upon cooling down by liquid nitrogen to an estimated final temperature of about 100 K.

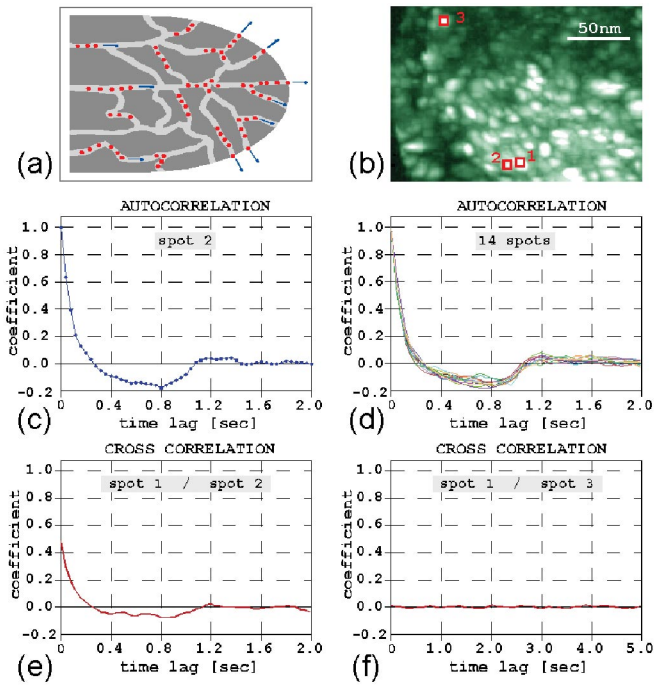

FIG. 3 (color). Quantitative evaluation of the silver ion emission patterns. (a) Schematic cut through an ion emitter tip exhibiting a network of ion channels. (b) Superposition of 3000 video frames, clearly showing the existence of distinct emission spots at the tip apex. (c) The intensity autocorrelation function for spot 2 with a temporal resolution of 40 ms. (d) The autocorrelation functions for 14 individual spots from the area shown in (b). (e),(f) Cross correlation between two neighboring spots (1 and 2) and between two farther apart spots (1 and 3).

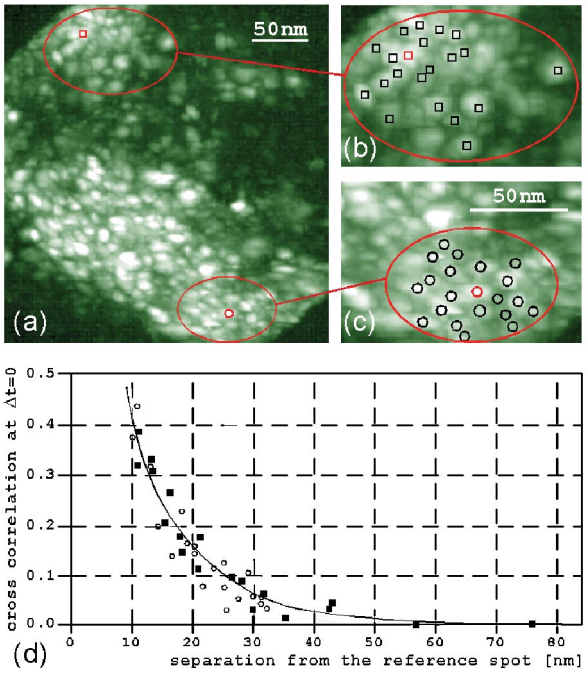

FIG. 4 (color). Distance dependence of the cross correlation. (a) Emission pattern from which two different regions have been arbitrarily chosen for further analysis. (b),(c) In these two regions, the cross-correlation function at $\Delta t = 0$ has been evaluated for several spots at different distances from a reference spot, marked in red. (d) Cross correlation for the two regions (circles and squares) on the apex of the solid-electrolyte ion source.

and Δt is the time lag. All autocorrelation functions displayed in Figs. 3(c) and 3(d) show a characteristic decay time of about 200 ms, up to which a positive correlation persists. Once this characteristic time has elapsed, a channel that did emit above the average current is exhausted for some time, which is reflected in a negative correlation, maintained for about 1 s. It is followed by a correlation function that is zero for all longer times, as expected.

As a consistency check for the picture drawn above, we also investigated the cross correlation between different ion emission spots. Neighboring spots separated by only 10 nm experience the same local over- or undersupply as has been seen in the autocorrelation experiment discussed before. This signifies that they are supplied by joined pathways in the bulk. However, spots that are separated by more than 100 nm show no correlation for any time [Fig. 3(f)].

To obtain information about the lateral extent of the ion pathway network, we have finally investigated the distance dependence of the cross-correlation coefficient for $\Delta t = 0$ as a function of the separation of two spots. The results are shown in Fig. 4. In accordance with the model, sketched in Fig. 3(a), the cross correlation gradually decays with increasing distance between two emission sites. A measure for the density of the network is given by the lateral distance over which a positive correlation between spatially separated ion channels is maintained. It turns out that individual ion pathways of the network "communicate" over distances up to about 60 nm [Fig. 4(d)].

In summary, field ion microscopy studies have made it possible to identify individual ion emission centers at the surface of a solid electrolyte. They are assumed to be the end points of bulk ion conduction pathways. The ion conduction pathway model for solid electrolytes, predicted by theory some time ago, has been confirmed on a microscopic scale. Auto- and cross-correlation measurements of the currents from individual nanometer-sized ion channels provide an insight into the dynamics of charge transport through a network of such conduction pathways in a solid electrolyte.

We are grateful to J. P. Malugani for the recipes of $(AgI)_{0.5}(AgPO_3)_{0.5}$ and to J. Toquant and R. Mouras for providing the raw material. We are also thankful to C. Andreoli and S. Thomann for their assistance in the field ion microscopy studies. D. W. P. acknowledges financial support by the National Center of Competence in Research (NCCR) Nanoscale Science as part of the Swiss National Science Foundation (SNF).

[1] C. A. Angell, Annu. Rev. Phys. Chem. **43**, 693 (1992).
[2] R. C. Agrawal and R. K. Gupta, J. Mater. Sci. **34**, 1131 (1999).
[3] E. W. Mueller and T. T. Tsong, *Field Ion Microscopy: Principles and Applications* (American Elsevier, New York, 1969).
[4] C. Escher, S. Thomann, C. Andreoli, H.-W. Fink, J. Toquant, and D. W. Pohl, Appl. Phys. Lett. **89**, 053513 (2006).
[5] J. P. Malugani, A. Wasniewski, M. Doreau, G. Robert, and A. Al Rikabi, Mater. Res. Bull. **13**, 427 (1978).
[6] M. Mangion and G. P. Johari, Phys. Rev. B **36**, 8845 (1987).
[7] See EPAPS Document No. E-PRLTAO-97-057639 for a video sequence showing the dynamics of the Ag ion emission. For more information on EPAPS, see http://www.aip.org/pubservs/epaps.html.
[8] J. D. Wicks, L. Börjesson, G. Bushnell-Wye, W. S. Howells, and R. L. McGreevy, Phys. Rev. Lett. **74**, 726 (1995).
[9] P. Mustarelli, C. Tomasi, and A. Magistris, Phys. Rev. B **63**, 144203 (2001).
[10] A. Bunde, K. Funke, and M. D. Ingram, Solid State Ionics **86–88**, 1311 (1996).
[11] J. Swenson, R. L. McGreevy, L. Börjesson, and J. D. Wicks, Solid State Ionics **105**, 55 (1998).
[12] J. E. Shelby and D. E. Day, J. Am. Ceram. Soc. **52**, 169 (1969).
[13] C. A. Angell, Chem. Rev. **90**, 523 (1990).
[14] A. P. Sokolov, A. Kisliuk, M. Soltwisch, and D. Quitmann, Phys. Rev. Lett. **69**, 1540 (1992).
[15] C. Rousselot. *et al.*, Solid State Ionics **78**, 211 (1995).
[16] J. H. Lee and S. R. Elliott, Phys. Rev. B **54**, 12 109 (1996).

[17] E. Kartini *et al.*, Phys. Rev. B **61**, 1036 (2000).
[18] A. Bunde, M. D. Ingram, and P. Maass, J. Non-Cryst. Solids **172–174**, 1222 (1994).
[19] A. Hunt, J. Non-Cryst. Solids **175**, 129 (1994).
[20] R. Peipst, St. Schott, and P. Maass, Phys. Rev. Lett. **95**, 115901 (2005).
[21] See EPAPS Document No. E-PRLTAO-97-057639 for a video sequence showing the dynamics of the Ag ion emission upon cooling with liquid nitrogen. For more information on EPAPS, see http://www.aip.org/pubservs/epaps.html.

II.8. Appendix II

II.8.1. Appendix II.1: Patent Specification; Solid Ion Beam Generator

(12) INTERNATIONAL APPLICATION PUBLISHED UNDER THE PATENT COOPERATION TREATY (PCT)

(19) World Intellectual Property Organization
International Bureau

(43) International Publication Date
5 October 2006 (05.10.2006)

PCT

(10) International Publication Number
WO 2006/103524 A1

(51) International Patent Classification:
H01J 37/08 (2006.01) *H01J 27/26* (2006.01)

(21) International Application Number:
PCT/IB2006/000706

(22) International Filing Date: 29 March 2006 (29.03.2006)

(25) Filing Language: English

(26) Publication Language: English

(30) Priority Data:
0507245.9 29 March 2005 (29.03.2005) GB

(71) Applicants *(for all designated States except US)*: **UNIVERSITY OF BASEL** [CH/CH]; Wtt-stelle, Petersgraben 35, CH-4003 Basel (CH). **UNIVERSITY OF ZÜRICH** [CH/CH]; Künstlergasse 15, CH-8001 Zürich (CH).

(72) Inventors; and

(75) Inventors/Applicants *(for US only)*: **POHL, Dieter** [DE/CH]; Felsenhofstrasse 10, CH-8132 Adliswil (CH). **FINK, Hans-Werner** [DE/CH]; Probsteistrasse 115, CH-8051 Zürich (CH). **TOQUANT, Julien** [FR/CH]; Strassburgerallee 75, CH-4055 Basel (CH). **ESCHER, Conrad** [CH/CH]; Rotachstrasse 19, CH-8003 Zürich (CH). **THOMANN, Sandra** [CH/CH]; Zwinglistrasse 33, CH-8004 Zürich (CH). **ANDREOLI, Cornel** [CH/CH]; Frohburgstrasse 325, CH-8057 Zürich (CH).

(74) Common Representative: **UNIVERSITY OF BASEL**; Wtt-stelle, Petersgraben 35, CH-4003 Basel (CH).

(81) Designated States *(unless otherwise indicated, for every kind of national protection available)*: AE, AG, AL, AM, AT, AU, AZ, BA, BB, BG, BR, BW, BY, BZ, CA, CH, CN, CO, CR, CU, CZ, DE, DK, DM, DZ, EC, EE, EG, ES, FI, GB, GD, GE, GH, GM, HR, HU, ID, IL, IN, IS, JP, KE, KG, KM, KN, KP, KR, KZ, LC, LK, LR, LS, LT, LU, LV, LY, MA, MD, MG, MK, MN, MW, MX, MZ, NA, NG, NI, NO, NZ, OM, PG, PH, PL, PT, RO, RU, SC, SD, SE, SG, SK, SL, SM, SY, TJ, TM, TN, TR, TT, TZ, UA, UG, US, UZ, VC, VN, YU, ZA, ZM, ZW.

(84) Designated States *(unless otherwise indicated, for every kind of regional protection available)*: ARIPO (BW, GH, GM, KE, LS, MW, MZ, NA, SD, SL, SZ, TZ, UG, ZM, ZW), Eurasian (AM, AZ, BY, KG, KZ, MD, RU, TJ, TM), European (AT, BE, BG, CH, CY, CZ, DE, DK, EE, ES, FI, FR, GB, GR, HU, IE, IS, IT, LT, LU, LV, MC, NL, PL, PT, RO, SE, SI, SK, TR), OAPI (BF, BJ, CF, CG, CI, CM, GA, GN, GQ, GW, ML, MR, NE, SN, TD, TG).

Published:
— *with international search report*

[Continued on next page]

(54) **Title:** HIGH BRIGHTNESS SOLID STATE ION BEAM GENERATOR, ITS USE, AND METHOD FOR MAKING SUCH A GENERATOR

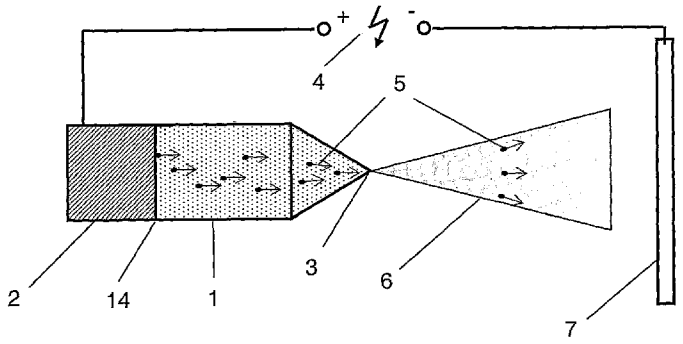

(57) **Abstract:** Ion sources or generators for focused ion beam emission (FIB) applications emitting ion beams into vacuum or a gas are used in industry and research for the characterization and processing of surfaces. With appropriate focusing, such ion beams can be confined to diameters of a few nanometers. The tip of technical FIB generators for producing such focused beams consists of a liquid metal, gallium in general, which tends to fluctuate during operation. This has a negative influence on the stability of the emission current and the focus definition. It is also possible to generate an FIB with solid tips, consisting of a solid metal, but such tips detoriorate rapidly during operation due to erosion of material from the tip apex. The present invention concerns a novel FIB source generating free space ion beams from a solid source but does not exhibit the above-mentioned erosion effect at the apex. The novel FIB generator consists of a combination of two essentially unitary bodies, a solid electrolyte body with a sharp tip and a solid ion reservoir body, both bodies having close contact with each other. The reservoir is made of or contains the same material, in general a metal as the mobile ions. Loss of ions from the electrolyte body due to emission is compensated by an inflow of ions from the reservoir body during operation. This practically preserves electro-neutrality which is a precondition for continuous mode operation. Erosion of the tip of the electrolyte body does not occur since the counter ions form a solid matrix and the emitted ions are replenished during operation.

WO 2006/103524 A1

— *before the expiration of the time limit for amending the claims and to be republished in the event of receipt of amendments*

For two-letter codes and other abbreviations, refer to the "Guidance Notes on Codes and Abbreviations" appearing at the beginning of each regular issue of the PCT Gazette.

DESCRIPTION

High brightness solid state ion beam generator, its use, and method for making such a generator

Field of the Invention

This invention concerns a solid state ion source or generator suitable for focused ion beam emission (FIB) applications. Ion beams emitted into vacuum or a gas are used in industry and research for the characterization and processing of surfaces. With appropriate focusing, such ion beams can be confined to diameters of a few nanometers.

Focusable ion beams require a point source in the shape of a sharp tip. Commercial FIB tools use liquid gallium (Ga) for that purpose. The gallium floats from a reservoir to the end of a needle where it forms a droplet. A large voltage applied between needle and an extraction electrode generates a high electric field at the tip that deforms the droplet into the shape of a tip and field-ionizes Ga atoms at the apex of that tip. The ions are expelled into a surrounding vacuum which contains means for acceleration, focusing, and deflection. Design and operation of stable liquid ion emitting tips are demanding and mastered by few, highly specialized companies only.

A simple alternative would be the use of sharp solid metallic tips, but such tips tend to erode during operation, whereby the emission current and the focus of the beam deteriorate significantly.

The present invention relates to an FIB source capable of generating free space ion beams from a solid-state body, but does not exhibit the typical erosion effect at the tip. To this, the FIB generator of the present invention basically consists of two essentially unitary bodies, a solid electrolyte, super-ionic conductor body having a sharp tip and a solid ion reservoir body in close contact with each other.

Preferably, the reservoir is made of or contains the same material as the mobile ions. Erosion of the tip of the super-ionic conductor body is avoided by the existence of a solid matrix of counter ions and a continuous ion flux from the reservoir body into the ionic conductor body and the tip. In other words, the erosion is shifted from the tip to the reservoir body which may be made sufficiently large to enable a nearly unlimited production of an ion beam.

Background and Prior Art

As mentioned above, ion beams emitted into vacuum or a gas are used in industry and research for the characterization and processing of surfaces. Several techniques are known for such FIB tools and applications. FIB tools are being used for implanting ions locally into a sample, for cutting away ("milling") material from a defined area with very small dimensions, for depositing material onto a sample, or for selectively etching a material surface by interaction with (organic) gases introduced into a reaction chamber.

Somewhat more specific, FIB tools are used for site-specific cross-sectioning, for interfacial microstructure studies, in particular for removing of certain metals or oxides, for editing or modifying semiconductor devices, for preparing site-specific TEM samples, and for grain imaging.

Also, high resolution microscopic images of a surface may be generated, similar to those obtained with an electron microscope (SEM). FIB tools for this latter application, i.e. processing and imaging, are therefore generally named FIB microscopes.

Usual FIB generators provide an ion beam emitted by a source, which beam is limited in its angular spread by a suppressor, accelerated by an extractor, collimated by a first lens and confined another time by an aperture. The source has to be lined up precisely with respect to the beam-shaping elements for optimum performance. Since this alignment procedure usually has to be repeated every time the source is replaced, a source with a long service life and/or integrated, pre-aligned beam-shaping elements has many advantages. The resulting beam is then directed onto a selected spot of the target by means of octupoles, deflectors and further lenses.

Especially for such an FIB microscope, a number of specific requirements must be fulfilled:

- Brightness: The FIB source or generator has to provide a strong current of ions per unit source area.
- Low divergence: The ions must be emitted at a narrow and constant angle.
- Monochromaticity: The ions must be emitted with small energy spread. This is required since the "focal length" of an ion lens depends on the initial energy, i.e. the "color" of the ion. The resulting chromatic aberration leads to a blurred images.

Further desirable features are stability, low cost, compact size, ease of operation and, as mentioned above, long service life of the source.

In many applications it is necessary that the implantation of FIB ions must not jeopardize the planned application of the FIB-treated work piece. In other applications, however, implantation is the very purpose of the FIB process, for instance the formation of optical waveguides with or without light-amplifying properties.

The standard ion source in an FIB generator is a sharp tip made - at least partly - from a conductive material. A voltage in the kV-range applied between the tip and an extraction electrode generates a strong electric field at the tip's apex. For sufficient field strength, ions at the tip surface are field evaporated, i.e. they experience a force strong enough to overcome the binding force to the rest of the tip material and to be expelled in direction of the electric field. The emission is usually restricted to the highly curved tip apex since the field enhancement is proportional to the curvature of the surface. Very bright ion emitters can be generated by minimizing the radius of this apex curvature.

In principle, any conductive sharp tip is suitable for ion emission. Solid metallic tips, however, erode during operation such that the tip becomes more and more blunt. The electric field strength at the apex is correspondingly reduced and so is the emission current. For this reason, tips suitable for operation over extended periods of time must maintain their shape while allowing for a continuous flow of ions to the tip.

The most common FIB generators use a tip formed by a molten metal, gallium (Ga), in general. Gallium has the advantage of a very low melting point and a relatively low level of toxicity. As described by J. Melngailis in "Ion sources for nanofabrication and high resolution lithography", IEEE Proceedings of the 2001 Particle Accelerator Conference, Chicago 2001, p. 76, molten Ga is pulled from a reservoir along a needle of solid metal towards its apex by the electric field and capillary forces. The droplet of liquid at the apex itself takes on the shape of a sharp tip under the influence of the electric field. This source is fairly stable, bright, has an acceptable energy spread ($\Delta E \sim$ 5eV), and a long lifetime (~1000 hours). However, due to the liquid flow condition, there are frequent fluctuations in the emission current. Sources with other metals, e.g. In, and with alloys such as Au/Si, Au/Si/Bi, and Pd/As/B have also been developed but are more difficult to handle and are not as stable or long-lived.

An alternative to the liquid metal source is the gas field ion source. The geometry of such a source is similar to the liquid metal source, except that the needle is cooled to cryogenic temperatures and gaseous species such as H, He, Ne, or Ar are condensed

on the needle. Again the ions are extracted by applying a voltage between the tip and a concentric electrode below the tip. With a sharpened tungsten needle tip of a few microns radius, the ion source characteristics are similar to those of the liquid metal source described above. Under particular conditions, it can have an extraordinary brightness, as described by R. Boerret, K. Jousten, K. Boehringer, and S. Kalbitzer in J. Phys. D, Appl . Phys. 21, p. 1835.

However, both sources described above are in general difficult to operate and appear not to have been incorporated into commercial systems to date, as described by J. Melngailis, supra.

A third, and somewhat more promising approach consists in the use of a solid ionic conductor for the FIB generator. One such ion (and atom) source is disclosed in Seidl USP 4 783 595, "Solid-state source of ions and atoms". The Seidl USP shows a source of a beam of positive ions or atoms comprising an ion-emitting pellet consisting essentially of a solid electrolyte.

Preferred solid electrolytes for the pellet are described as being alkali or alkali-earth mordenites. These materials have a room temperature conductivity of $<10^{-10}$ S/cm^{-1}, cf. Table 1 below and the article by A.N. Pargellis and M. Seidl "Thermionic emission of alkali ions from zeolites", J. Appl.Phys. 49, 4933 (1978). They are "poor-ionic solids" according to the classification of R.C. Agrawal & R.K. Gupta in the review article "Superionic solids: composite electrolyte phase – an overview" (Journal of Materials Science 34 (1999) 1131 – 1162). The classification is reproduced in the following table.

Table 1

Materials		Conductivity at 27°C (S/cm)
Electronic conductors	Metals	ca. 10^{-5}
	Semiconductors	ca. 10^{-5} to 10^{0}
Ionic conductors	Superionic solids	ca. 10^{-1} to 10^{-4}
	Normal-ionic solids	ca. 10^{-5} to 10^{-10}
	Poor-ionic solids	$< 10^{-10}$

Poor ionic solids have a sizeable conductivitiy at elevated temperatures only. The Seidl USP consequently includes a heater filament that is capable to heat the pellet to

a temperature of about 1000°C, at which ions are emitted from the pellet due to field-enhanced thermionic emission. A beam-forming electrode contacts an ion-emitting surface of the pellet, this beam-forming electrode having a passageway extending through it for ions from the ion-emitting surface. The ion-emitting surface of the pellet may be coated with a layer of porous tungsten or another refractory, high-work-function, material to establish an essentially equal potential across the surface and to neutralize ions emitted from the surface when the source is operated as an atom source.

The above-described apparatus may have some advantages over the prior described liquid metal or gas field ion sources, in particular by its use of a solid electrolyte. But since the ion (or atom) beam is emitted from an extended source according to the above Seidl USP, it cannot to be focused. This device hence cannot be called an FIB generator, which latter requires a well focusable ion beam, as explained above. Another serious limiting factor is the use of the high temperature of about 1000°C which prohibits the use of this device in any temperature-sensitive environment.

Materials that can be emitted in the form of ions by said apparatus are alkali or earth alkali metals. These materials are highly reactive (oxidation, etc.) which can be desirable for certain applications, but will generally be a disadvantage. Furthermore, high currents are obtained in pulsed mode only as described by A.N. Pargellis and M. Seidl in J. Appl.Phys. 49, 4933 (1978) and by J. Matossian and M.Seidl in J.Appl.Phys. 53, 6376 (1982).

Another solid electrolyte source is disclosed in Matossian USP 4 994 711, "High brightness solid electrolyte ion source", showing a solid electrolyte ion source with an emitting tip which is small enough to concentrate an electric field from an extraction plate. The material used for the solid electrolyte is either Cs mordenite (one of the mordenites also disclosed in the above-cited Seidl USP) or yttrium-doped zirconia which also belongs to the class of poor-ionic solids. Reportedly, the tip shape significantly increases the extracted current density compared to the prior solid electrolyte source. The source was heated to a temperature on the order of 1100°C (mordenite) and 1850°C (zirconia), sufficient to induce a thermionic ion emission from the respective tips. The ion emission can be varied independent of the extraction field by varying the degree of heating, thereby reportedly preserving a constant focused ion beam spot size during changes of beam brightness. The tip is said to have a radius in the approximate range of 1-10 µm. Use for ion-microprobe surface analysis and micro-circuit fabrication applications previously unavailable with solid electrolyte sources is contemplated.

Though this appears to be a viable approach fulfilling most of the above-listed requirements, it has three significant disadvantages:

1. The ions are emitted thermionically at temperatures of about 1100°C and 1850°C, respectively, which prohibits the use of this device in any temperature-sensitive environment.
2. The tip preferentially has a radius of curvature of 1 - 10 µm. This is too large for a true point source which should have a radius of curvature clearly in the sub-micron regime, preferably around 100 nm or less for strong focusing.
3. The emitted ions are Cs, an alkali metal, and oxygen, respectively. Due to their high chemical reactivity, these materials are undesirable in many applications.

Even more important, it remains uncertain in both the Seidl USP and the Matossian USP how the loss of ions and the resulting imbalance of charge in the source can be compensated over an extended period of time. It is apparently foreseen to replace ionic material emitted from the surface of the source (in the Matossian USP restricted to the tip) by material from the bulk of the source, cf. Matossian USP p.5, line 42-44. Diffusion of ions from the bulk to the surface indeed can keep the variation in the stochiometry at a low level for a long period of operation but it does not prevent the charging of the source, i.e. loss of electro-neutrality during operation. As a result, the voltage between source and extraction electrode will continuously decrease, accompanied by a corresponding decrease in ion current until the emission process comes to an end. Such behavior indeed was reported by A.N. Pargellis and M. Seidl in their article "Thermionic emission of alkali ions from zeolites", J. Appl.Phys. 49, 4933 (1978), see Fig. 2 of this paper. To compensate for this effect during operation, new charges have to be injected at a sufficient rate into the source. This requires an additional mechanism provided neither in the Seidl USP nor in the Matossian USP. Hence it appears questionable whether the two above-discussed ion sources are suitable for extended periods of operation.

The present invention resolves these shortcomings and devises an FIB generator which provides a long-term stable operation of such a generator with regard to brightness, low dispersion, and monochromaticity. Furthermore, it allows for operation at room temperature or slightly above by exploitation of field emission instead of thermionic emission. It also features relatively low cost and compact size and is easily operated.

The Invention

The invention is based on the novel idea to generate a continuously operable ion source by combining a solid electrolyte with a separate reservoir for the ions. This is achieved by arranging two essentially unitary bodies, a solid-state electrolyte body and a solid ion reservoir body, in close contact. The contact between the two bodies en-

ables transfer of ions in sufficient quantities to avoid ion depletion in the electrolyte body.

The resulting FIB source or generator is solid and still does not erode at its tip during operation, i.e. when generating free space ion beams from the electrolyte body. The FIB source also can be operated in continuous mode since electro-neutrality is preserved by the inflow of ions from the reservoir, thus avoiding charging during operation.

The electrolyte body is preferentially made from a super-ionic solid and the tip is sufficiently sharp or pointed, i.e. the curvature of its apex is sufficiently small, to enable field emission of ions from the tip at room temperature or slightly above room temperature.

Some general properties of solid electrolytes shall be described in the following. Most solid electrolytes are salts, composed of partially or completely ionized constituents. One of said constituents is loosely localized in the crystal lattice or amorphous network of the residual constituents. The loosely bound constituent is a small metal cation in most of the known solid electrolytes. When such a solid electrolyte is sandwiched between two electrodes and a voltage is applied, the ions migrate from one electrode to the other. In contrast to liquid electrolytes, the residual constituents form a solid matrix that forces the mobile ions to move along fixed migration pathways. The latter probably result from accumulations of vacancies along a path between the two electrodes. Most solid electrolytes accept a certain species of cations only. The ion-emitting electrode, i.e. the anode for metal ions, hence has to consist of the same metal as the ions if a continuous current is to be sustained. Otherwise, the charging effect mentioned above will stop the ionic current after a short period of operation.

Many salts, such as halogenides, phosphates, and chalcogenides are regularly used as solid electrolyte materials. Very often, silver is the mobile cation in these solid electrolytes. Other metals showing electrolytic mobility in the solid state are Li, Na, K, Ca, Cu, Al, and rare earths such as Er, Sc and Y. Ion beam sources made from the respective electrolytes will enlarge the choice of ions available. This will be of particular importance for the local doping of semiconductors. There are also compounds showing anionic conductivity, e.g. for oxygen and fluor at elevated temperatures. Ion beam sources made from such compounds are of particular interest for local surface processing.

Solid electrolytes are classified, cf. Tab. 1 above, according to their room temperature conductivity as superionic (10^{-1} - 10^{-4} S/cm), normal-ionic (10^{-5} - 10^{-9} S/cm), and poor-ionic ($\leq 10^{-10}$ S/cm). Only the first group can sustain a current sufficiently large for room temperature FIB operation which requires beam currents of at least 1 – 10 µA.

Among the known solid electrolytes (SEs), the highest room temperature conductivities are achieved by silver and copper halides, phosphates and mixtures thereof. For the experiments which led to the present invention, a-AgPO3:AgI (API), an amorphous SE was chosen. It has one of the highest known ionic conductivities at room temperature, is stable at ambient conditions over a long time and can be fabricated conveniently in different shapes.

Erosion of the tip of the electrolyte body is compensated by a continuous ion flux from the reservoir body into the electrolyte body which has the shape of a sharply pointed tip. The tip's apex may have a conical, pyramidal, or irregular shape, as will be understood by someone skilled in the art. Important is that, as mentioned above, the curvature of the apex is sufficiently small to enable field emission of ions at approximate room temperature.

When mounted in an ion beam generator, ions are field-emitted from the apex of the tip upon application of an extraction voltage in the range of 5 - 20 kV. They are replenished by migrating ions from the electrolyte body so that no erosion takes place at the apex and the tip preserves its shape during operation.

In the present invention, size and shape of the first of the unitary bodies, the electrolyte body, can be selected to achieve the best possible tip structure and shape, independent of any other requirements regarding volume, shape, or similar properties. This is possible because the bulk of the electrolyte body must only compensate for the ions emitted from the tip - it has no reservoir function apart from that, i.e. there is no need to provide ions to the tip from the bulk for an extended period of operation. The tip must just be replenished with ions and the electrolyte body must have a shape appropriate to allow for the necessary throughput of ions. A concave short cone, for instance, is a favourable shape, a long thin fibre an unfavourable one.

The ions required for operation over an extended period of time are provided by the second of the unitary bodies, the reservoir body, which may be made of or contain the material constituting the mobile ions, preferably a metal. Since it serves no other purpose it can be made sufficiently large, in any shape, and from any material that serves this single purpose best.

To provide the necessary flux of ions from the reservoir body to the electrolyte body, the two bodies must be in sufficiently close contact, preferably pressed against each other with adequate force to achieve a low contact resistance that allows transfer of enough ions from the reservoir body to the electrolyte body.

The invention also includes a new use for such a two-bodied FIB generator, referring in particular to its use at room temperatures.

A method for making a two-bodied FIB generator according to the invention is a further aspect, focusing on pulling a thin fiber from a melt close to its solidification temperature, thereby creating a front tip with the desired small apex.

The basic principle and details of the invention shall be explained in the following.

Brief Description of the Drawings

Various examples and modifications for carrying out and using the invention shall be explained together with the drawings. These show in

Fig. 1	a schematic illustration of the principle of the present invention;
Fig. 2	a first embodiment of the invention;
Fig. 3	a second embodiment of the invention;
Fig. 4	a third embodiment of the invention;
Fig. 5	a fourth embodiment of the invention; and
Figs. 6a – 6d	an exemplary manufacturing method for an FIB tip.

Detailed Description of Several Exemplary Embodiments

Several implementations of the invention are disclosed in the following. They differ in shape and arrangement of the two bodies, the solid electrolyte body and the reservoir body. However, the same reference numbers in the drawings always refer to the same functional parts of the different embodiments, though they sometimes look very different.

Fig. 1 shows the principle of FIB source according to the invention, namely the combination of a solid electrolyte body 1 and an ion reservoir body 2. The pointed tip 3 of the is electrolyte body is placed opposite an extraction electrode 7. The tip 3 may possess a conical, pyramidal, or irregular shape, important is the curvature at its apex. In such an ion beam generator, ions 5 are field-evaporated from the apex of the tip 3. These ions are replenished by migration from the ion reservoir 2 through the bulk of electrolyte

body 1 to the tip. This avoids excessive charging of the electrolyte body as well as erosion at the apex of the tip. The curvature of tip 3 must be kept sufficiently small to allow emission 6 of ions 5 at normal temperature, i.e. at room temperature, or somewhat above, e.g. up to 300°C , with a voltage in the kV range, for instance 15...20 kV between ion reservoir 2 and extraction electrode 7.

The voltage is generated by high voltage source 4 and generates an electric field essentially between the tip 3 of the electrolyte body 1 and the extraction electrode 7. To avoid depletion of ions 5 in the electrolyte body 1, ion reservoir 2 provides ions of the same kind as those emitted from the tip 3 in sufficient quantities to the electrolyte body. This is done by appropriately selecting the material of the reservoir body 2 and by providing an interface or contact area 14 of sufficient conductivity, i.e. with low resistivity, between the reservoir body 2 and the electrolyte body 1. By shaping this interface 14 suitably and by pressing the two bodies against each other, the resistivity can be kept low enough to enable easy migration of the ions from the reservoir body 2 to the electrolyte body 1. The process of erosion, which usually takes place at the tip 3, is thus shifted to the reservoir body 2 where it can be compensated for an extended period of operation.

Preferred electrolyte materials are super-ionic conductors whose conductivity is large enough to allow for a sufficiently large current through the electrolyte body at room temperature or slightly above (< 300° C). Sufficiently large here means currents required for FIB processing, at least 1 µA, but preferentially > 10 µA. A particularly favourable material is API (Ag_4IPo_4) for the electrolyte body 1 and silver (Ag) for the reservoir body 2, but other suitable materials and material combinations may be chosen. Examples for providing the desired metal ions are Li, Na, K, Ca, Cu, Al, and rare earths such Sc and Y, mentioned above and described in the literature. Other examples for the electrolyte body 1 are Li-, Na, and K-doped β-aluminas, mixed bromides such as $C_6H_{12}N_{2.2}HBr$-CuBr(87.5m), $Ca_2P_2O_7$, and tungstates of the type $R_2(WO_4)_3$ with R = Al, Sc, Y, and Er. Extensive tables of solid electrolytes may be found in the literature, especially in the above-cited review article by R.C. Agrawal and R.K. Gupta.

As mentioned above, API (Ag_4IPo_4) was chosen for the electrolyte body 1 and silver (Ag) for the reservoir body 2. The reason is that among the known silver halides, phosphates and mixtures thereof are among the super-ionic conductors with the highest conductivity. API, an amorphous solid electrolyte, was chosen because it has one of the highest known ionic conductivities at room temperature, is stable at ambient conditions over a long time and can be fabricated conveniently in different shapes.

Fig. 2 shows a first practical embodiment of the invention. As in Fig. 1, a combination of ion reservoir 2 and solid electrolyte body 1 with its pointed tip 3 is placed opposite an extraction electrode (not shown in this figure), emitting an ion beam 6 which is field-evaporated from the apex of the tip 3. The ions are replenished by migration of ions from the reservoir body 2 to the bulk of the electrolyte body 1 and from there to the tip 3. A high voltage source 4 is connected with its positive pole to the reservoir body 2 and with its negative pole to a (not shown) extraction electrode, equivalent to the extraction electrode shown in Fig. 1.

A casing 9 from isolating material holds the electrolyte body 1, the reservoir body 2, and a spring 8 pressing the two bodies against each other. Regarding the transfer of a sufficient number of metal cations from the reservoir body 2 to the tip 3, the following considerations are being made.

In an FIB source according to the invention, the process of erosion during ion beam emission from the tip 3 is shifted to the reservoir body 2 via the interface between the electrolyte body and the reservoir body. The continuous abrasion of metal, silver in the present example, from the reservoir body 2 would break the contact to the solid electrolyte 1 after a while if this was not prevented by appropriate measures.

The most straightforward measure is the generation of a large contact area between the electrolyte body and the reservoir body. For example, a monolayer of silver with an area of 1 mm^2 can supply a 1 µA ion beam for about 10 days. Further increase of the contact area, for instance by the formation of a rough and/or otherwise non-planar interface may increase the contact lifetime accordingly.

A better solution for the contact problem is the exertion of mechanical force between the electrolyte body and the reservoir body, for instance by spring-loading one against the other. Various spring-loaded embodiments are shown in Figs. 2, 3, and 4. Note that electrolyte body and the reservoir body need not be in perfect contact at the beginning of the operation since the erosion preferentially abrades the points of contact which results in an increasingly intimate contact between the two bodies.

Fig. 3 shows a second embodiment of the invention, displaying again, as in Figs. 1 and 2, a combination of ion reservoir 2 and solid electrolyte body 1 with its pointed tip 3 and an ion beam 6 field-emitted from the apex of the tip 3. A high voltage 4 source is connected with its positive pole to the reservoir body 2 and with its negative pole to a not shown extraction electrode. The solid electrolyte body 1 has the shape of a relatively thin hollow cone with a pointed front end whose inner surface matches the front end of the reservoir body 2 which is essentially a round cone.

A front casing 9, relocatably holding the front end of the reservoir body 2 and the electrolyte body 1, is connected to a rear casing 13 by one or more tension springs 8. The rear casing 13 is fixed to the rear part of the reservoir body 2, thus pressing the latter into the inner surface of the electrolyte body 1.

Minimizing the spot of emission is a requirement for strong focusing of an FIB, desired in most applications. Emission from several spots or from a large one is not desirable. Selection of a single spot can be achieved by using very sharply pointed probes and/or installing a small aperture in the path of the ion beam. The latter may be achieved by covering the tip with an isolating, emission-suppressing casing everywhere except for a very small opening at the apex. Openings with a diameter as small as 30 nm, possibly even less at tip apices, can be formed by electrolytic erosion, plastic deformation or FIB processing. An alternative is the use of a micropipette or a similar device filled with the solid electrolyte, as described further down. An example for an embodiment employing some measures along these lines is illustrated in Fig. 4.

Fig. 4 shows a somewhat more complex third embodiment of the invention. Again, a combination of ion reservoir 2 and solid electrolyte body 1 with its pointed tip 3 emits an ion beam 6 from the tip's apex. Dissimilar to the previously described embodiments, the reservoir body 2 here envelops the electrolyte body 1 and, at the same time, provides the holding means for the latter. For that, the reservoir body 2 has an inner conical surface matching the outside cone of the electrolyte body 1, with an opening for the tip 3.

An isolating front casing 14 provides a holding means for the reservoir body 2 and for one or more beam focusing means. Shown in Fig. 4 are a suppressor 12, electrically connected to the positive pole of the high voltage source 4, and an extractor 11 connected to the negative pole, but the number and arrangement of such beam shaping means depends on the desired form of the ion beam 6. A rear casing 13 is fixed to the electrolyte body 1 and, by means of tension springs, presses the latter into the inner conical surface of the reservoir body 2.

Depending on the intended use of an FIB source, comparatively large ion currents may be required. It was found that the ion current may be maximized by avoiding or reducing the limitation created by the diffusion of ions from the electrolyte body or reservoir to the emission point, i.e. the tip. Hence the ion beam current may be maximized by (1) choosing a material with inherently high conductivity, i.e. a super-ionic conductor (such as API), and/or

(2) minimizing the ion current path length between ion reservoir and emission point, and/or
(3) raising the temperature of the electrolyte body which increases the mobility of the ions and hence the ionic conductivity.

It should be clear from the above, that an embodiment according to Fig. 4 provides good solutions for each of the first two maximization possibilities above, i.e. choosing an effective material, here API, and minimizing the diffusion lengts between reservoir and tip.

Focusing onto the third possibility, the solid electrolyte/reservoir assembly can be combined with heating elements, of course with or without beam-shaping members as shown in Fig. 4, into one integrated device.

Fig. 5 shows in a fourth embodiment a device with heating or cooling means. The arrangement is somewhat similar to the first embodiment shown in Fig. 2.

A unitary isolating casing 9, for instance a glass tube in the shape of a micro-pipette, envelops the combination of reservoir body 2 and the electrolyte body 1, leaving a small opening for the tip of the latter, from which tip 3 the ion beam is emitted. The spring means for pressing the two bodies together is not shown. The casing 9 carries heating means 10, shown as several windings of a preferably electrically heated wire or a radiator coil.

The embodiment allows for heating up to a few hundred °C, e.g. up to 300°C. This is sufficient for many super-ionic conductors to raise the conductivity into the required range. 300°C is a fraction only of the temperatures required for thermionic emission from a poor-ionic conductor, typically above 1000°C, even up to 1850°C, as described in the above-cited prior art.

For certain applications, cooling of the FIB source can be of advantage. Cooling reduces the thermal spread of the velocities of the individual ions - the beam becomes more "monochromatic". This results in a better focusing capability since the electrostatic and magnetic lenses used in FIB tools suffer from large chromatic aberrations quite generally. Improved focusing is of particular interest for imaging with FIB and implantation of ions into minimum size volumes. Cooling of the FIB source can be achieved with essentially the embodiment of Fig.5 by replacing the heater coil by a cooling element, e.g. a liquid nitrogen filled outer tube or a Peltier element.

A different issue with regard to FIB sources is the necessary shaping of the tips of the electrolyte body. A sharp tip is mandatory for high brilliance in field emission, and it is also required for the formation of a sharp focus. This can be understood by the analogy between particle beams and light beams: The size of a focused spot is proportional to the spot size of the source as long as the wavelength is small compared to that spot. The quantum mechanical wavelength of the ions used in typical FIB applications is in the range of sub-angstroms, hence irrelevant for most applications.

Several inventive methods may be applied to create the tips of any of the above-described FIB sources, especially when using API, the preferred material for the electrolyte body.

In a first method, illustrated in Figs.6a and 6b, a thin API fiber is produced by pulling a fiber 20 from an API melt 21 near the melt's solidification temperature, about 300°C, with an appropriate tool 19. A sharp tip 22 at the end of such a fiber 20 may be generated with a modified micro-pipette puller 23, shown schematically in Figs. 6c and 6d. Such a fiber tip 22 provides stable currents at least in the nA range. As shortcoming, fiber tips sometimes may undergo mechanical rupture under the influence of electric fields generated at the tip.

In a second method (not shown in the drawings), the API is encapsulated inside a glass pipette. The pipette is stretched and narrowed with a micro-pipette puller to form an opening in the sub-micron range at one end. The pipette provides a stiff isolating mantle around the electrolyte that prevents rupture of the brittle material. In addition, it allows for in-situ heating by means of an electrically heated wire or a radiator coil attached to the pipette. This leads to a stable source that delivers currents in the μA range. The embodiments shown in Figs. 3 and 5 are examples for the application of an FIB source made according to this method.

In a third method, sharp tips are obtained by cleaving a piece of API in such a way that three faces are formed which meet at a sharp apex. Tetrahedral tips made from regular glass slides with atomically sharp apices are reported in the literature, e.g. by J. Koglin, U. C. Fischer, and H. Fuchs, Phys. Rev. B 55, 7977 (1997), and by A. Naber et al., Phys.Rev.Lett.89, 210801 (2002). Cleaving of amorphous API according to the same or a similar method will provide similar results.

A fourth method is based on the use of a FIB microscope. Tips prefabricated by one of the previous methods (or any other method) can be sharpened and/or given a desired shape in the nanometer range. The method and techniques used for the purpose are well known to any person trained in the use a FIB microscope.

The invention has been described using some detailed and some exemplary preferred embodiments. However, it is to be understood that the scope of the invention is not limited to the disclosed embodiments and that other applications and modifications of the invention by a person skilled in the art are encompassed by the following claims.

CLAIMS

1. A focused ion beam (FIB) generator with a solid electrolyte and an electric field adapted to create a focused beam of mobile ions,
characterized by
- a unitary solid electrolyte body (1) comprising a non-eroding first material and having a front tip (3) with an apex of predetermined curvature, from which front tip (3) said focused beam (6) of mobile ions exits and
- a unitary solid reservoir body (2) of a second material contacting said electrolyte body (1), said reservoir body comprising material suitable to forward mobile ions to said solid electrolyte body.

2. The FIB generator according to claim 1, *wherein*
the electrolyte body (1) is held in a predetermined position and has a transfer surface (14) remote from its front tip (3), the reservoir body (2) being in close contact with said transfer surface (14), thus allowing essentially continuous transfer of ions (5) from said reservoir body to said electrolyte body (1).

3. The FIB generator according to claim 2, *wherein*
the transfer surface (14) of the electrolyte body (1) is a rear surface essentially opposite of the tip (3) of said body.

4. The FIB generator according to claim 2, *wherein*
the transfer surface (14) of the electrolyte body (1) is essentially flat, as is the corresponding transfer surface of the reservoir body (2).

5. The FIB generator according to claim 2, *wherein*
the electrolyte body (1) is essentially a cone-shaped shell whose inner surface is a close contact with a cone-shaped reservoir body (2) to enable the desired ion transfer.

6. The FIB generator according to claim 2, *wherein*
the reservoir body (2) is in close contact and at least partly envelops the electrolyte body (1), leaving the front tip (3) of said electrolyte body (1) free.

7. The FIB generator according to claim 2, *wherein*
- the reservoir body (2) is a shell whose inner surface is essentially cone-shaped and
- the electrolyte body (1) has a similarly cone-shaped outer surface in close contact with said reservoir body's (2) inner surface.

8. The FIB generator according to any preceding claim, *wherein*
the close contact between the electrolyte body (1) and the reservoir body (2) is provided by an appropriately arranged resilient member (8).

9. The FIB generator according to any preceding claim, *further including*
a heater (10) for warming at least the region of the front tip (3) of the electrolyte body (1) above ambient temperature, in particular to a temperature of no more than about 300°C.

10. The FIB generator according to any of the claims 1 to 8, *further including*
a cooling apparatus capable of reducing the temperature of at least the region of the front tip (3) of the electrolyte body (1) below ambient temperature.

11. The FIB generator according to any preceding claim, *further including*
a casing (9, 13), especially an isolating casing, said casing providing a fixed support for either the electrolyte body (1) or the reservoir body (2) and a spring-loaded support for the corresponding other body.

12. The FIB generator according to claim 11, *wherein*
the casing (9, 13) is in two parts, spring-loaded against each other, one part holding the electrolyte body (1), the other part holding the reservoir body (2).

13. The FIB generator according to claim 11 or 12, *further including* ion beam extraction means (12) and, preferably, suppression and/or focusing means (11), in

particular an extraction electrode (7, 12) and a suppression electrode (11) fixed to one part of the casing (13) in the vicinity of the front tip (3) of the electrolyte body (1).

14. The FIB generator according to any preceding claim, *further including* a high voltage contact (4) directly connected to the reservoir body (2).

15. The FIB generator according to any preceding claim, *wherein* the first material is a halogenide, especially silver halide, or a phosphate, especially silver phosphate, or a chalcogenide or a mixture thereof, in particular amorphous API, and the second material is a metal, in particular silver.

16. The FIB generator according to any preceding claim, *wherein* the mobile ion is a cation, especially Ag^+, Li^+, Na^+, K^+, Ca^{2+}, Cu^+, Al^{3+}, or a rare earth metal ion.

17. The FIB generator according to any of the claims 1 to 15, *wherein* the mobile ion is an anion, especially O^{2-} or F^-.

18. Use of an FIB generator according to any preceding claim, *wherein* the electrolyte body (1), especially the tip (3) of said body, is kept at room temperature.

19. Use of an FIB generator according to any of the preceding claims, *wherein* the electrolyte body (1), especially the tip (3) of said body, is heated to a temperature above ambient temperature, especially to a temperature of less than about 300°C.

20. Use of an FIB generator according to any of the claims 1 to 18, *wherein* the electrolyte body (1), especially the tip (3) of said body, is cooled to a temperature below ambient temperature.

21. A method for making an FIB generator according to any of the claims 1 to 17, *characterized by*

- providing a melt (21) of the first material, especially API, having a temperature near its solidification temperature,
- pulling a thin fiber (20) from said melt (21), and
- tearing said thin fiber (20) apart in a micropipette puller, the ends of the broken fiber providing the front tip (22) of the electrolyte body with the desired apex.

22. A method for making an FIB generator according to any of the claims 1 to 18, *characterized in that*
the apex of the front tip (3) of the solid electrolyte body (1) is generated by cleaving or cutting a piece of solid electrolyte material.

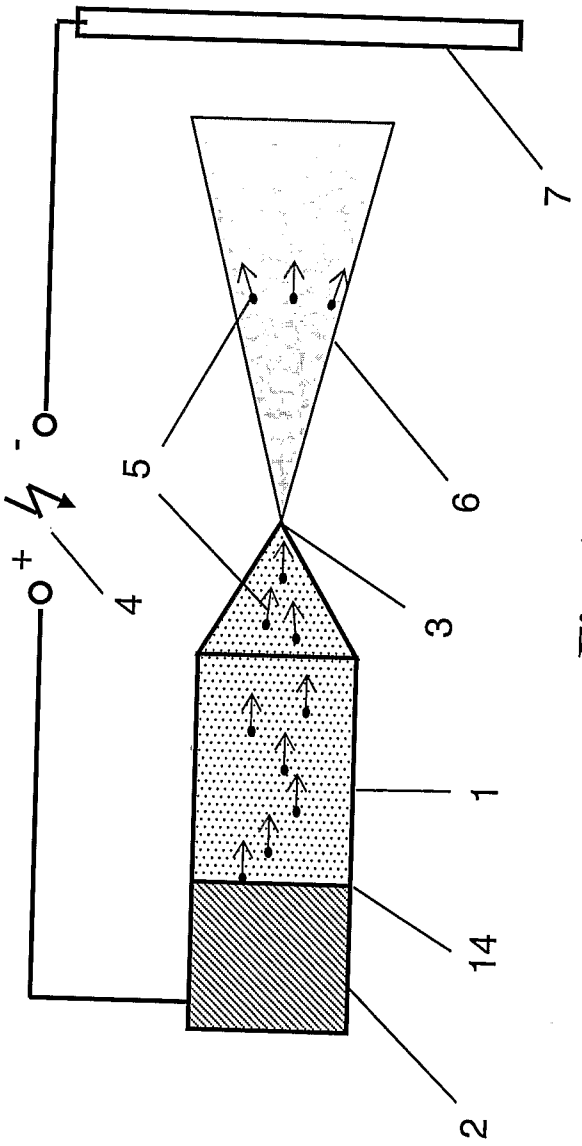

Fig. 1

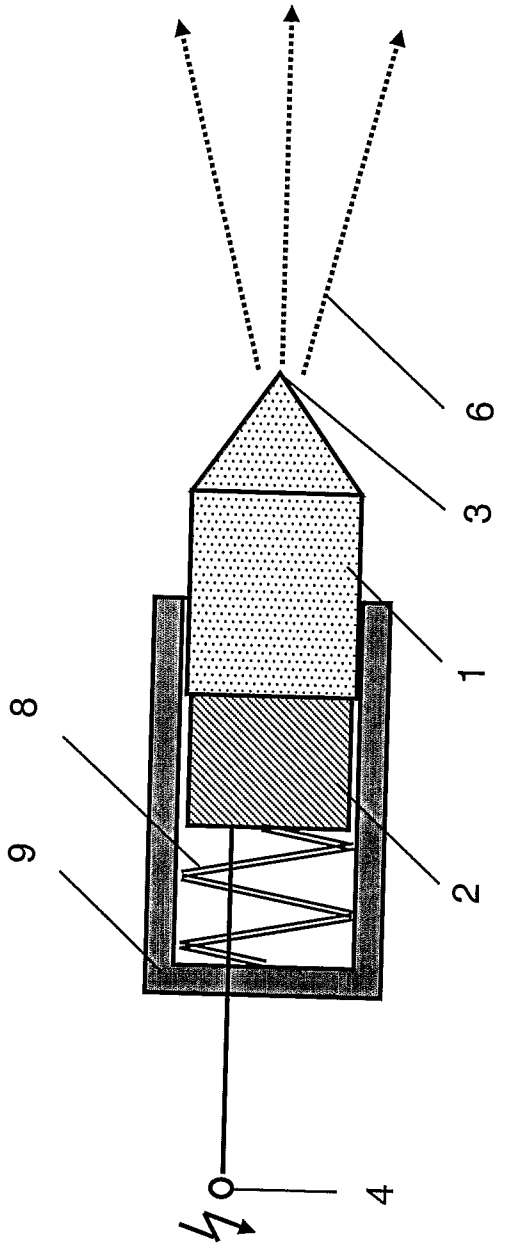

Fig. 2

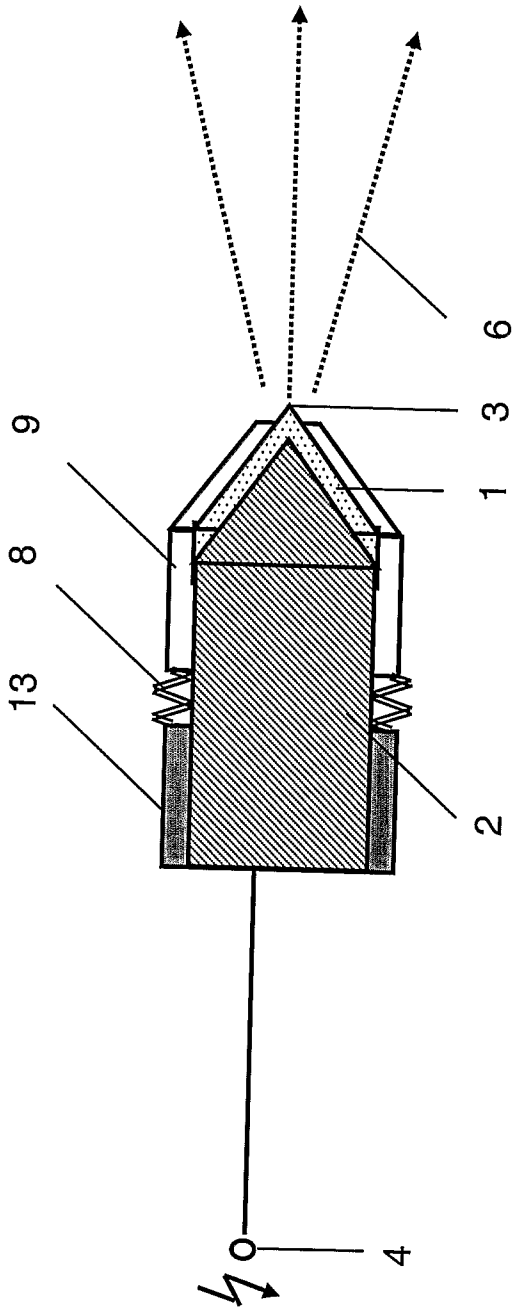

Fig. 3

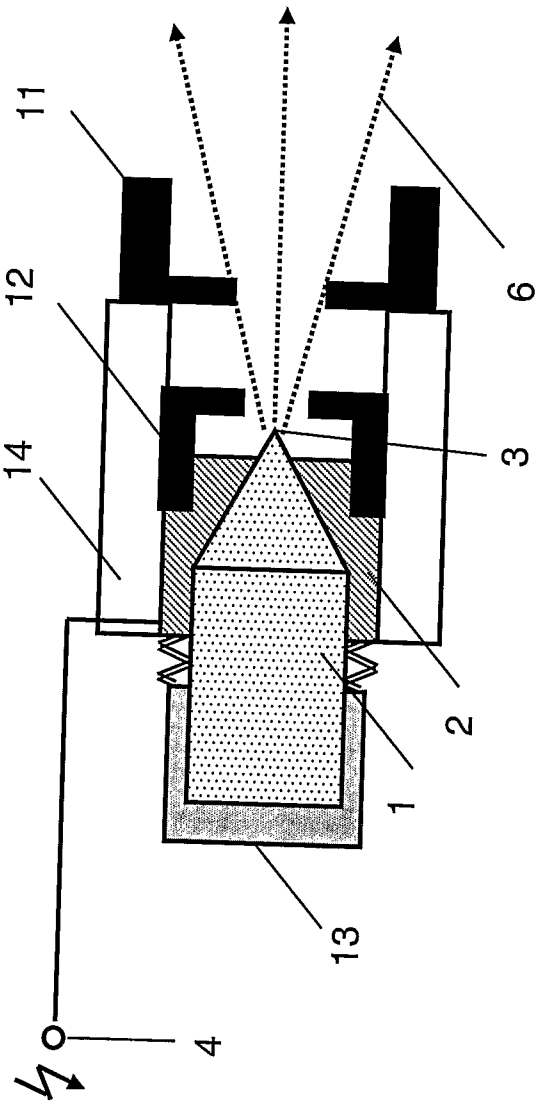

Fig. 4

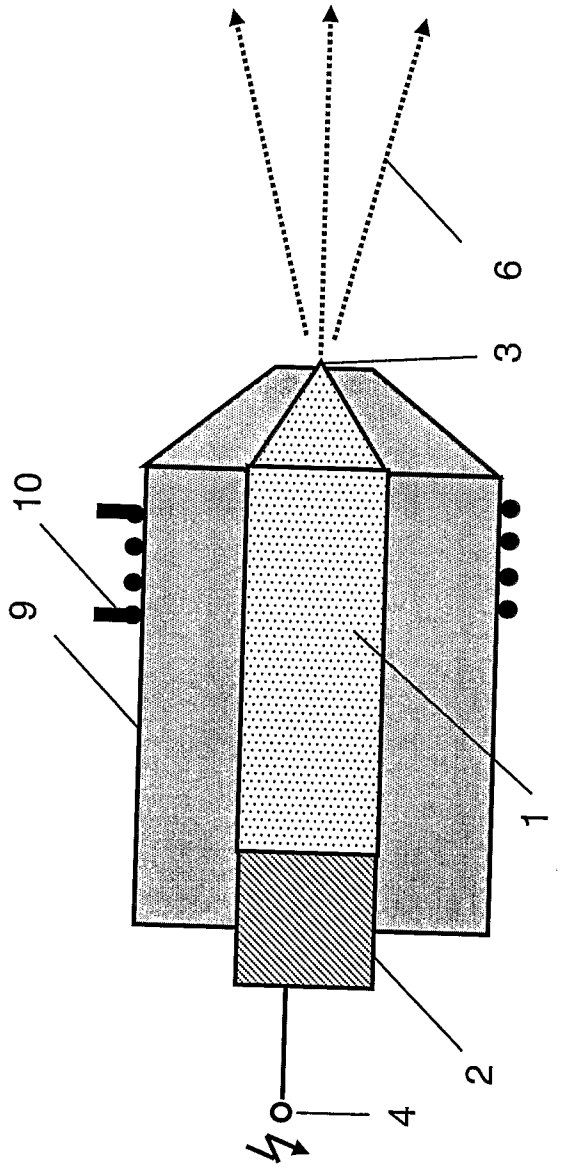

Fig. 5

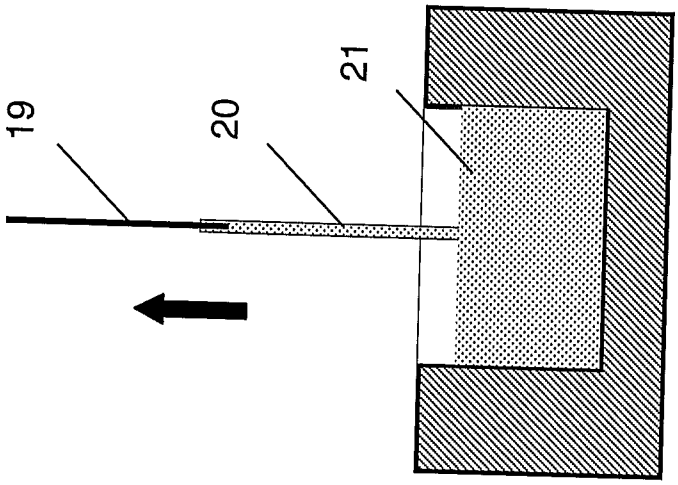

Fig. 6b

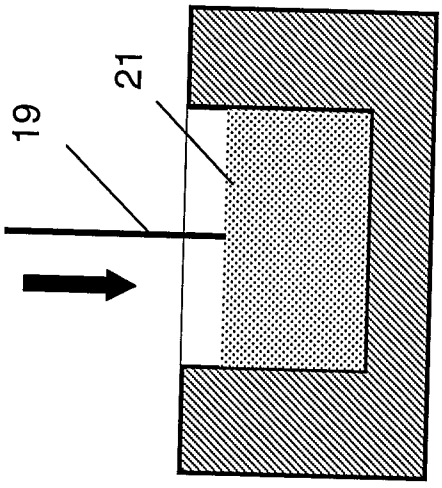

Fig. 6a

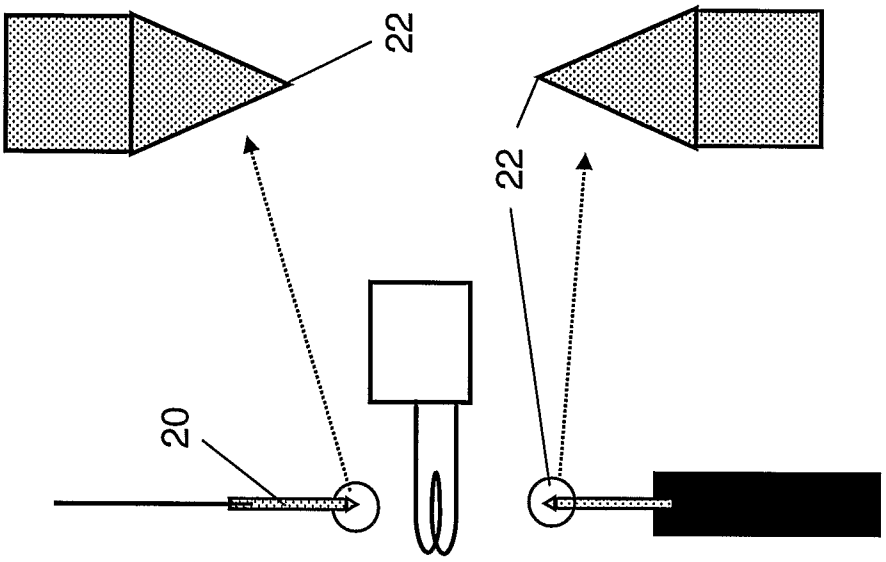

Fig. 6d

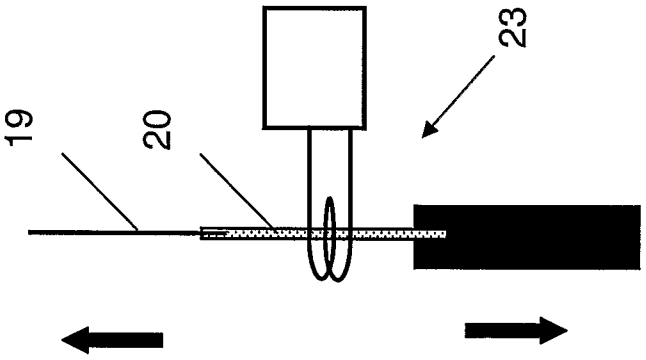

Fig. 6c

INTERNATIONAL SEARCH REPORT

International application No
PCT/IB2006/000706

A. CLASSIFICATION OF SUBJECT MATTER
INV. H01J37/08 H01J27/26

According to International Patent Classification (IPC) or to both national classification and IPC

B. FIELDS SEARCHED

Minimum documentation searched (classification system followed by classification symbols)
H01J

Documentation searched other than minimum documentation to the extent that such documents are included in the fields searched

Electronic data base consulted during the international search (name of data base and, where practical, search terms used)
EPO-Internal, PAJ

C. DOCUMENTS CONSIDERED TO BE RELEVANT

Category*	Citation of document, with indication, where appropriate, of the relevant passages	Relevant to claim No.
A	US 4 994 711 A (MATOSSIAN ET AL) 19 February 1991 (1991-02-19) the whole document	1-22
A	US 4 783 595 A (SEIDL ET AL) 8 November 1988 (1988-11-08) cited in the application the whole document	1-22
A	US 4 721 878 A (HAGIWARA ET AL) 26 January 1988 (1988-01-26) the whole document	1-22

☐ Further documents are listed in the continuation of Box C.

☒ See patent family annex.

* Special categories of cited documents :

"A" document defining the general state of the art which is not considered to be of particular relevance

"E" earlier document but published on or after the international filing date

"L" document which may throw doubts on priority claim(s) or which is cited to establish the publication date of another citation or other special reason (as specified)

"O" document referring to an oral disclosure, use, exhibition or other means

"P" document published prior to the international filing date but later than the priority date claimed

"T" later document published after the international filing date or priority date and not in conflict with the application but cited to understand the principle or theory underlying the invention

"X" document of particular relevance; the claimed invention cannot be considered novel or cannot be considered to involve an inventive step when the document is taken alone

"Y" document of particular relevance; the claimed invention cannot be considered to involve an inventive step when the document is combined with one or more other such documents, such combination being obvious to a person skilled in the art.

"&" document member of the same patent family

Date of the actual completion of the international search	Date of mailing of the international search report
9 August 2006	18/08/2006

Name and mailing address of the ISA/	Authorized officer
European Patent Office, P.B. 5818 Patentlaan 2 NL – 2280 HV Rijswijk Tel. (+31–70) 340–2040, Tx. 31 651 epo nl, Fax: (+31–70) 340–3016	Zuccatti, S

INTERNATIONAL SEARCH REPORT

Information on patent family members

International application No
PCT/IB2006/000706

Patent document cited in search report	Publication date	Patent family member(s)	Publication date
US 4994711 A	19-02-1991	NONE	
US 4783595 A	08-11-1988	NONE	
US 4721878 A	26-01-1988	DE 3677062 D1	28-02-1991
		EP 0204297 A2	10-12-1986

INTERNATIONALER RECHERCHENBERICHT

Internationales Aktenzeichen
PCT/IB2006/000706

A. KLASSIFIZIERUNG DES ANMELDUNGSGEGENSTANDES
INV. H01J37/08 H01J27/26

Nach der Internationalen Patentklassifikation (IPC) oder nach der nationalen Klassifikation und der IPC

B. RECHERCHIERTE GEBIETE

Recherchierter Mindestprüfstoff (Klassifikationssystem und Klassifikationssymbole)
H01J

Recherchierte, aber nicht zum Mindestprüfstoff gehörende Veröffentlichungen, soweit diese unter die recherchierten Gebiete fallen

Während der internationalen Recherche konsultierte elektronische Datenbank (Name der Datenbank und evtl. verwendete Suchbegriffe)
EPO-Internal, PAJ

C. ALS WESENTLICH ANGESEHENE UNTERLAGEN

Kategorie*	Bezeichnung der Veröffentlichung, soweit erforderlich unter Angabe der in Betracht kommenden Teile	Betr. Anspruch Nr.
A	US 4 994 711 A (MATOSSIAN ET AL) 19. Februar 1991 (1991-02-19) das ganze Dokument	1-22
A	US 4 783 595 A (SEIDL ET AL) 8. November 1988 (1988-11-08) in der Anmeldung erwähnt das ganze Dokument	1-22
A	US 4 721 878 A (HAGIWARA ET AL) 26. Januar 1988 (1988-01-26) das ganze Dokument	1-22

☐ Weitere Veröffentlichungen sind der Fortsetzung von Feld C zu entnehmen ☒ Siehe Anhang Patentfamilie

* Besondere Kategorien von angegebenen Veröffentlichungen :
"A" Veröffentlichung, die den allgemeinen Stand der Technik definiert, aber nicht als besonders bedeutsam anzusehen ist
"E" älteres Dokument, das jedoch erst am oder nach dem internationalen Anmeldedatum veröffentlicht worden ist
"L" Veröffentlichung, die geeignet ist, einen Prioritätsanspruch zweifelhaft erscheinen zu lassen, oder durch die das Veröffentlichungsdatum einer anderen im Recherchenbericht genannten Veröffentlichung belegt werden soll oder die aus einem anderen besonderen Grund angegeben ist (wie ausgeführt)
"O" Veröffentlichung, die sich auf eine mündliche Offenbarung, eine Benutzung, eine Ausstellung oder andere Maßnahmen bezieht
"P" Veröffentlichung, die vor dem internationalen Anmeldedatum, aber nach dem beanspruchten Prioritätsdatum veröffentlicht worden ist
"T" Spätere Veröffentlichung, die nach dem internationalen Anmeldedatum oder dem Prioritätsdatum veröffentlicht worden ist und mit der Anmeldung nicht kollidiert, sondern nur zum Verständnis des der Erfindung zugrundeliegenden Prinzips oder der ihr zugrundeliegenden Theorie angegeben ist
"X" Veröffentlichung von besonderer Bedeutung; die beanspruchte Erfindung kann allein aufgrund dieser Veröffentlichung nicht als neu oder auf erfinderischer Tätigkeit beruhend betrachtet werden
"Y" Veröffentlichung von besonderer Bedeutung; die beanspruchte Erfindung kann nicht als auf erfinderischer Tätigkeit beruhend betrachtet werden, wenn die Veröffentlichung mit einer oder mehreren anderen Veröffentlichungen dieser Kategorie in Verbindung gebracht wird und diese Verbindung für einen Fachmann naheliegend ist
"&" Veröffentlichung, die Mitglied derselben Patentfamilie ist

Datum des Abschlusses der internationalen Recherche	Absendedatum des internationalen Recherchenberichts
9. August 2006	18/08/2006

Name und Postanschrift der Internationalen Recherchenbehörde	Bevollmächtigter Bediensteter
Europäisches Patentamt, P.B. 5818 Patentlaan 2 NL – 2280 HV Rijswijk Tel. (+31–70) 340–2040, Tx. 31 651 epo nl, Fax: (+31–70) 340–3016	Zuccatti, S

INTERNATIONALER RECHERCHENBERICHT

Angaben zu Veröffentlichungen, die zur selben Patentfamilie gehören

Internationales Aktenzeichen
PCT/IB2006/000706

Im Recherchenbericht angeführtes Patentdokument	Datum der Veröffentlichung	Mitglied(er) der Patentfamilie	Datum der Veröffentlichung
US 4994711 A	19-02-1991	KEINE	
US 4783595 A	08-11-1988	KEINE	
US 4721878 A	26-01-1988	DE 3677062 D1	28-02-1991
		EP 0204297 A2	10-12-1986

Mein herzlicher Dank gilt Jewgeni Ermantraut, Dieter Pohl und Hans-Werner Fink für ihr Interesse und die Unterstützung im Zusammenhang mit der vorgelegten Arbeit.